ARTIFICIAL SAND PRODUCTION FOR LABORATORY USES

by

Murat Cenk Erdurak

B.S., Civil Engineering, Boğaziçi University, 2009

Submitted to the Institute for Graduate Studies in
Science and Engineering in partial fulfillment of
the requirements for the degree of
Master of Science

Graduate Program in Civil Engineering

Boğaziçi University

2011

ACKNOWLEDGEMENTS

I am heartily thankful to my thesis supervisor, Prof. Gökhan Baykal for his continuous support, thoughtful guidance and encouragement.

I would also like to express my gratitude to members of my thesis committee, Assoc. Prof. İsmail Hakkı Aksoy and Assist. Prof. Özer Çinicioğlu who devoted their invaluable time for reading and commenting on my thesis.

I want to convey heartfelt thanks to Emrah Kılıç, Yusuf Eşidir, Cihan Cengiz, Anıl Yıldız, Elif Çiçek and Arshiya Abadkon for their help during my experiments and during preparation of this thesis and spending their valuable time with me in Karl-Terzaghi Soil Mechanics Laboratory.

And finally, I owe special thanks to my mother Türkan Erdurak and my sister, Ceren Erdurak. They have always supported me and believed in me throughout my whole life.

This thesis is dedicated to my father and my grandparents.

ABSTRACT

ARTIFICIAL SAND PRODUCTION FOR LABORATORY USES

Natural sands, like standards sands, are used for geotechnical purposes in laboratory experiments. However, they have some certain drawbacks such as variability even in the same deposit, high cost of collecting samples or becoming unavailable over the time. So, they are not suitable for parametric study concerning geotechnical laboratory experiments. The objective of this M.S. thesis is producing artificial sand in order to use in geotechnical laboratory experiments for parametric studies and examining its geotechnical properties. The usability of the pellets as artificial sand for laboratory uses can be decided by evaluating and comparing the parameters such as mineralogy, roundness, sphericity, specific gravity, water absorption, grain size distribution and internal friction angle with those of the natural or standard sands. In order to evaluate the performance of artificial sand; natural sand samples, crushed sand samples and artificial sand samples produced from cement and fly ash, alternatively, were prepared. Constrained modulus tests are conducted to specify the strain-stress behavior of the samples at rest, in K_0 condition and to find crushability values. Internal friction angles of pellets, produced both from fly ash and cement, are close to the internal friction angle values of crushed sand. Crushed sand and Sakarya sand have internal friction angle values ranging between 33.6^o and 41^o. Whereas pellets produced from fly ash and cement have internal friction angle values between 32.8^o to 42^o. Lastly, stress path tests and cyclic triaxial tests were conducted. The samples produced from fly ash and cement reaches to the failure after 25 and 23 cycles, whereas Sakarya sand and crushed sand reaches to the failure after 19 and 21 cycles with amplitude of 50 kPa and 2 Hz cyclic sinusoidal loading. It is seen that pellets have similar or better performance than the performance of natural and crushed sands under the condition of cyclic loading.

ÖZET

LABORATUVAR DENEYLERİ İÇİN YAPAY KUM ÜRETİMİ

Doğal kum numuneleri, standart kumlar gibi, zemin mekaniği laboratuvar deneylerinde kullanılırlar. Ancak aynı ocaktan dahi olsalar değişkenlik gösterme, örnek almadaki yüksek maliyeti ve zamanla tükeneme gibi dezavantajları vardır. Zemin mekaniği laboratuvar deneyleri açısından düşünüldüğünde parametrik çalışmaya uygun değillerdir. Bu yüksek lisans tezinin amacı zemin mekaniği deneylerinde parametrik çalışmalar için kullanılacak yapay kum üretilmesi ve zemin mekaniği özelliklerinin incelenmesidir. Laboratuvarda pelletlerin yapay kum olarak kullanılabilirliğine mineraloji, küresellik, yuvarlaklık, özgül ağırlık, su emilimi, dane boyutu dağılımı ve içsel sürtünme açısı bulunarak ve doğal ya da standard kumlarınkiyle kıyaslanarak karar verilebilir. Yapay kumların performansının belirlenebilmesi için doğal kum numuneleri, kırma kum numuneleri çimento ya da uçucu külden üretilen yapay kum numuneleri hazırlanmıştır. Sınırlı modül testleri, numunelerin sükunette deformasyon - gerilme davranışları ve kırılabilirliğinin belirlenmesi için yapılmıştır. Uçucu kül ve çimentodan üretilen peletlerin içsel sürtünme açıları, kırma kumun içsel sürtünme açısı değerlerine yakındır. Kırma kum ve Sakarya kumu 33.6^o ve 41^o arasında değişen içsel sürtünme açılarına sahiptir. Uçucu kül ve çimentodan üretilmiş peletlerin içsel sürtünme açısı $32,8^o$ ile 42^o arasındadır. Son olarak gerilme izi ve dinamik üçeksenli deneyleri, peletlerin zemin mekaniği yönünden performansları hakkında bilgi toplanması için yapılmıştır. Sakarya kumu ve kırma kum numuneler 50 kP'lık genlik ve 2 Hz'lik döngüsel sinüs yük altında 19 ve 21 yüklemede kırılırken uçucu kül ve çimentodan üretilen numunelerin, sırasıyla 25 ve 23 döngüde kırıldığı gözlemlenmiştir. Peletlerin periyodik yük altında doğal ve kırma kumun performansına benzer ya da daha iyi bir performansa sahip oldukları görülmüştür.

TABLE OF CONTENTS

LIST OF FIGURES

LIST OF TABLES

LIST OF SYMBOLS

C_c	Coefficient of uniformity
C_u	Uniformity coefficient
D_{50}	Mean grain size
d	Diameter of the spherical particle
D	Disc diameter (m),
e_{max}	Maximum void ratio
e_{min}	Minimum void ratio
e	Void ratio
E	Modulus of elasticity
G_s	Specific gravity
m_v	Equivalent oedometer coefficient of compressibility
n_{cr}	Critical revolutions per minute
P_c	Pressure at the point of contact
α_i	Angle of disc inclination in degrees
β	Central angle of the meniscus and
ϕ	Angle of friction
γ_{max}	Maximum density
γ_{min}	Maximum density

1. INTRODUCTION

According to the definition of ASTM specification Standard Specification for Standard Sand standard sand is silica sand, composed almost entirely of naturally rounded grains of nearly pure quartz, used for preparing mortars in the testing of hydraulic cements (ASTM C778 - 06).

Standard soils are used worldwide as reference materials with which new model or single element experiments may be performed, assessed and calibrated. The testing databases associated with these are valuable resources that are particularly important when developing new procedures. So, continuous access to standard test sands is essential to geotechnical researchers. However, the finite extent and variability of all natural deposits creates the possibility that standard soils may vary, or become unavailable, over time (Takahashi and Jardine, 2007).

There are many types of standard soils for laboratory uses. Generally, they are used very frequently for the geotechnical experiments in the teritories where they are available. The most known example for standard sands is Ottawa Sand. Ottawa is a city located in LaSalle County, Illinois, USA. It has been a major sand center over the years. The geotechnical properties of the Ottawa Sand has been researched over that time because it has been used in many civil engineering projects until today. Further information about standard sands will be given in following chapters.

The biggest advantage using a standard soil is having some of the data about that standard soil that was searched by other researchers before. However, it is not cheap to get samples of those standard soils for the laboratories in far distances. Furthermore, the characteristic properties of the soil may vary with the changing samples, even if they are called standard soils. It is also very limiting to conduct experiments if the chemical structure of the soil is taken into consideration.

Because of the reasons stated above, a geotechnical experiment, that is conducted in order to investigate only one parameter of a sand, is almost impossible. As an example, an experiment can be given, where only the effect of shape of grains on the shear strength is researched. The chemical composition of the sand samples is also a changing parameter in the experiments because the sand samples will be from different quarries in order to have sand samples with different particle shapes. So, the shear strength of these different soil samples are changing according to their shapes and their crushability which is affected by chemical composition. The parameter that is in the focus of the research cannot be isolated out of other factors.

There are some replacement materials that are used in geotechnical researches in order to minimalize the changing factors in the experiment. One of them is glass beads. They are used in geotechnical researches because they have a similar chemical composition like sand. Glass beads are produced mainly from silica. Their perfectly sphere shape eliminates the shape factor that is effecting the shear strength. Furthermore, they are chosen for the researches about granular packing. The reason for being chosen in this topic is again their shape that provides good observation on the particle behaviour and movement with a simplified manner.

In his research, (Vallejo, 2001) has studied natural slopes and rockfill stuructures. As it is known, any natural slopes and rockfill structures are made of a mixture of rock fragments and sand-size particles. To analyze the stability of such natural slopes and rockfills, a knowledge of how rock-sand mixtures develop their shear strength is needed. To gain an understanding of the reasons why limits of concentration by weight of gravel in gravel-sand mixtures exist at which it controls, partially controls, or has no control at all on the shear strength of the mixtures, laboratory and theoretical analyses of the changes in porosity (or grain concentration) developed by the mixtures of large (5 mm) and small (0.4 mm) spherical glass beads are presented. The changes in porosity that different proportions of the large and small glass beads develop when mixed together seem to explain why these limits exist. So, in his research glass beads are used to model the particle behaviour with a known particle shape (Vallejo, 2001).

Earthquake engineering cannot be thought without the influence of soil and structure interaction. A very important parameter that is used for the calculation and design in the concern of earthquake engineering is shear wave velocity. Patel *et al.*, stated that it is well recognized that shear wave velocity in the soil mainly depends on its type, state of compaction, and the confining stress. However, the influence of other geometrical parameters of soil particles (such as size, shape, roundness, and sphericity) on the shear wave velocity has not received much attention of the earlier researchers. With this in view, investigations were conducted to determine shear wave velocity in different types of granular materials (sands, glass beads). Glass beads are used to investigate the effects of shape, roundness and sphericity (Patel *et al.*, 2009).

Reinson *et al.*, researched the design of effective capillary barriess. In their research, it is argued that design of effective capillary barrier systems requires a thorough understanding of the soil-water interactions that take place in both coarse- and fine-grained unsaturated soils. Furthermore, experimental observations of water flow through coarse porous media are presented to gain greater understanding of the processes and mechanisms that contribute to the movement and retention of water in coarse-grained unsaturated soils. This experimental observations and experimental measurements of seepage velocity and volumetric water content were obtained for columns of 12 mm glass beads using digital videography to capture the movement of a dye tracer front at several infiltration rates (Reinson *et al.*, 2005).

In the paper of Kuwano and Jardine, it is set out the experimental conditions that had to be met to make representative creep observations in the course of research on Ham River sand (HRS) and Ballotini® glass beads (GB). HRS is a uniform, clean subangular-shaped quartz sand, with a mean particle size around 0.27 mm. The particle size of the GB was similar to that of the HRS. This paper is an example where a standard sand and also a replacement material, Ballotini® glass beads, are used. The main reason, why Ballotini® glass beads are used, is stated as the shape and size of the GB are compatible with HRS (Kuwano and Jardine, 2002).

More examples where glass beads are used in the experiments for geotechnical manner can be found when it is investigated. Another replacement material is metal beads. They are used to model sands in high pressures. In those high pressures natural sands and glass beads can be crushed and they can change their behavior.

In the researches of Kong *et al.*, it is stated that one of the major factors that affect the strength and deformation of rockfill materials is particle sliding. Based on triaxial tests of artificial rockfill materials of steel balls, the effect of micromechanics on strength and deformation of rockfill materials is investigated. Steel balls are chosen in the in this particular research because the effect of crushing can be ignored by this way (Kong *et al.*, 2010).

In the paper of Yun and Santamarina, a very different property of the soil is investigated: The thermal conductivity of the different soil components (mineral, liquids and air) are studied. The study is implemented to explore the role of contacts in heat conduction in dry granular materials Metal beads are used in these particular experiments to elucidate heat transfer at contacts, and it is complemented with a numerically based inversion analysis for different local and boundary conditions to extract proper material parameters (Yun and Santamarina, 2007).

2. LITERATURE REVIEW

In the geotechnical laboratories, standard soils are used to investigate new models or to develop new procedures. During this tedious work, the researchers do not need to worry about other properties of soil such as specific gravity or maximum and minimum void ratios. The only concern about the experiments is the parameters that are wanted to be observed.

Calcareous sands have been a problem for geotechnical engineers since 1960's. Construction on an area of calcareous sand deposits is sometimes a challenging project because the behavior of calcareous sands is unpredictable time to time. This can be concluded as a catastrophe, where considerable amount of money is wasted and, moreover, great loss of human life can be a result.

Pellets can be new unique testing materials with wide variety of changeable properties. At the time of production of pellets, the properties, that are wanted to be kept same, can be kept same and the properties, that are wanted to be changed, can be changed.

In the following part, some geotechnical properties of standard sand will be given. The problem of the calcareous sands will be explained. Also the geotechnical information about that type of sand till today will be summarized. The idea of pelletization and pellets as geotechnical testing materials is going to be implemented.

2.1. Standard Sands

The constituent particles of soils are of varying sizes, broadly grouped as clay, silt, sand, gravel, etc. Each size fraction contributes different properties to the soil. Particles with a diameter larger than 75 μm are classified as coarse grained, or they are named as granular materials (Bowles, 1998).

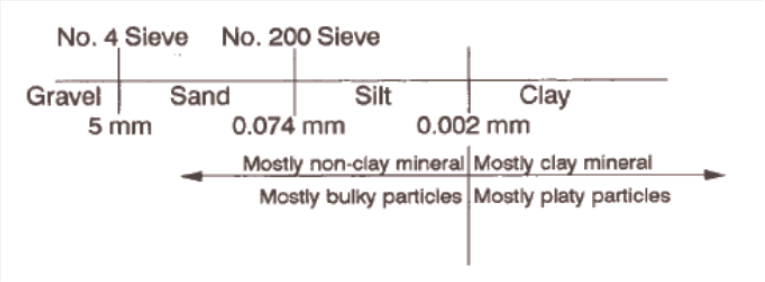

Figure 2.1. Particle size ranges in soils (Mitchell and Soga, 2005).

In all standard soil mechanics laboratory experiments the granular materials like sand and gravel are examined according to standards that are accepted by organizations regulating the standardization of soil mechanics experiments. For all laboratory experiments used in soil mechanics, the setup of the relevant experiments are needed to be calibrated, even if the setups are designed according to the standards and specifications. These calibrations are mostly made with the help of a standard sand of which the soil mechanics properties are known.

The American Society of Testing Materials (ASTM) has defined the stardard for the Standard Sand in the specification of Standard Specification for Standard Sand. Standard sand is silica sand, composed almost entirely of naturally rounded grains of nearly pure quartz, used for preparing mortars in the testing of hydraulic cements (ASTM C778-06).

There are two types of Standard Sand. First one is 20-30 sand, which is standard sand, predominantly graded to pass a 850-μm (No. 20) sieve and be retained on a 600-μm (No. 30) sieve. The second one is graded sand (well graded sand), which is standard sand, predominantly graded between the 600-μm (No. 30) sieve and the 150-μm (No. 100) sieve (ASTM C778-06).

Standard sands are also used in modeling of new procedures because of their known properties. Thus, most of the parameters, that must be examined before the modeling with the sand, are known and the valuable time for the laboratory work is decreased. This chapter presents an overview of the current work done with the help

of standard sands and a review of the soil mechanics parameters that are examined for the standard sands.

2.1.1. Ottawa Sand

Standard sands are mostly used in their territory where they are mostly available, as stated in the chapter before. The most known example for standard sands is Ottawa Sand. Ottawa is a city located in LaSalle County, Illinois, USA. Ottawa Sand has a relatively uniform size and shape for each grain. It is used for the manufacture of glass, for filter and molding sand, and for abrasives. Its purity is especially important to glassmakers. It is also important as a frac sand in oil and gas drilling - loose sand is pumped in a liquid mix under high pressure into an well where the sand grains wedge into and hold open any fractures in the rock, enhancing the extraction of hydrocarbons. The uniform particle size also makes the sand useful for laboratory experiments (Unklesbay and Vineyard, 1992).

Table 2.1. Internal friction angle, maximum and minimum void ratio values and coefficient of uniformity values of Ottawa Sand with different granulation (Rouse *et al.*, 2008).

Material Description	Ø: degrees	e_{max}	e_{min}	C_u	Roundness
Ottawa Sand 1	-	0.704	0.408	1.4	0.6
Ottawa Sand 2	-	0.772	0.407	1.4	0.42
Ottawa Sand 3	-	0.830	0.460	1.4	0.38
Ottawa 45	33.5	1.11	0.75	2.1	0.24
Ottawa 20/70	27.8	0.78	0.47	2.4	0.38
Ottawa 90	32.4	1.10	0.73	2.2	0.16
Ottawa 20/30	27	0.742	0.502	1.2	0.90
Ottawa F-110 Sand	31	0.848	0.535	1.7	0.70

As it is seen on the table, the values for some important geotechnical properties such as internal friction angle, maximum and minimum void ratio and coefficient of

uniformity varies greatly from one sample to another, even if the source of the sand is the same for all samples.

2.1.2. Toyoura Sand, Tongjiazhi Sand, Niigata Sand

Toyoura, Tongjiazhi and Niigata are different sand quarries of Japan. These sands are used for different applications like Ottawa sand. They are valuable with different granulation curves for modelling in geotechnical experiments.

Toyoura was a town located in Toyoura District, Yamaguchi, Japan. For the same applications, sand is supplied from this town to nearby industries. According to Yoshimi *et al.*, (1989), Toyoura sand has a D_{50} of 0.175 mm, uniformity coefficient of 1.52, maximum void ratio of 0.976 and minimum void ratio of 0.605 (Yoshimi *et al.*, 1989).

Like Toyoura sand, the origin of the name of Niigata sand is the city Niigata. Niigata is the capital and the most populous city of Niigata Prefecture, Japan. It lies on the northwest coast of Honsh$\bar{u}$, the largest island of Japan, and faces the Sea of Japan and Sado Island. Niigata sand has a D_{50} of 0.325 mm and the uniformity coefficient of 1.47 (Ishihara *et al.*, 2001).

According to Xia and Hu (1991), Tongjiazhi sand, which is one of the standard sands in Japan, has a D_{50} of 0.1 and the uniformity coefficient of 3.7. As mentioned before, those sands are used to model different granulation curves with different D_{50} values. Although it seems reasonable to use these different sands to model experiments for different granulation curves and D_{50} values, the results of the experiments may change because of the changing chemical composition with changing sand center (Xia and Hu, 1991).

Table 2.2. Maximum and minimum void ratio values and coefficient of uniformity values of Ottawa Sand with different granulation (Xia and Hu, 1991).

Material	D_{50}	C_u	e_{max}	e_{min}
Toyoura sand	0.175	1.52	0.976	0.605
Tongjiazhi sand	0.1	3.7	-	-
Niigata sand	0.325	1.47	-	-

2.1.3. Ham River Sand (HRS)

The Ham River Sand (HRS) was quarried originally from one of the Thames River terraces at Ham, a site near Richmond Surrey lying about 12 km southwest of Heathrow Airport and the Staines Reservoir. In the paper of Takahashi and Jardine (2007), it is mentioned that, batches of sharp HRS graded for use in building mortars were selected by Skempton and Bishop for use as standard research sands, and they have been used for this purpose at Imperial College London, and elsewhere, for almost 50 years. However, the operational life time of such quarries may be limited to just a few years in the Thames Valley and the Ham pit closed many years ago. A large database of HRS laboratory tests exists, making it vital to maintain continuity by locating a similar replacement. A substitute, termed the new Ham River Sand was located by Jardine (aided by Walker (1991)), from a pit south of Heathrow near Chertsey but this pit is also closed (Takashi and Jardine, 2007; Walker, 1991).

Although there are different values of Gs for HRS, they lie inbetween 2.70 and 2.66. Maximum void ratios are between 0.94 - 0.81 and minimum voids ratios are between 0.462 - 0.456 (Takashi and Jardine, 2007).

As it is mentioned above, to find and work for several years with a unique type of sand is very hard. Even if the quarries of the sand are very close to each other, they may differ in physical and geotechnical properties.

2.1.4. Leighton Buzzard Sand

Leighton Buzzard is a a town in Bedfordshire, England near the Chiltern Hills and lying between Luton and Milton Keynes. The town has a sizeable sand quarrying industry. Because of that the sand from this quarries are called Leighton Buzzard sand.

In their paper, Cabalar *et al.*, (2010) investigate the results of laboratory experiments and numerical simulations conducted to examine the behavior of mixtures composed of coarse (i.e. Leighton Buzzard Sand fraction B) and fine (i.e. Leighton Buzzard Sand fraction E) sand particles. The Leighton Buzzard Sand fraction B used in the experiments has a specific gravity, minimum and maximum dry densities of 2.65, 1.48 and 1.74 g/cm^3, respectively. More than 90% of the coarse sand particles, which are rounded and mainly quartz, are between 0.6 and 1.1mm. Leighton Buzzard Sand Fraction E is an uniform fine sand, with 85% by weight falling between 90 and 150 μm. Its minimum and maximum dry densities were found to be 1.33 and 1.62 g/cm^3, respectively. Its specific gravity was found to be 2.65 (Cabalar *et al.*, 2010).

According to the article of Brendan and Naughton, the Leighton Buzzard sand has the geotechnical properties stated in Table 2.3. In this article, Leighton Buzzard sand is used to study theplastic yield behavior of Leighton Buzzard sand under generalizedstress conditions by using a state-of-the-art hollow cylinder torsional apparatus (HCTA)developed at University College Dublin (UCD) (Brendan and Naughton, 2009).

Table 2.3. Physical properties of Leighton Buzzard sand.

Coefficient of uniformity, C_U	1.32
Coefficient of curvature, C_C	0.96
Effective grain size, D_{10}	0.44 mm
Specific gravity of solids	2.64
Maximum void ratio	0.80
Minimum void ratio	0.53

2.2. Calcareous Sands

Offshore costruction encountered calcareous sediments in the Arabian Gulf in the mid - 1960's and since then in many other world areas. Calcareous sediments cover approximately 40% of the ocean floor, according to (Holmes, 1978). Foundation surprises and diappointments have been recurrent because land - based design experience has proved inappropriate, especially for driven pile design. Depositional environments control the structure of carbonate sediments and also the mechanical behavior of the material. A variety of soft carbonate grains cemented with precipitated calcite from a porous structure that experiences diagenetic changes after deposition. The resultant soil structure responds to load in a brittle manner, tends to contract during shear, is very susceptible to cyclic strength degradation, is highly compressible under bearing pressures. Still remaining to be determined, in support of general design procedures for foundations on such materials, are: relevant parameters, means to quantify the parameters, and methods to apply them. For the present, design is largely emprical and dependent upon site - specific, full - scale field load tests (Holmes 1978, McClelland, 1988).

They are especially widespread in tropical and subtropical shallow waters of the Pacific Ocean where seismic hazards are oftenvery high. The potential for damages caused by strong shaking of calcareous sediments has been made painfully clear by numerous catastrophic earthquakes such as the Guam earthquake of 1993, the Hawaii earthquake of 2006, the Haiti earthquake of 2010 and many others. In each of these cases, calcareous sediments were observed to liquefy and spread, causing extensive damage to port facilities and other offshore structures. It is well known that calcareous sediments pose a challenge to offshore construction, particularly the installation of driven piles and their response to dynamic loads (McClelland, 1988).

The character of biogenic calcareous sands is quite different from that of quartz sands, yet our understanding of the dynamic behavior of granular soils comes primarily from studies conducted on quartz sands of terrigenous origin. Calcareous sands typically have lower grain hardness, larger intragranular porosity, a wider range of grain

shapes, more complex structural arrangements that reflect unique post-depositional processes of cementation, dissolution,recrystallization, and other diagenetic changes. It is not surprising then that there are significant differences in mechanical behavior among various types of calcareous sands, and with respect to quartz sands (Celestino and Mitchell 1983).

Field and laboratory investigations have highlighted differencesin terms of compressibility, volume changes and graincrushing during shearing, yielding, friction, and waterpermeation (Datta *et al.*, 1979, Semple 1988, Al-Douri and Poulos, 1991, Jewell 1993, Kwag *et al.*, 1999, Ong *et al.*, 1999, Coop and Airey, 2003). Although there have been a few studies that have addressed the dynamic behavior of calcareous sediments (Lo Presti *et al.*, 1993, Kwag *et al.*, 1999, Sharma and Fahey, 2003 a,b, Mao and Fahey, 2003, Seidman 2007, Porcino *et al.*, 2008), most of them have not sought todraw particular distinctions with the corresponding behavior of terrigenous soils (Datta *et al.*, 1979, Semple, 1988, Al-Douri and Poulos, 1991, Jewell, 1993, Kwag *et al.*, 1999, Ong *et al.*, 1999, Coop and Airey, 2003, Lo Presti *et al.*, 1993, Kwag *et al.*, 1999, Sharma and Fahey,2003a,b, Mao and Fahey, 2003, Seidman, 2007, Porcino *et al.*, 2008).

What evidence exists islimited and sometimes contradictory. Some laboratory studies indicate that the cyclic strength of loose calcareous sands is higher than that of quartz sands at equivalent densities and stress conditions (Chen, Morioka and Nicholson, Nicholson). Rollins *et al.*, suggest that liquefaction istriggered at different stress levels in reefoidal calcareous sand deposits compared to quartz sand deposits,again suggesting that cyclic strengths are different. On the other hand, Mejia and Yeung report similarliquefaction behavior for both classes of sands basedon observations of field liquefaction (Chen 1985; Morioka and Nicholson 2000; Nicholson 2006, Rollins *et al.*, 2004, Mejia and Yeung 1995).

In the following Figure 2.2 and Figure 2.3, Tampa Bay and Kawaihae Sand are compared. Tampa Bay Sand, which is chemically composed of mainly quartz, shows the general behaviour of sands that are in loose condition (Brandes, 2011).

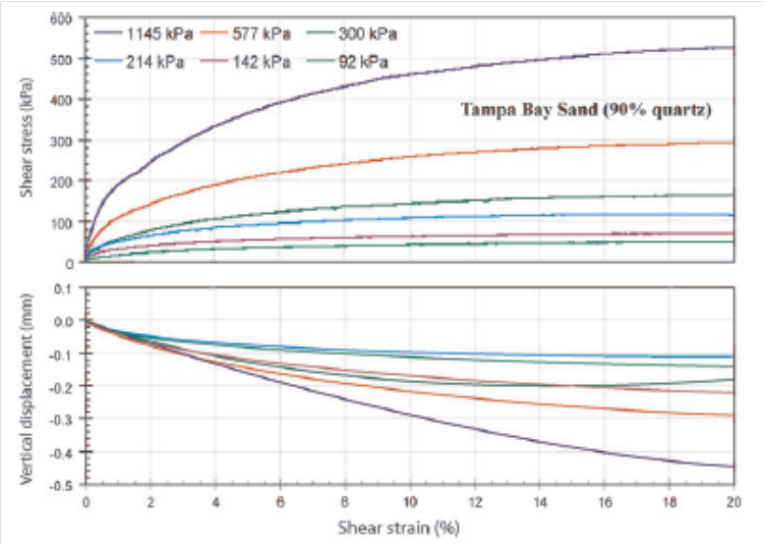

Figure 2.2. Tampa Bay Sand Direct Simple Shear drained strength test (Brandes, 2011).

In the Direct Simple Shear tests, Kawaihae Harbor Sand behaves significantly different than quartz sand. Even in the loose state, a dilation behavior can be seen and this behavior occurs at the large deformations (Brandes, 2011).

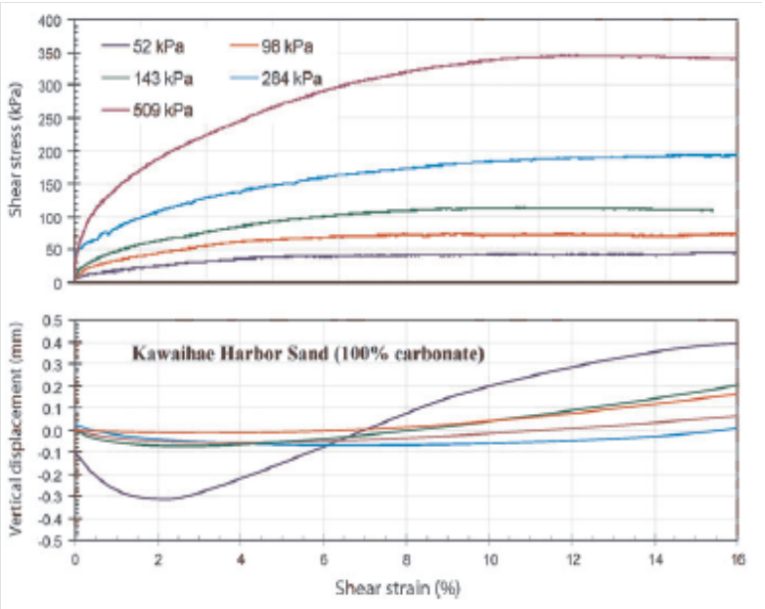

Figure 2.3. Kawaihae Sand Direct Simple Shear drained strength test (Brandes, 2011).

2.3. Fly Ash

To understand the theory of pelletization with fly ash or cement and the behavior of pellets produced from fly ash, the material fly ash is needed to be understood. According to the American Concrete Institute (ACI) Committee 116R, fly ash is defined as the finely divided residue that results from the combustion of ground or powdered coal and that is transported by flue gasses from the combustion zone to the particle removal system (ACI Committee 232, 2004).

Fly ash is a major byproduct of coal burning in thermal power plants. The disposal of such fly ash is creating a serious problem because of its storage space and cost involved in its storage. At the same time there is a lot of pollution of the environment due to the fineness of the fly ash. The effects for its utilization for many gainful purposes have been made since late sixties of this century by various research institutions and public enterprises. Some researchers have investigated methods to beneficiate high-carbon fly-ash into a marketable product. High percentage of fly ash is utilized in developed countries. The majority of the fly-ash produced every year is not being used; nearly 80% of the fly ash produced is still land filled (Danyıldız, 2007).

Fly ash consists of inorganic matter present in the coal that has been fused during coal combustion. This material is solidified while suspended in the exhaust gases and is collected from the exhaust gases by electrostatic precipitators. Fly ash is made up of fine, spherical particles with a diameter range of 0.074 to 0.005 mm. These hard and round particles are so small that in laboratory tests for fineness. Under a microscope, fly ash particles look like tiny ball bearings. A SEM of typical fly ash particles is given in Figure 2.2 (Danyıldız, 2007).

Silica is the primary compound in fly ash. Fly ash is a pozzolan. A pozzolan is primarily a siliceous or siliceous and aluminous material, in a finely divided form and in the presence of water, chemically reacts with calcium hydroxide at ordinary temperatures to form compounds possessing cementitious properties (Danyıldız, 2007).

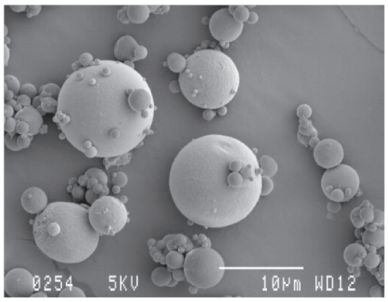

Figure 2.4. SEM of typical fly ash particles (Danyıldız, 2007).

Formation of cementitious material by the reaction of free lime (CaO) with the pozzolans (AlO3, SİO2, Fe2O3) in the presence of water is known as hydration. For class C fly ash, the calcium oxide (lime) of the fly ash can react with the siliceous and aluminous materials (pozzolans) of the fly ash itself. Since the lime content of class F fly ash is relatively low, addition of lime is necessary for hydration reaction with the pozzolans of the fly ash. For lime stabilization of soils, pozzolanic reactions depend on the siliceous and aluminous materials provided by the soil. The pozzolanic reactions are as follows:

- $Ca(OH)_2 \Rightarrow Ca^{++} + 2[OH]^-$
- $Ca^{++} + 2[OH]^- + SiO^2 \Rightarrow$ CSH (Silica gel)
- $Ca^{++}+ 2[OH]^- + Al^2O^3 \Rightarrow$ CAH (Alumina gel) (Danyıldız, 2007)

Hydration of tricalcium aluminate in the ash provides one of the primary cementitious products in many ashes. The rapid rate at which hydration of the tricalcium aluminate occurs results in the rapid set of these materials, and is the reason why delays in compaction result in lower strengths of the stabilized materials. The hydration chemistry of fly ash is very complex in nature. So the stabilization application must be based on the physical properties of the ash treated stabilized soil and cannot be predicted based on the chemical composition of the fly ash (Danyıldız, 2007).

Fly ash has been classified into two classes, F and C, based on the chemical composition of the fly ash. According to ASTM C 618, the chemical requirements to

classify any fly ash are shown in Table 2.4 (Danyıldız, 2007).

Table 2.4. Chemical requirements for fly ash classification.

Properties	Fly Ash Class	
	Class F	Class C
Silicon dioxide (SiO2) plus aluminum oxide (Al2O3) plus iron oxide (Fe2O3), min,%	70.0	50.0
Sulfur trioxide (SO3), max,%	5.0	5.0
Moisture Content, max,%	3.0	3.0
Loss on ignition, max,%	6.0*	6.0

Fly ash can be used in various developmental and construction activities. Some of the prominent uses of fly ash are given as under:

- For development of various value added products, fly ash based bricks, blocks, mosaic tiles, glazed floor, wall tiles, partition boards, concrete products, cellular light weight concrete blocks etc.
- For reclamation of waste land/filling of low lying areas, soil amendment.
- As mine fills in open cast mines and the underground mines can be stowed with ash.
- Production of cement.
- For use in concrete as lightweight aggregate.
- In construction of embankments, dykes, road sub-base and base course.
- In agriculture as a source of micronutrient for improvement of soil condition.
- Road-building applications (Danyıldız, 2007)

2.4. Pelletization Process

Artificial lightweight aggregates which consist primarily of fly ash, fine and/or coarse aggregates and a small amount of Portland cement are being used increasingly in the construction industry. Pelletization is a promising process for making artificial

aggregates from fine-grained materials like fly ash, which facilitates its high volume utilization as lightweight aggregate in concrete (Danyıldız, 2007).

2.4.1. Definition and Objectives of Pelletization

Anderson was the first to put the idea of pelletization process. Brackbelserg revised process with the addition of binder to the fines being pelletized and the pellets would be strengthened at elevated temperatures during production (Yukio *et al.*, 1999).

Two basic steps have to be performed to produce an aggregate from fly ash: bonding of the material in the pellets by firing, hydrothermal processing, and cold bonding which gives the pellets strength and other properties necessary to meet the criteria for a lightweight aggregate, and agglomeration of the fine fly ash particles to form aggregate size pellets (Bijen, 1986).

Agglomeration (also called pelletization) can be performed by two distinct methods. One is by agitation, where fly ash particles are introduced onto an inclined rotating disk along with a wetting agent and an appropriate binder. Balling of the material occurs by the formation of seeds which ultimately grow into pellets of a certain maximum size. The product obtained at the end of the process is termed as fresh pellet. The crushing strength of the fresh pellet must be adequate for hauling and stockpiling purposes (Döven, 1998).

The other method is the pressure or extrusion method where agglomeration is accomplished by using a continuous piston-type press where more or less rectangular or cylindrical pellets are formed. The extrusion process generally results in a product having a higher density than the spherical pellets produced by agitation (Bijen, 1986).

Regardless of which manufacturing process is used, pellets have to meet the following requirements (Vuppala *et al.*, 1997):

- They should be near spherical and have a smooth surface; both considered opti-

mum characteristics for subsequent film coating.

- The particle size range should be as narrow as possible. The optimum size of pellets for pharmaceutical use is considered to be between 600 and 1000 μm.
- The pellets should contain as much as possible of the active ingredient to keep the size of the final dosage form within reasonable limits.

The pellets may also be sintered during a specified interval of time after production depending on concerns like properties of the fines used in pelletization process, the purpose of use and the rate of increment in engineering performance of pellets. Besides that, several advantages of cold bonding process based on experiences to date show that:

- Cold bonded process plants tend to have lower capital costs than sintering/rotary kiln firing plants.
- Cold bonded processes tend to have lower operating costs than sintering/rotary kiln firing.
- Cold bonded process plants have less environmental impact than sintering/rotary kiln firing plants (no exhaust gases). Both processes require particulate emission controls and may have waste water streams.
- Finished material costs tend to be lower for cold bonded material than for sintered material (Danyıldız, 2007).

2.4.2. The Theory of Pelletization

Pelletization depends on the size of particles and their distribution, moisture content, along with the process related parameters. Only limited studies have been reported on the pelletization of fly ash aggregates. The previous studies showed that the performance of pelletization process is a function of;

(i) speed of revolution of pelletizer disc,
(ii) angle of pelletizer disc,
(iii) moisture content, and

(iv) duration of pelletization (Doven, 1998).

When a fine grained material is moisturized, there forms a thin liquid film on the surface of the grains, which forms meniscus between the grains (Figure 2.5). In case the particles are rotated in a balling drum or disc, then there forms ball shape structures with enhanced bonding forces between grains due centrifugal and gravitational forces (Figure 2.5) (Yukio *et al.*, 1999).

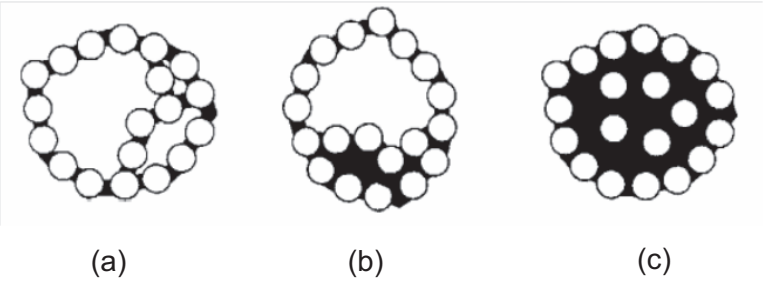

Figure 2.5. Mechanism of pellet formation.

As described in Figure 2.5 the initial bonding between particles is a meniscus formed due to water film, however it does not provide sufficient cohesion between particles to hold them together. As the amount of water increases, the particles begin to coalesce due to increased surface tension formed by increased liquid column. There are also voids in the structure formed (Yukio *et al.*, 1999).

The primary structure forms the nucleus of the pellet and the pellet gradually grows in size as more moisturized particles are coated on the nucleus. When these structures are rotated in the balling drum or disc, the pellets are compacted in denser state under the mechanical forces developed by the balls bumping against each other and against the walls of the balling device as well as centrifugal gravitational forces. At this stage of process, the forces developed on pellets expel the air that fills the free space between the individual particles, leaving the gaps to particles and water. As the particles get closer, the structure becomes denser, and the height of capillary rise increases, which improves the structure coherence and makes the fresh pellets have sufficient strength for handling and stockpiling conditions. As the particles get denser, the engineering performance of the fresh pellets is improved as well as their performance

for the rest of their service life (Yukio *et al.*, 1999).

The strength of the pellets depends on the pelletization process parameters, and finally the resultant magnitude of pressure being exerted on the pellets. Moreover, the capillary forces (surface tension generated by the height of liquid column) play a greater role in the magnitude of the coherence of the pellets. The coherence of the structure is directly proportional to the mechanical and capillary forces exerted on the pellets. In this respect, the capillary force theory was developed by Sastry (Sastry, 1995);

$$h = \frac{2^{*}\sigma,^{*} cos\delta_c}{r^{*}\rho^{*}g}(cm) \tag{2.1}$$

where h is the height of the liquid column (cm), σ_s is the surface tension of the liquid (N cm-1), δ_c is the angle of contact between the liquid and the solid phase (^{o}), r is the density of the liquid (g/cm^{-3}), ρ is the radius of capillary (cm), g is the acceleration of gravity (cm s^{-2}) (Sastry, 1995).

As defined in the formula above, the cohesiveness of the structure and, consequently, the strength of the pellet are directly proportional to the capillary rise and inversely proportional to the radius of capillaries. The minimization of void ratio of the final product and the radius of capillary during pelletization process may be provided by a wider range of granulometric distribution as well as process efficiency (Danyıldız, 2007).

If the liquid used in the pelletization process is assumed to be water and assumedthat all fines are uniformly wetted with water, then;

$$\delta_c = 0, cos\delta_c = 1, \rho = 1gr/cm^3(20^oC) \tag{2.2}$$

$$k_c = \frac{2^*\sigma,^* cos\delta_c}{\rho^* g} \tag{2.3}$$

The capillary constant k_c an be defined as in the formula above. When the values in Equation 2.2 are substituted in Equation 2.3, then the equation simplifies into;

$$k_c = 0.15 \tag{2.4}$$

and

$$h = 0.15/r \tag{2.5}$$

The radius of capillary (r) that takes place in equations is found by the help of the specific surface area and the specific gravity of the material. Then the height of the liquid column, h is found by substituting the value of radius of capillary, r, in Equation 2.5 (Sastry, 1995).

The experimental studies showed that the strength of fresh pellets is directly proportional to the height of liquid column found out by the help of above equations. At this stage, it is obvious that the maximum strength (the strength of fresh pellets and, consequently, the strength of cured pellets) may only be reached if all the capillaries are filled with water during production. The lack of sufficient water causes air voids to be entrapped inside the structure, which restricts the capillary action. On the other hand, excessive water causes a water film on the surface of the ball, which destroys the capillary forces resulting in particle cohesiveness limited to the magnitude of the surface

tension water. Sastry, 1995 defined pelletization process in three steps depending on the degree to which the inter-granular spaces are filled with water (Sastry, 1995).

According to Sastry, 1995, the pelletization process may be analyzed in three steps depending on the degree to which the intergranular spaces are filled with water:

- The pendular state: The water is present at only the point of contacts of grains.
- The funicular state: In this state, in addition to the conditions present in pendular state, some of the pores are completely filled with water.
- The capillary state: In this state, all inter-granular spaces are completely filled with water and no water film exits on the surface of the pellet (Sastry, 1995).

The force being exerted on the particles can be expressed in terms of equation below;

$$P = \frac{2\pi d\sigma_s}{tan\beta/2} \tag{2.6}$$

where P is the pressure at the point of contact, σ_s is the surface tension of the liquid, β is the central angle of the meniscus and d is the diameter of the spherical particle.

There are two factors determining the strength of the fresh pellet:

- The magnitude of cohesive force acting on the particles during the process,
- The interlocking effects (Sastry, 1995).

The strength of the fresh pellet is equivalent to the superposition of the strength gained by these two factors. The magnitude of the cohesive force is determined by the void ratio of the structure, whereas the strength gained due to interlocking effect is a

function on the surface texture of the fresh particles. However, for the ideal condition of fully rounded particles, the strength of the fresh pellet may be assumed to be equal to the cohesive force that is formed during process (Sastry, 1995).

Yukio *et al.*, (1999) introduced the following assumptions and simplifications, formulized the capillary and cohesive forces being exerted on the particles;

- all particles are spherical and have uniform diameters;
- the bonding pattern is uniform throughout the ball section;
- the particles in the ball are evenly distributed;
- effective bonding forces fluctuate around the average value(Yukio et al., 1999).

Then, according to the above assumptions, following equation may be derived for cohesive forces in the capillary state;

$$P_c = 8\frac{(1-\varepsilon)\sigma_s}{\varepsilon d} \tag{2.7}$$

where σ is the surface tension of the liquid, P_c is the cohesive force exerted on the structure in capillary state, ε is the ball porosity and d is the diameter of the spherical particle (Sastry, 1995).

Schematic views for ball formation are given in Figure 2.6 and Figure 2.7. In Figure 2.6 the mechanism of ball formation is sketched for the moisture content less than the optimum state. In this state, the moisturized particles move closer, become connected with water bridges. As more particles join the structure, the formation tightens under mechanical forces. The degree of saturation increases by decreasing volume of voids, since the air is expelled leaving the pore spaces to particles and water. In this state, if the structure is fed with additional moisture, then the capillary bonding occurs (Arslan, 2003).

Figure 2.6. Mechanism of ball nuclei formation (water content below optimum state) (Yukio *et al.*, 1999).

When the water content is above optimum state as in Figure 2.5, the particles are wetted excessively to form the nucleus by means of the surface tension of water. The formation is weaker than capillary force diminished. The formations are also random sized, and they may easily degrade upon mechanical forces created in balling drum disc. This methodology has disadvantages, since the granulometric distribution of pellets cannot be controlled during pelletization process (Arslan, 2003).

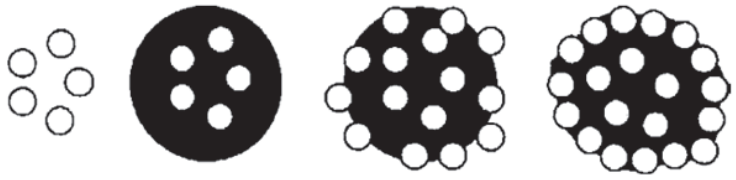

Figure 2.7. Mechanism of ball nuclei formation (water content above optimum state) (Yukio *et al.*, 1999).

The variations of movements of pellets in the pelletization disc with respect to the revolution speed are given in Figure 2.8. As described in figure as well, for low revolution speed the movement of pellets is governed by gravitational force, and for high speeds the movement is governed by centrifugal force. If one of these forces becomes dominant on the movement, then either pellet formation is ceased or the pellets formed have loose structure. Especially if the dominant force is centrifugal force, the pellet formation is almost ceased since all the particles will stick to the sidewall of the disc by means of adherence created by moisture (Baykal and Doven, 2000).

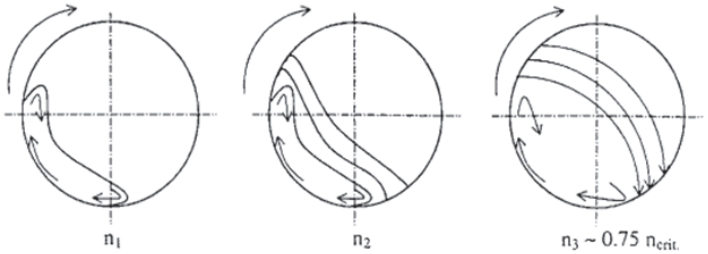

Figure 2.8. Motion of material in disc pelletizer revolving at various speeds (Yukio *et al.*, 1999).

The optimization studies of Baykal and Döven showed that the critical revolutions per minute is (Baykal and Döven, 2000);

$$n = \frac{43.2}{\sqrt{D}}\sqrt{sin\alpha_i} \tag{2.8}$$

where n is the critical revolutions per minute (rpm), D is the disc diameter (m), α_i is the angle of disc inclination in degrees.

2.4.3. Factors Affecting the Pelletized Product Quality

The amount of water used in pellet production is of extreme importance since the formation and structure of pellet is dependant on moisture content regardless of other mechanical factors of the process. The effect of moisture content on pellet formation, diameter and structure are described in Figure 2.9 (Döven, 1998).

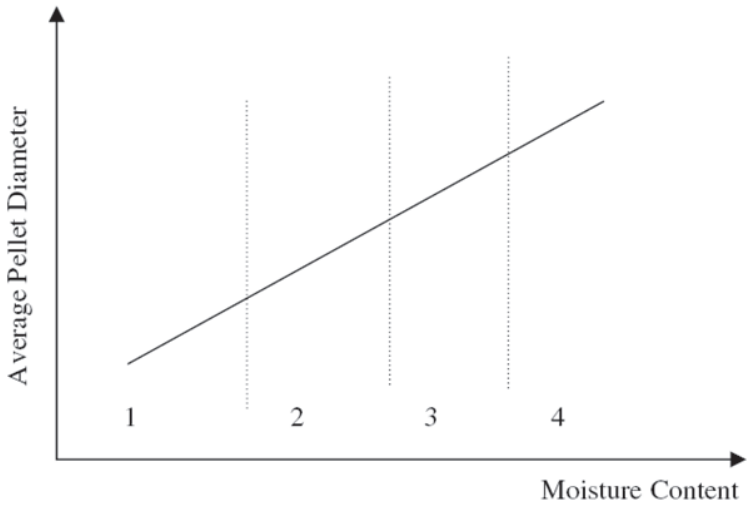

Figure 2.9. The effect of moisture content on pellet formation, diameter, and structure (Yukio *et al.*, 2000).

The moisture content used for pelletization process affects the residence of time of pellets in the pan and the rate of production besides the size of pellets. The general relationship is shown in Figure 2.10. The diagonal lines represent the moisture content (f_i) increasing from lower right to upper left.

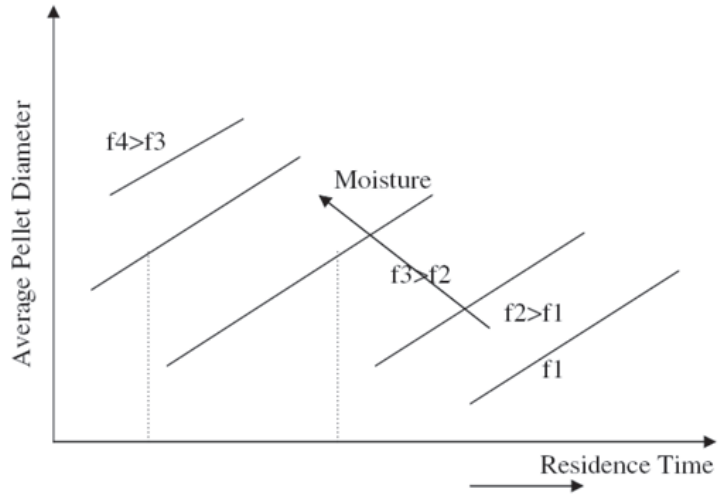

Figure 2.10. The effect of moisture on the duration time of fresh pellet (Yukio *et al.*, 1999).

2.5. Pellets

Firstly, the paper Utilization of fly ash as engineering pellet aggregates written by Arslan and Baykal gives the idea of pelletization process and the experiments that can be done in order to specify the properties of the produced pellets (Arslan and Baykal, 2006).

By making use of the idea presented in this paper, artificially produced pellets for laboratory uses are investigated in this dissertation. The data found after the experiments in previous dissertations are given in this section as reference data.

Table 2.5. Pellets produced of fly ash and different cement ratios by weight (Arslan, 2003).

The name of manufactured granular materials	FA (only Fly ash)	FC10 (Fly ash with 10% cement)	FC20 (Fly ash with 20% cement)	FC30 (Fly ash with 30% cement)
Internal friction angle(^{o})	29.8	34.9	40	42.5

In the table above, the data from the dissertation of Arslan is presented. After pelletization of fly ash, fly ash with 10% cement, fly ash with 20% cement and fly ash with 30% cement, the sand sized particles are sheared in direct shear equipment and the internal friction angles are given, as it can be seen in table. Not a big crushing effect, not a big change in sieve analysis results are seen after shearing in direct shear test equipment at normal stresses of 50 and 100 kPa. Some crushing behaviour are seen at normal stress of 200 kPa (Arslan, 2003).

In the further review of literature, it is seen that there are also academic researches with larger particle diameter. In the dissertation of Döven (1998), pellets with only fly ash, with fly ash and 8% cement by weight, with fly ash and 8% lime by weight are produced. The particle diameters are varying between 22.6 mm and 2 mm. Specific gravity, water absorption, crushing strength, maximum and minimum index density,

California Bearing Ratio and shear strength results are givin in the tables below (Döven, 1998).

Table 2.6. Specific gravity and water absorption test results of groups with respect to grain sizes (Döven, 1998).

Group	Sieve Size (mm)	Apparent G_s	G_s (SSD)	Bulk G_s	Water Absorption (%)
FA	22.6+	2.00	1.60	1.19	33.85
	16 - 22.6	2.02	1.62	1.22	32.38
	8 - 16	2.09	1.66	1.26	31.84
	4 - 8	2.11	1.66	1.26	31.77
	2 - 4	2.17	1.70	1.29	31.38
FC8	22.6+	2.17	1.71	1.33	29.31
	16 - 22.6	2.03	1.65	1.28	28.65
	8 - 16	2.09	1.68	1.31	28.66
	4 - 8	2.18	1.72	1.34	28.83
	2 - 4	2.35	1.81	1.40	28.77
FL8	16 - 22.6	2.10	1.66	1.26	31.61
	8 - 16	2.08	1.65	1.25	31.73
	4 - 8	2.11	1.67	1.27	31.53
	2 - 4	2.28	1.75	1.33	31.42

The apperent specific gravity, saturated - surface dry specific gravity, bulk specific gravity and water absorption values are given for different sieve size ranges. The sizes of the granular material can be describe as coarse to fine gravel. The materials are selected as uniform graded, so that the changing properties of material with changing sizes can be discussed (Döven, 1998).

Table 2.7. Specific gravity and water absorption test results of groups with respect to grain sizes (Döven, 1998).

	Curing Period	7 Days	14 Days	28 Days
Group	Sieve Size (mm)	Crushing Strength (N)	Crushing Strength (N)	Crushing Strength (N)
FA	19	173.6	197.2	211.9
	16	147.2	160.9	170.7
	12.5	93.2	120.7	141.3
	10	71.6	74.6	85.3
	8	45.1	51.0	51.0
	6.3	29.4	35.3	38.3
	4.75	17.7	21.6	23.5
FC8	19	387.5	585.7	660.2
	16	353.2	516.0	570.0
	12.5	247.2	306.1	366.9
	10	155.0	193.3	246.2
	8	108.9	142.2	151.1
	6.3	84.4	93.2	105.9
	4.75	52.0	71.6	74.6
FL8	19	299.2	540.5	740.7
	16	253.1	411.0	687.7
	12.5	145.2	290.4	476.8
	10	113.8	187.4	312.0
	8	65.7	120.7	215.8
	6.3	33.4	79.5	141.3
	4.75	20.6	51	91.2

The crushing strength tests are conducted with uniformly graded samples. The

sizes of the materials are given in the table. Materials with different curing period and sizes are compared (Döven, 1998).

Table 2.8. The maximum and minimum index density test results (Döven, 1998).

Group	γmin (kN/^3)	γmax (kN/^3)	Relative Density, Dd (%)	Relative Compaction, Rc (%)	Density Index Id (%)
FA	7.7	12.7	50.2	75.6	38.0
FC8	8.4	13.6	585.7	76.5	38.5
FL8	8.0	13.1	540.5	75.6	37.3

The maximum and minimum index densities are given as the mean of the groups, namely FA, FC8 and FL8 in the Table 2.7 (Döven, 1998).

Table 2.9. The optimum water content, dry unit weight and CBR values of groups with respect to grain size distribution used in the performance tests (Döven, 1998).

Group	Optimum Water Content (%)	Dry Unit Weight (kN/^3)	CBR (%)
FA	34.4	12.0	58
FC8	34.0	12.6	82
FL8	34.5	12.2	82

The optimum water content, dry unit weight and CBR values are given as the mean of the groups, namely FA, FC8 and FL8 in Table 2.8, similar to Table 2.7 (Döven, 1998).

Table 2.10. The shear strength parameters of the groups- angle of internal friction angle (Döven, 1998).

Angle of Internal Friction (degrees)		
Group	Ultimate	Residual
FA	29.4	22.4
FC8	45.4	37.7
FL8	44.4	38.0

Similiarly in table of the maximum and minimum index densities, the angle of internal friction angles, both ultimate and residual, are given as the mean of the groups, namely FA, FC8 and FL8 in the Table 2.9 (Döven, 1998).

3. METHODOLOGY

3.1. Materials and Preparation of Samples

In the experiments mentioned in this thesis, four types of materials are used. Fly ash and cement are two materials that are pelletized and used in the experiments to research the performance of these artificially produced pellets in comparison with natural sand samples like Sakarya sand and crushed sand.

Portland cement 42.5 and type C fly ash are materials used in this study. The physical properties of cement and fly such as specific gravity, specific surface fineness (Blaine fineness) obtained from laboratory tests are given in Table 3.1 (Danyıldız, 2007).

Table 3.1. Specific gravity and surface fineness of cement and fly ash (Danyıldız, 2007).

	Cement	Fly Ash
	PC 42.5	Type C
Specific Gravity (gr/cm^3)	3.18	2.35
Blaine Fineness (cm^2/gr)	3600	3490

The average grain size of fly ash and cement was 22.91 μm, 19.95 μm respectively. The grain size distribution of fly ash and cement are presented in Figure 3.1 (Danyıldız, 2007).

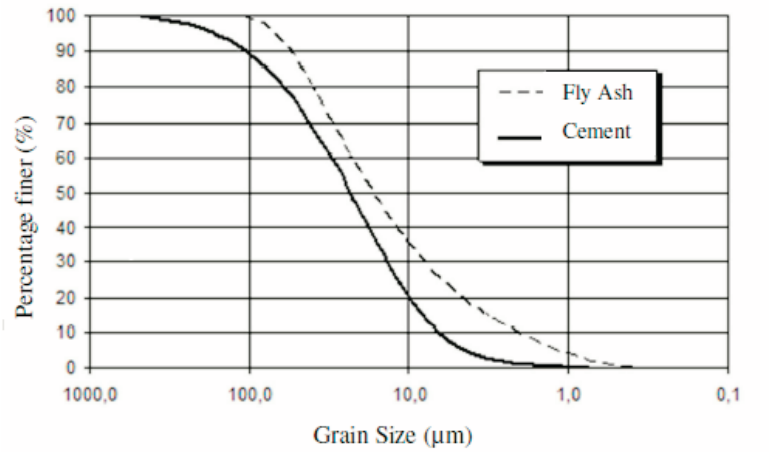

Figure 3.1. Grain size distribution of fly ash and cement (Danyıldız, 2007).

The geotechnical experiments conducted in this thesis are specific gravity, water absorption, roundness and sphericity, constrained modulus, direct shear and triaxial tests. Before and after constrained modulus and direct shear tests, the sieve analyses of the specimens are conducted.

3.1.1. Fly Ash

Coal is one of the major sources of energy and its consumption is about 31.9% in thermal plants in Turkey. This is predicted to increase in the future in order to meet the continuous demand for electric power generation (Danyıldız, 2007).

Although the mineralogical properties of fly ash obtained from different power plants maybe somehow similar, the physical and chemical properties may vary depending on the operational conditions. The chemical analyses of fly ashes from various power plants in Turkey are given in Table 3.2 (Danyıldız, 2007).

Table 3.2. Chemical analysis tests results of samples obtained from various thermal plants in Turkey (Doven, 1998).

ASTM	Soma	Yeniköy	Kangal	Afşin	Tunçbilek
Classification	Type C	-	Type C	Type C	Type C
SiO_2 (%)	49.00	17.54	38.67	30.78	53.00
Al_2O_3 (%)	24.22	9.94	16.63	10.41	19.63
Fe_2O_3 (%)	7.78	0.37	6.41	10.81	10.74
CaO (%)	11.60	33.10	23.63	32.59	12.02
MgO (%)	0.49	2.46	3.90	4.06	2.04
SO_3 (%)	4.35	33.75	6.00	12.23	0.57
Loss on Ignition (%)	2.08	0.45	2.54	0.27	1.15

The fly ash used in this study is obtained from Soma Thermal Plant located 2 km out of Soma, Manisa. The plant is made of eight units 1034 MW energy capacity, consumes low-quality lignite reserves of SomaBasin. At the Soma thermal power plant, approximately 30000 tons of coal is burnt and approximately 12000 tons of fly ash is produced per day. The chemical analyses on fly ash used in this study are given in Table 3.3 (Danyıldız, 2007).

Table 3.3. Chemical analysis tests results of fly ash used in this study (Danyıldız, 2007).

	FlyAsh
InsolubleResidue (%)	—
SiO_2 (%)	43.42
Al_2O_3 (%)	19.66
Fe_2O_3 (%)	5.60
CaO (%)	23.66
MgO (%)	1.32
SO_3 (%)	3.60
Cl^-	0.0007
Na_2O	0.54
K_2O	1.33
Loss on Ignition (%)	0.13

3.1.2. Cement

The Portland cement used in this study was provided from Akçansa B. Çekmece cement plant which supplies 8% of Turkey's cement requirement with its products that comply with global quality standards. Cements produced by the plant and their properties are shown in Table 3.4. The physical and chemical properties of fly ash used in this study were obtained in Akçansa cement factory laboratories in Büyükçekmece, Istanbul. The chemical analyses on cement used in this study are given in Table 3.4(Danyıldız, 2007).

Table 3.4. Cements produced by Akçansa B. Çekmece plant and their properties (Danyıldız, 2007).

Akçansa B. Çekmece cement plant			Strength (N/mm^2)		Strength (h)		Blanine Specific Surface Area cm^2/g
			7 days	28 days	Initial Set	Final Set	
PC 42,5	Portland Cement	TS EN 197-1 Standard	40	51	02:28	03:08	3550
PCC 32,5	Portland Composite Cement	TS EN 197-1 Standard	23	36	02:50	03:15	4200
SRC 32,5	Sulphate Res. Cement	TS 10157 Standard	35	47	02:40	03:17	3075

Table 3.5. Chemical analysis tests results of cement used in this study.

Insoluble Residue	Cement
(%)	0.47
SiO_2 (%)	21.08
Al_2O_3 (%)	4.77
Fe_2O_3 (%)	3.23
CaO (%)	63.61
MgO (%)	1.15
SO_3 (%)	2.49
Cl^-	0.0251
Na_2O	0.20
K_2O	0.94
Loss on Ignition (%)	1.78

3.1.3. Pelletization

The details of the pelletization disc are given in Figure 3.2 and Figure 3.3. The pelletization disc is a combination of five main units; a pelletizing disc with a diameter of 40 cm, a motor reduction unit, a divisor table with 1/30 degree sensitivity to adjust the normal of disc, a carrying frame and a speed controller unit which is capable of changing revolution speed of the disc between 0 and 7 with 0.15 rpm sensitivity (Arslan,

2003).

Scraping blades are placed from centre to one edge of the disc with 6 cm intervals. (Figure 3.3) The properties of the blades are:

- to remove any mix that sticks to the bottom and walls of the disc,
- to create an energy barrier before either free or radial rotating balled material to compact them more and
- to let different grain size of balled material move in different path for ease in screening the grain size distribution (coarse size material in interior path, and fine size in outer path) (Döven, 1998).

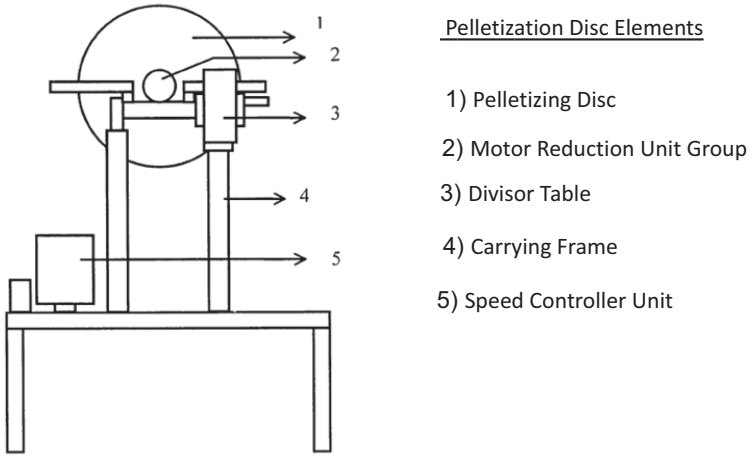

Figure 3.2. Sketch of pelletization disc unit (back view) (Döven, 1998).

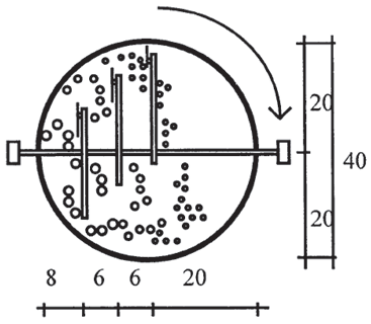

Figure 3.3. Sketch of scraping blades positioning (plan view / units in cm) (Döven, 1998).

Trial pellet production was done by observing of pellet formation stages, the shape and apparent strength of pellets with changing the angle and the revolution speed of the pelletizing disc. During the optimization, firstly, the angle and revolution speed parameters were tried to be determined for the desired pelletization process. A simple method was used for the determination of apparent strength of fresh pellets to investigate if they have adequate strength for hauling and stockpiling conditions in which the pellets are let to fall from a 115 cm height (Danyıldız, 2007).

The result of optimization study was in accordance with Döven (1998). The execution of theoretical equations with defined parameters and observations on fresh pellet formation and strength showed that operation angle should change between 35 and 50^o and revolution speed between 35 and 55 rpm (Döven,1998).

It is found that 45 rpm and anoperation angle of 45^o are adequate for pellet formation both for fly ash and cement. During the production process of pellets, it is observed that the water droplets are smaller with a tight nozzle of water spray and it causes production of pellets with smaller diameter.

The formation of pellets occurred between 6 and 9 minutes. The total pelletization time was about 20 minutes, since it was found that under the mechanical and capillary forces, the saturation point in volume compression was reached around this time. Avoiding water film on the surface of the pellets was of extreme care during production. The pellets were kept in plastic bags in the curing room in which the temperature and relative humidity were 21^oC and 70% respectively.Cement or fly ash was mixed with water in pelletization disc and the samples were put in curing room, in order to get the needed strength before they were used in experiments(Döven, 1998).

3.1.4. Sakarya Sand

Sakarya sand is an alluvial sand that is transported by Sakarya River from weathered rocks till the shore of Black Sea. During the transportation process the weathered sand loses it edges and gets a more rounded and spherical shape.

The grains are the closed in comparison with other types of sand that can be found in the market if the roundness and sphericity is the concern. The grains are looking spherical and round with a quick eye inspection with the help of a optical microscope. In the picture below, a photo of the Sakarya sand can be seen.

Figure 3.4. Sakarya Sand.

3.1.5. Crushed Sand

Crushed sand is produced when the big pieces of rocks are crushed in order to produce gravels or crushed sand can be made when the sizes of gravel produced from rocks are wanted to be decreased. Crushed sand is the distant one if the natural sand samples are arranged according to their similarity to pellets. This type of sand is chosen for the experiments conducted in this thesis in order to determine the upper limit of marginality in the test results.

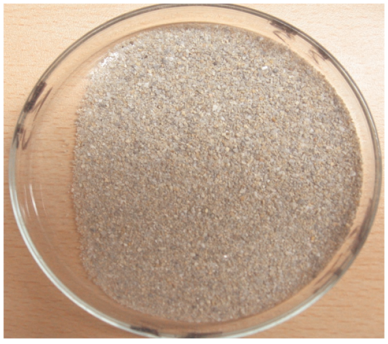

Figure 3.5. Crushed Sand.

3.2. Experimental Setups and Procedure

3.2.1. Specific Gravity and Water Absorption

The specific gravity of soil solids is used in calculating the phase relationship parameters for soils, such as void ratio and degree of saturation.For all groups of pellets (fly ash and cement), bulk specific gravity, saturated surface dry specific gravity, apparent specific gravity, and water absorption values were obtained with respect to ASTM C127-04.

Bulk specific gravity (SSD) is used if the aggregate is wet, that is, if its absorption has been satisfied. Conversely, bulk specific gravity (OD) is used for computations when the aggregate is dry or assumed to be dry.Apparent specific gravity pertain to the solid material making up the constituent particles not including the pore space within the particles which is accessible to water (ASTM C127-04).

500 mL Labware pycnometers are used in the test. According to ASTM C127-04 recommended mass for test specimen when using 500 mL pycnometer is given as 100±10 g. 100 g of sand is used for the test. The lab temperature was 20^oC, therefore no correction is made for temperature.

The equipment for determination of specific gravity includes (Bowles, 1998):

- Volumetric flasks (250 or 500 mL) with stoppers numbered and calibrated. (Figure 3.8)
- Vacuum pump.
- Balance accurate to 0.01 g.
- Distilled deaired water.
- Thermometer, ranging from 0 to 50^oC accurate to 0.5^oC.
- Drying oven.
- Evaporating dish.

Figure 3.6. Specific Gravity Experiment Setup.

Water absorption values are used to calculate the change in the mass of an aggregate due to water absorbed in the pore spaces within the constituent particles, compared to the dry condition, when it is deemed that the aggregate has been in contact with water long enough to satisfy most of the absorption potential. The definitions of the terms are given below;

Table 3.6. Chemical analysis tests results of cement used in this study.

IBulk Specific Gravity (Oven Dry, OD)	A / (B-C)
Bulk Specific Gravity (Saturated Surface Dry, SSD)	B / (B-C)
Apparent Specific Gravity (Apparent Relative Density)	A / (A-C)
Water Absorption (%)	((B-A) / A) x 100

where A is the weight of the oven-dry specimen in air, gr, B is the weight of saturated surface dry specimen in air, gr, C is the weight of saturated specimen in water, gr (ASTM C127-04).

3.2.2. Law of Large Numbers

To understand the logic of repetition of the experiments and accepted that number of repetition as enough in order to make a comment on them, the probability theorem of law of large numbers must be understood. According to the probability theorem of law of large numbers, the average of a sample approaches the mean of the population as the sample size increases. The number of grains that are examined is selected as 30 according to law of large numbers, therefore a brief description of the theory is given here, taken from Moore and Mc Cabe (Moore and Mc Cabe, 2003).

If X is a discrete random variable taking values $x_1, x_2, ..., x_k$ with probabilities $p_1, p_2, ...p_k$ the mean and variance can be computed from its distribution as follows (Eşidir, 2010):

$$\mu_x = x_1 p_1 + x_2 p_2 + ... + x_k p_k \tag{3.1}$$

$$\sigma_x^2 = (x_1 - \mu_x)^2 p_1 + (x_2 - \mu_x)^2 p_2 + ... + (x_k - \mu_x)^2 p_k \tag{3.2}$$

The mean and variance of a continuous random variable can be computed from the density curve, but to do so require more advanced mathematics (Eşidir, 2010)

The mean of a random variable is by definition the average outcome of the random variable as computed from the distribution. It is a striking fact that the mean of a random variable is also the average outcome in a different sense. If it is actually observed a large number outcomes of a random variable and calculated their mean (arithmetic average), this random mean will be close to the fixed mean of the distribution (Esidir,

2010).

Suppose that four coins are tossed repeatedly and the number X of heads obtained in each trial is recorded. A computer is used to toss four coins 1000 times and to record the number of heads among the four coins on each trial. Then it is found that the relative frequency of the outcome exactly two heads after each trial. The result of the few trials were (Eşidir, 2010):

Table 3.7. The result of first 6 trials of the toss of four coins.

Trial	Outcome	Relative frequency of exactly 2 heads
1	3 heads	$\frac{0}{1} = 0$
2	0 heads	$\frac{0}{2} = 0$
3	0 heads	$\frac{0}{3} = 0$
4	2 heads	$\frac{1}{4} = .25$
5	4 heads	$\frac{1}{5} = .20$
6	2 heads	$\frac{2}{6} = .33$

The first toss gave $X = 3$, the second toss $X = 0$, then another 0, then 2, 4, 2, and so on. The relative frequency of each outcome in many repetitions will be close to its probability as Figure 3.6 illustrates for the outcome $X = 2$ (Eşidir, 2010).

The probabilities of all possible outcomes make up the probability distribution of discrete random variable X. What happens to the average number of heads observed? The numbers of heads obtained on each of the first n trials form n observations. The average number of heads in the first n trials is the familiar mean $\bar{x}$ of these observations. The mean $\bar{x}$ is a random variable that takes different values if the tosses are repeated. Here are the values of observations and the mean $\bar{x}$ of all observations to date after each of the first few trials (Eşidir, 2010).

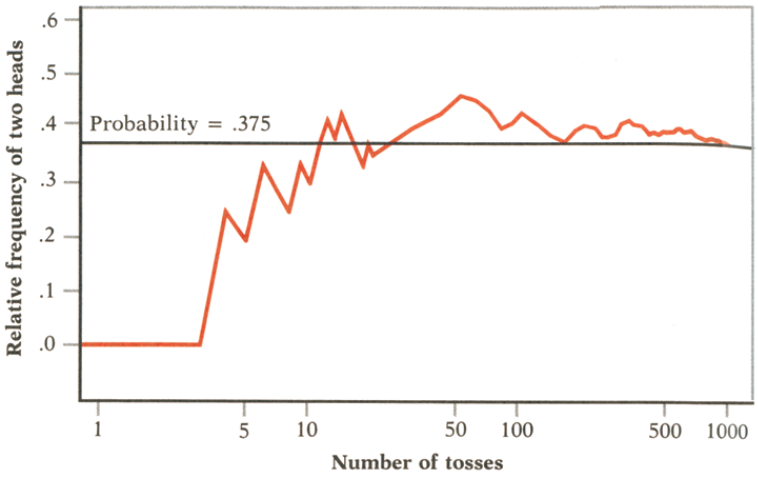

Figure 3.7. The long term behavior of the relative frequency of two heads in many tosses of four coins. The relative frequency approaches the probability 0.375 (Eşidir, 2010).

Figure 3.7 shows the behavior of $\bar{x}$ as the number of trials n increases. At first the value of $\bar{x}$ is unstable, but in the long run observed mean $\bar{x}$ approaches and remains close to the distribution mean $\mu_x = 2$. After 100 trials $\bar{x} = 1.86$; at the end of our series of 1000 tosses of four coins $\bar{x} = 2.012$. If the work is repeated, a different sequence of outcomes would be obtained and the graph of the progress of $\bar{x}$ would differ from Figure 3.7. But $\bar{x}$ will always approach $\mu_x = 2$ ever more closely as the number of trial grows (Eşidir, 2010).

Starting from the basic laws o probability, it can actually be proved that the sample mean outcome calculated from repeated independent observations of a random variable must approach the mean of the distribution. It should be noticed, though, that the behavior of $\bar{x}$ is similar to intuitive idea of probability - in long run, relative frequencies of outcomes get close to the probability distribution, and the average outcome gets close to the distribution mean. These facts, especially when they are considered as mathematical results that can be derived from basic laws of probability, are called the law of large numbers. An essential requirement for the law of large numbers to apply is that the successive trials of the random phenomenon be independent (Eşidir, 2010).

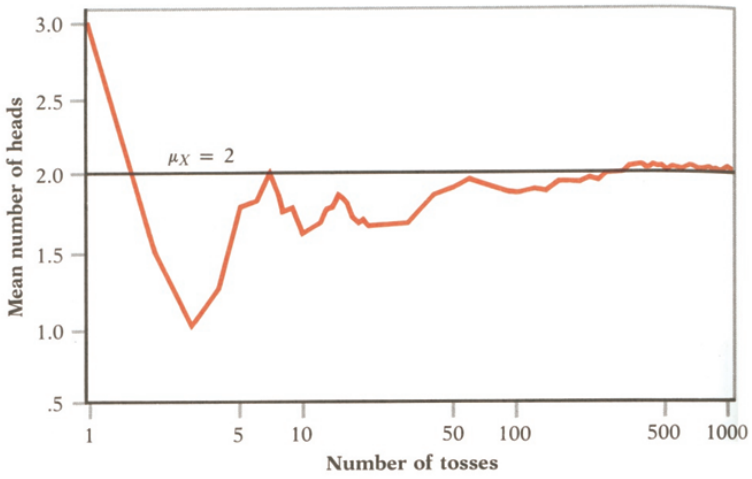

Figure 3.8. The long term behavior of the mean outcome of many trials. The mean number of heads $\bar{x}$ observed when four coins are tossed many times approaches the mean $\mu_x = 2$ of the probability distribution (Eşidir, 2010).

Table 3.8. The mean $\bar{x}$ of all observations to date after each of the first few trials (Eşidir, 2010).

Trial	Outcome	Average number of heads per trial
1	3	$\bar{x} = \frac{3}{1} = 3.00$
2	0	$\bar{x} = \frac{3}{2} = 1.50$
3	0	$\bar{x} = \frac{3}{3} = 1.00$
4	2	$\bar{x} = \frac{5}{4} = 1.25$
5	4	$\bar{x} = \frac{9}{5} = 1.80$
6	2	$\bar{x} = \frac{11}{6} = 1.83$

3.2.3. Roundness and Sphericity

There are three important scales in particle shape. Definitions and their conventional evaluation in the form of dimensionless parameters follow (Figure 4.1) (Wadell 1932; Krumbein 1941; Powers 1953; Krumbein and Sloss 1963; Barrett 1980):

(i) Sphericity S(eccentricity or platiness) refers to the global form of the particle and reflects the similarity between the particle's length, height, and width. Sphericity

can be quantified as the diameter of the largest inscribed sphere relative to the diameter of the smallest circumscribed sphere.

(ii) Roundness R (angularity) describes the scale of major surface features which are typically one order of magnitude smaller than the particle size. Roundness is quantified as the average radius of curvature of surface features relative to the radius of the maximum sphere that can be inscribed in the particle.

(iii) Smoothness (roughness). Roughness describes the particle surface texture relative to the radius of particle. (Cho *et al.*, 2006)

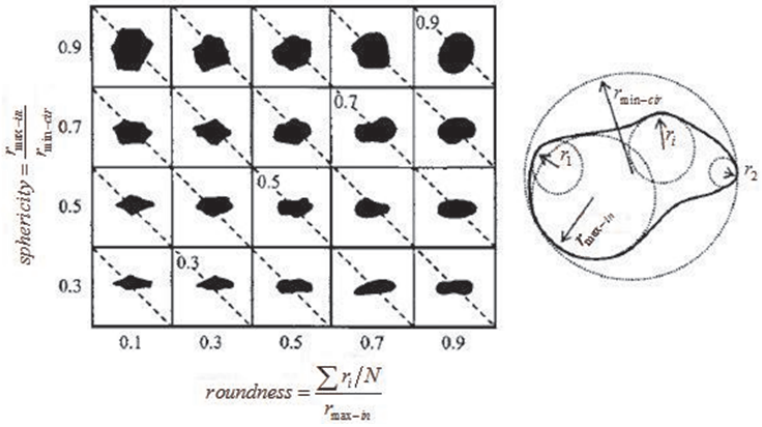

Figure 3.9. TParticle shape determination chart (Cho *et al.*, 2006).

According to Cho *et al.*, shape varies with particle size, particularly in crushed sands. Smaller particles are more planar and have sharp corners (Cho *et al.*, 2006). By the help of a stereomicroscope, pictures of individual grains are taken from four different sands for three different sieve gaps. Shape dispersion is minimized in this study by placing emphasis on specimen's uniformity. Based on previous studies (Rouse *et al.*, 2008) and the probability theorem law of large numbers the average of a sample approaches the mean of the population as the sample size increases (Moore and McCabe, 2003). In Section 3.1 brief description of the theory of law of large numbers can be found. Applying it to a sample size equal to 30 or more, roundness, sphericity, and regularity values are calculated using chart shown in Figure 3.1, and fitting 30 random grains.

The values of roundness, sphericity, and regularity are important because the behavior of particulate materials is directly affected by their fabric, the imposed state of stress and the inherent characteristics of particles, for example mineralogy, size, material strength and stiffness, angularity and surface characteristics (Santamarina, 1998).

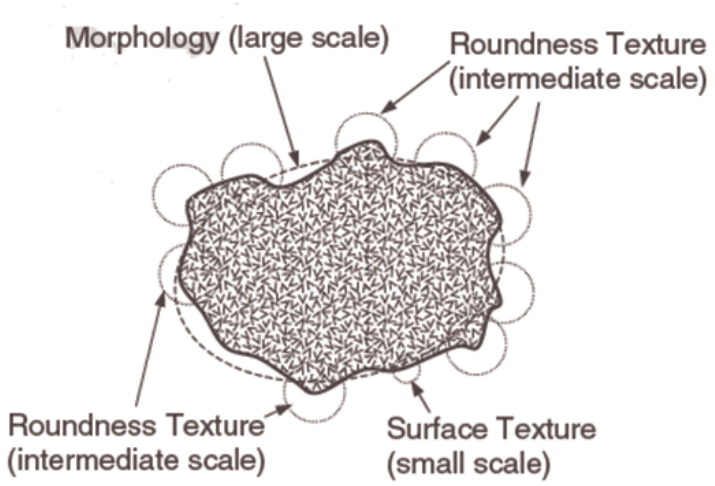

Figure 3.10. A sample of calculation of shape parameters (Mitchell and Soga, 2005).

3.2.4. Constrained Modulus

Consolidation settlements can be estimated using the 1-D constrained modulus, M, (Marchetti, 1999);

$$M = 1/m_v = \delta\sigma_v/\delta\varepsilon = 2.3(1 + e_o)\acute{\sigma}_{vo}/C_c \tag{3.3}$$

where m_v is the equivalent oedometer coefficient of compressibility, σ_v is the vertical total stress, $\delta\varepsilon$ is the vertical displacement, e_0 is the void ratio, $\acute{\sigma}_{vo}$ is the vertical effective stress, C_c is the compression index.

The constrained modulus experiment is conducted with a odeometer cell. The

granular material is put in the cell and the cap is closed. The vertical load is exerted by a lever arm which has a ratio of 10 : 1. So a load which is put on the arm of the lever will give a load of ten times higher than the actual load on the specimen.

Figure 3.11. Constrained modulus test.

Constrained modulus can be estimated from CPT results using the followingempirical relationship (Marchetti, 1999);

$$M = \alpha_M(q_t - \sigma_{vo} \tag{3.4}$$

where q_t is the cone resistance.

Sangrelat suggested that α_M varies with soil plasticity and natural water content for a wide range of fine grained soils and organic soils, although the data were based on q_c. Meigh suggested that α_M lies in the range 2 - 8, whereas Mayne suggested a general value of 8 (Sangrelat, 1970; Meigh, 1987; Mayne, 2001).

Estimates of drained 1-D constrained modulus from undrained cone penetration

will be approximate.Estimates can be improved with additional information about the soil, such as plasticity index and natural moisture content, where α_M can be lower in organic soils (Marchetti, 1999).

In order to conduct this test, the stresses of 10 kPa, 20 kPa, 50 kPa, 100 kPa, 200 kPa, 400 kPa, 800 kPa and finally 1600 kPa were applied to the each specimen. After the application of these stresses, the stresses were reduced from 1600 kPa to 400 kPa, 200 kPa, 50 kPa and finally to 10 kPa. The specimens were taken out of the odeometer cell and they were sieved. Their grain size distributions are specified.

3.2.5. Direct Shear

In principle, the shear box test is an angle of friction test, in which one portion of soil is made to slide along another by the action of a steadily increasing horizontal shearing force, while a constant load is applied normal to the plane of relative movement. These conditions are achieved by placing the soil in a rigid metal box, square in plan, consisting of two halves. The lower half of the box can slide relative to the upper half when pushed (or pulled) by a motorized drive unit, while a yoke supporting a load hanger provides the normal pressure (Head, 1981).

The direct shear test is simple to perform, but it has some inherent shortcomings. The reliability of the results may be questioned because the soil is not allowed to fail along the weakest plane but is forced to fail along the plane of split of the shear box. Also, the shear stress distribution over the shear surface of the specimen is not uniform (Danyıldız, 2007).

In terms of stress, Coulomb's law of friction can be expressed as

$$\tau_f = \sigma_n tan(\phi) \tag{3.5}$$

Digital direct shear apparatus EL26-2112 equipped with a 60x60x28 mm direct shear box was used in this study (Figure 3.12). The device was fully capable of providing variable speeds between 0.00001 to 9.99999 mm/min. The speed of displacement was chosen 1 mm/min which resulted in the failure occur in approximately 10 minutes (Danyıldız, 2007). Minimum three specimens of all groups of aggregates were tested under 50 kPa, 100 kPa and 200 kPa to investigate the relationship between normal stress and shear stress parameters of manufactured aggregates. According to ASTM D 3080, the minimum specimen width for square specimen shall be 50 mm or not less than ten times the maximum particle size diameter, the minimum initial specimen thickness shall be 12 mm, but not less than six times the maximum particle diameter, and minimum specimen width to thickness ratio shall be 2 : 1. Therefore, according to ASTM D 3080, 60x60 mm square box was used in the test because the maximum diameter of the aggregates is 0.850 mm, and the height of the box is 28 mm that is bigger than six times of the maximum particle size (ASTM D 3080).

Figure 3.12. Direct shear box with dimensions of 60x60x28 mm.

A load ring with a 3 kN capacity was used for measurement of shear loads. A maximum displacement of 6 mm was chosen because of the limitations of the direct shear device.

The crushability of samples have great importance in this study; therefore the crushing ratio of grains was obtained by comparing the grain size distributions before and after the tests according to ASTM D 421 - ASTM D 422.

The tests were conducted in dense and loose condition. The density was obtained by pouring the grains very slowly into the shear box from a constant height of 50 mm for loose condition and tamping the granular to reach desired density level for dense condition. The target normal pressure was achieved by applying vertical loads on the beam hanger that transfer loads to the load cap by $10:1$ ratio.

3.2.6. Stress Path

The stress path method was described by Lambe, in 1967, as a systematic approach to stability and deformation problems in soil mechanics. During a laboratory test on a soil sample, or as load applied to a mass of soil in the ground by a foundation, each element of soil experiences changes in its state of stress. A stress path gives a continuous representation of the relationship between the components of stress at a given point as they change. Use of a stress path provides a geotechnical engineer with an easily recognizable pattern which assists him in identifying the mechanism of soil behavior. It also provides a means of selecting and specifying the sequence of stresses to be applied to a sample in a test for a particular purpose.

Soils in general are not elastic materials and their behavior in - situ depends on many factors. These include the magnitude of the imposed stress changes; the way in which they change; and the previous history of loading, whether due to normal causes (geomorphological) or to changes imposed by man (e.g. previous loading, excavation, alteration of ground water level). It is therefore desirable to trace the states of stress of an element of soil throughout its loading history, and a stress path provides a convenient and easily understood means of conveying that information.

Usage of the stress path method in the laboratory enables the field stress changes, past, present and future, to be modeled much more realistically than by using conven-

tional test procedures alone. The conventional approach may be good enough in many instances, but for certain problems a closer approach to field conditions is necessary.

Stress paths are diagrams that represent the results of triaxial tests. A stress path is a line that connects a series of points, each of which represents a successive stress state experienced by a soil specimen during the progress of a test. There are several ways in which a stress path can be drawn. Three types of them will be mentioned in the following chapters. The first one is plotting $\acute{\sigma}_1$ and $\acute{\sigma}_3$. The second one is plotting $\acute{p}$ vs. $\acute{q}$ and the last one is plotting $\acute{s}$ vs. $\acute{t}$. Detailed information about those concepts will be given and for a better explanation of the stress path concept, the triaxial shear tests will be introduced beforehand (Das, 2007).

3.2.6.1. Triaxial. A triaxial shear test is a common method to measure the mechanical properties of many soils (e.g. sand, clay) and rock, and other granular materials or powders. There are several variations on the test.

3.2.6.2. Experimental setup. For granular materials like sand or gravel, the material is contained in a cylindrical latex sleeve with a flat, circular metal plate or platen closing off the top and bottom ends. This cylinder is placed into a bath of water (mostly water but may be any other fluid) to provide pressure along the sides of the cylinder. The top platen can then be mechanically driven up or down along the axis of the cylinder to squeeze the material. The distance that the upper platen travels is measured as a function of the force required to move it, as the pressure of the surrounding water is carefully controlled. The net change in volume of the material is also measured by how much water moves in or out of the surrounding bath.The test for cohesive (non-loose) materials (e.g. clay, rock) is similar to the test for granular materials (Head, 1998).

3.2.6.3. Basic concepts. The principle behind a triaxial shear test is that the stress applied in the vertical direction (along the axis of the cylindrical sample) can be different from the stresses applied in the horizontal directions perpendicular to the sides of the cylinder, i.e. the confining pressure). In a homogeneous and isotropic material

this produces a non-hydrostatic stress state, with shear stress that may lead to failure of the sample in shear. In non-homogeneous and anisotropic samples (e.g. bedded or jointed samples) failure may occur due to bending moments and, hence, failure may be tensile. Also combinations of bending and shear failure may happen in inhomogeneous and anisotropic material (Bardet, 1997).

A solid is defined as a material that can support shear stress without moving. However, every solid has an upper limit to how much shear stress it can support. The triaxial test is designed to measure that limit. The stress on the platens is increased until the material in the cylinder fails and forms sliding regions within itself, known as shear bands. A motion where a material is deformed under shear stress is known asshearing. The geometry of the shearing in a triaxial test typically causes the sample to become shorter while bulging out along the sides. The stress on the platen is then reduced and the water pressure pushes the sides back in, causing the sample to grow taller again. This cycle is usually repeated several times while collecting stress and strain data about the sample (Head, 1998).

During the shearing, a granular material will typically have a net gain or loss of volume. If it had originally been in a dense state, then it typically gains volume, a characteristic known as Reynolds dilatancy. If it had originally been in a very loose state, then contraction may occur before the shearing begins or in conjunction with the shearing (Head, 1998).

From the triaxial test data, it is possible to extract fundamental material parameters about the sample, including its angle of shearing resistance, apparent cohesion, and dilatancy angle. These parameters are then used in computer models to predict how the material will behave in a larger-scale engineering application. An example would be to predict the stability of the soil on a slope, whether the slope will collapse or whether the soil will support the shear stresses of the slope and remain in place. Triaxial tests are used along with other tests to make such engineering predictions (Head, 1998).

3.2.7. Types of triaxial test

3.2.7.1. Consolidated Drained (CD). In a consolidated drained test the sample is consolidated and sheared in compression with drainage. The rate of axial deformation is kept constant, i.e. is strain controlled. The idea is that the test allows the sample and the pore pressures to fully consolidate (i.e. adjust) to the surrounding stresses. The test may take a long time to allow the sample to adjust, in particular low permeability samples need a long time to drain and adjust stain to stress levels (Head, 1998).

3.2.7.2. Consolidated Undrained (CU). In a consolidated undrained test the sample is not allowed to drain. The shear characteristics are measured under undrained conditions and the sample is assumed to be fully consolidated under the stresses applied that should be similar to the field conditions. Test in particular used if a change in stress is to happen without time for further consolidation (Head, 1998).

3.2.7.3. Unconsolidated Undrained (UU). In an unconsolidated undrained test the sample is not allowed to drain. The sample is compressed at a constant rate (strain-controlled) (Head, 1998).

3.2.7.4. Stress Path Plotting. As mentioned before, there are mainly three types of plotting of stress paths in geotechnical engineering. In the following sections, those types of plotting will be explained and a brief summary of interpretation of stress paths will be given.

3.2.7.5. Plot of $\acute{\sigma}$ vs. τ. This type of stress path plot can be explained with the aid of Figure 3.13 below. The effective principal stresses are plotted and the Mohr circle is drawn at the stress state of failure.

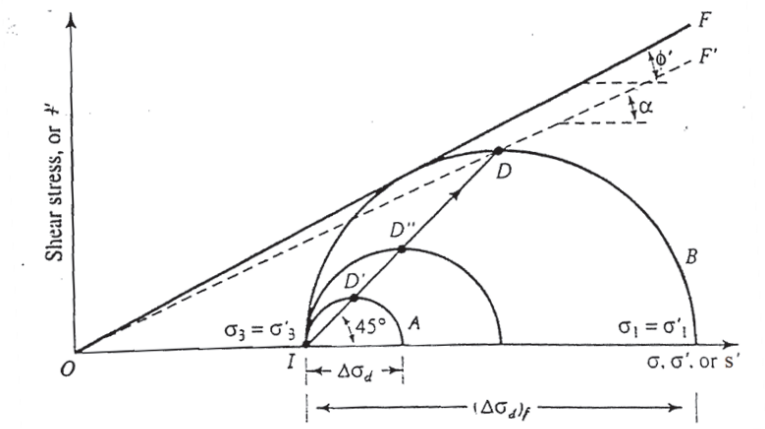

Figure 3.13. Stress path - plot of $\acute{\sigma}$ vs. τ and $\acute{s}$ vs $\acute{t}$.

3.2.7.6. Plot of $\acute{s}$ vs. t. This type of plotting of stress path is called MIT Stress Field. Let us consider a normally consolidated clay specimen subjected to an isotropically consolidated - drained triaxial test. At the beginning of the application of deviator stress, $\acute{\sigma}_1 = \acute{\sigma}_3 = \sigma_3$, so

$$\acute{s} = \frac{\acute{\sigma_3} + \acute{\sigma}_3}{2} = \acute{\sigma}_3 = \sigma_3 \tag{3.6}$$

and

$$t = \frac{\acute{\sigma}_3 - \acute{\sigma}_3}{2} = 0 \tag{3.7}$$

For this condition, $\acute{s}$ and $\acute{t}$ will plot as a point (that is I in the Figure 3.13). At some other time during deviator stress application, $\acute{\sigma}_1 = \acute{\sigma}_3 + \triangle\sigma_d = \sigma_3 + \triangle\sigma_d$; $\acute{\sigma}_3 = \sigma_3$. The Mohr's circle marked as A in the Figure 3.13 corresponds to this state of

stress on the soil specimen. The values of $\acute{s}$ and $\acute{t}$ for this stress condition are

$$\acute{s} = \frac{\acute{\sigma}_1 + \acute{\sigma}_3}{2} = \frac{(\acute{\sigma}_3 + \triangle\sigma_d) + \acute{\sigma}_3}{2} = \acute{\sigma}_3 + \frac{\triangle\sigma_d}{2} = \sigma_3 + \frac{\triangle\sigma_d}{2} \tag{3.8}$$

and

$$t = \frac{(\acute{\sigma}_3 + \triangle\sigma_d) - \acute{\sigma}_3}{2} = \frac{\triangle\sigma_d}{2} \tag{3.9}$$

If the values of s and t were plotted in the figure 3.13, they would be presented by point D at the top of the Mohr's circle. So, if the values of s and t at various stages of the deviator stress application are plotted and these points are joints, a straight line like ID will result. The straight line ID is referred to the stress path in $\acute{s}$ - $\acute{t}$ plot for a consolidated - drained triaxial test. Note that the line ID makes an angle of 45^o with the horizontal. Point D represents the failure condition of the soil specimen in the test. Also, we can see that Mohr's circle B represents the failure stress condition.

3.2.7.7. Plot of p vs. q. This type of plotting stress path is also called as Cambridge Stress Field. At year 1958, Roscoe, Schofield and Wroth at the University of Cambridge, England, developed the use of the mean of the three principal effective streses $(\sigma_1, \sigma_2, \sigma_3)$ instead of the mean of the major and minor principal stresses. This method of plotting is known as the Cambridge Stress Path Plot, in which the parameter $\acute{p}$ is defined in terms of effective stress by the equation below:

$$\acute{p} = \frac{\acute{\sigma}_1 + \acute{\sigma}_2 + \acute{\sigma}_3}{3} \tag{3.10}$$

The parameter q is defined as being equal to the deviator stress:

$$q = \acute{\sigma}_1 - \acute{\sigma}_3 = \sigma_1 - \sigma_3 \tag{3.11}$$

In the triaxial test two of the principal effective stresses are equal to the horizontal effective stress, and the equation is expressed as:

$$\acute{p} = \frac{\acute{\sigma}_1 + 2\acute{\sigma}_2}{3} \tag{3.12}$$

The mean of the total stress is similarly defined as:

$$p = \frac{\sigma_1 + 2\sigma_2}{3} \tag{3.13}$$

The concept that the volumetric behavior of soil is dependent upon a mena effective stress written as $\frac{1}{3}$ $(\acute{\sigma}_1 + \acute{\sigma}_2 + \acute{\sigma}_3)$ is central to this type of stress path plot. The introduction of the intermediate principal effective stress leads to a more fundamental representation of the state of the stress with regard to yield and the elastic behavior of overconsolidated soils. By plotting volume changes, in terms of void ratio e (or as v = 1+e) in the plane perpendicular to the $(\acute{p}, \acute{q})$ surface, a three - dimensional space for representing stresses and deformations is obtained which has been extensively used for critical state analysis at Cambridge and elsewhere.

3.2.8. Cyclic Triaxial Test

Cyclic triaxial tests can be performed to determine the modulus of elasticity E and the damping ratio D of soils. In these tests, in most cases, the soil specimen

is subjected to a confining pressure $\sigma_0 = \sigma_3$. After that, an axial cyclic stress $\triangle\sigma_d$ is applied to the specimen, as shown in Figure 3.14. The tests conducted for the evaluation of the modulus of elasticity and damping ratio are strain-controlled tests. A servo-system is used to apply cycles of controlled deformation (Das, 2011).

Figure 4.15 shows the nature of a hysteresis loop obtained from a dynamic triaxial test. From this,

$$E = \frac{\triangle\sigma_d}{\varepsilon} \tag{3.14}$$

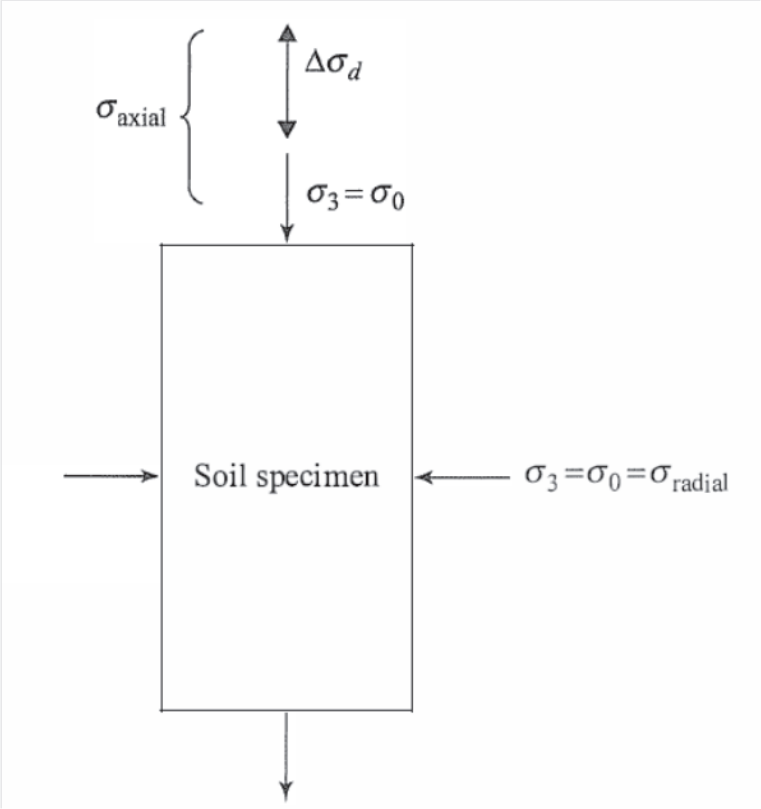

Figure 3.14. Cyclic triaxial test (Das, 2011).

Once the magnitude of E is determined, the value of shear modulus can be calculated by assuming a representative value of Poisson's ration, or

$$G = \frac{E}{2(1+\mu)} \tag{3.15}$$

Again referring to Figure 3.15, the damping ratio can be calculated as

$$D = \frac{1}{2\pi} \frac{area of the hysteresis loop}{area of triangle OAB and O\acute{A}\acute{B}} \tag{3.16}$$

Stress-controlled dynamic triaxial tests are used for liquefaction studies on saturated granular soils.

A more elaborate type of dynamic test device has also been used by several investigators to study the cyclic stress-strain history and shear characteristics of soils. Matsui, O-Hara, and Ito (1980) used a dynamic triaxial system that could generate sinusoidally varying axial and radial stresses (Das, 2011).

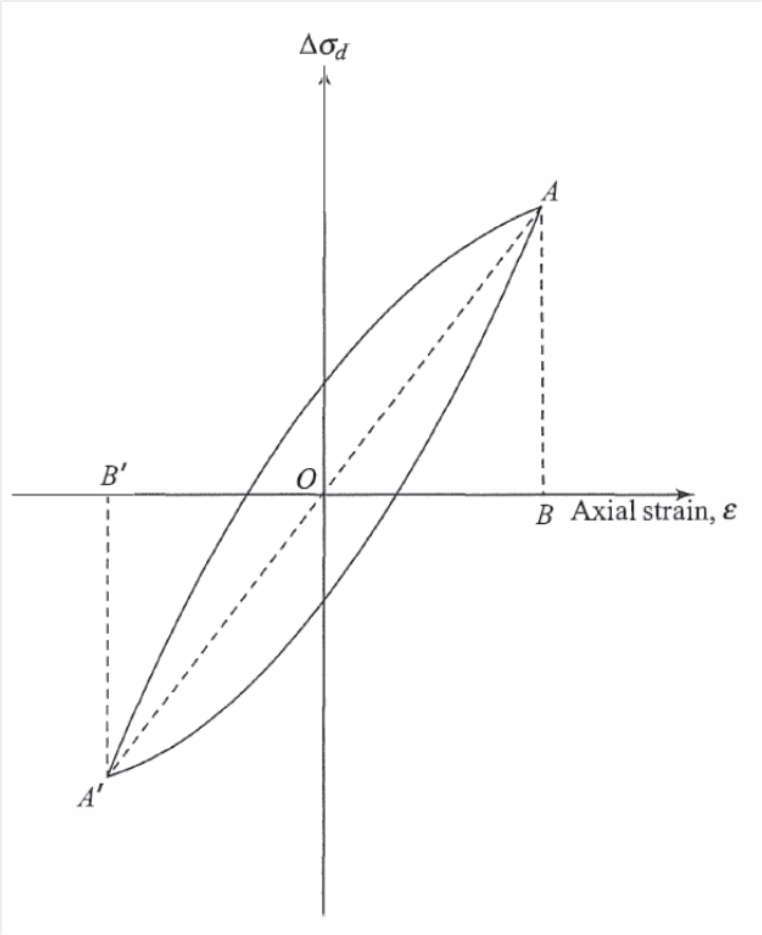

Figure 3.15. Determination of damping ratio from cyclic triaxial test (Das, 2011).

4. RESULTS AND DISCUSSION

The results of the experiments that are conducted with Sakarya sand, crushed sand, pellets with fly ash and pellets with cement are given in the following section. Specific gravity, water absorption, constrained modulus and direct shear tests are conducted with same material sample (and at the same stress conditions for the constrained modulus and direct shear tests) four times. The reason for that is to check if the produced materials like pellets from fly ash or cement are giving similar results at the same conditions and to mineralize the operator error. Also, the discussions about the test results are given in the relevant sections with the experiments.

4.1. Specific Gravity

The specific gravity test are done for the four types of granular material and apparent specific gravity is taken as the main G_s value from three types of G_s values, but also the water absorption values are taken into the consideration, especially for the triaxial experiments.

Table 4.1. The specific gravity and water absorption values of the pellets from fly ash and cement.

Fly Ash				Cement			
20-30		Well Graded		20-30		Well Graded	
w%	30.82	w%	24.81	w%	27.38	w%	21.67
AD	2.39	AD	2.36	AD	2.46	AD	2.43

Table 4.2. The specific gravity and water absorption values of the Sakarya sand and crushed sand.

Sakarya Sand				Crushed Sand			
20-30		Well Graded		20-30		Well Graded	
AD	2.68	AD	2.68	AD	2.84	AD	2.84

As it can be seen in the Table 4.1, the 20 - 30 pellets with larger diameter from fly ash have more water absorption percentages than the ones that are well graded and having smaller diameters, in other words smaller D_{50} values. Also, the 20 - 30 pellets with larger diameter produced from cement have more water absorption percentages than the ones that are well graded and so having smaller diameters. The reason for that may be the decreasing compaction effect in the pelletization disc for pellets with larger diameter. The pellets with larger diameter cannot be effectively compacted, because the compaction energy dissipates on the outer shell of the pellets and the voids those are closer to the core of the pellet stay without changing.

A further detail to discuss is the decreasing value of water absorption when pellets produced from cement are compared with pellets produced from fly ash. Because cement is a material which is produced with perfect ratios of the chemical substances as a binding material for concrete and cement mortar, more voids in the pellets produced from cement are filled with silica gel. So, the percentage of intragranular voids to the solid part is decreasing. For an absolute explanation and to prove above stated claim, different experiments and observations with different instruments like X - ray diffraction equipment or scanning electron microscope should be used.

4.2. Roundness and Sphericity

If the roundness, sphericity and regularity values of pellets produced with fly ash are compared with those values of the pellets produced from cement with grain size distribution of Standard sand well graded, it is obvious that these values are very close to each other. Those values are even the same if the samples from cement and fly ash with grain size distribution of Standard sand 20 - 30 are taken into the consideration. This result have also another meaning: The pelletization process is a totally physical process. Furthermore, at the hands of an experienced operator and with a proper device; the mean diameter of the grains, the roundness, the sphericity and the regularity values will be the same independent of the material that is used for pelletization.

The roundness values for pellets are higher than the natural and crushed sand samples in both grain size distributions. The decrease of the roundness value of Sakarya sand from the grain size distribution of Standard Sand 20 - 30 to the well graded can be explained by the decreasing shaping effect of the running water, here Sakarya River, with decreasing size of the grains. As the diameter of the grain is decreasing, the keen corners of the grain interact, i.e. crush, with other grains less often. That causes to an increase of the number of the corners of the grain and to a decrease of the value of roundness. The decrease of the roundness value of the Sakarya sand is so huge, that it is almost the same value with crushed sand. Except Sakarya sand, all roundness values of other sand types are increasing as the D_{50} value decreasing. The explanation for this behavior might be the increasing stability of chemical structure as the size of the grains is decreasing.

Table 4.3. Roundness, sphericity and regularity values of Sakarya sand, crushed sand, pellet produced with fly ash and with cement with grain size distribution of Standard sand 20 - 30.

Sand Type	Roundness	Sphericity	Regularity
Sakarya Sand	0.58	0.76	0.67
Crushed Sand	0.39	0.62	0.51
Pelet (Fly Ash)	0.68	0.85	0.77
Pelet (Cement)	0.69	0.85	0.77

Table 4.4. Roundness, sphericity and regularity values of Sakarya sand, crushed sand, pellet produced with fly ash and cement with grain size distribution of Standard sand well graded.

Sand Type	Roundness	Sphericity	Regularity
Sakarya Sand	0.45	0.76	0.61
Crushed Sand	0.43	0.68	0.56
Pelet (Flyash)	0.71	0.83	0.77
Pelet (Cement)	0.72	0.81	0.77

The sphericity values for pellets are still higher but the gap between the sphericity values of pellets and natural sands or crushed sands are smaller. Because the pellets with smaller diameter are more susceptible for deformation while they are taken put from the pelletization disc, they can have smaller sphericity values than the larger diameter pellets. On the other hand, the sphericity value of Sakarya sand is not changing with the change of the mean particle size. This is the shaping effect of the stream. Furthermore, the difference of the sphericity values of the Sakarya sand and crushed sand decreases as the mean particle size decreases. The excessive pressure, which is experienced on the smaller particles, so that they have this size, can increase the sphericity value.

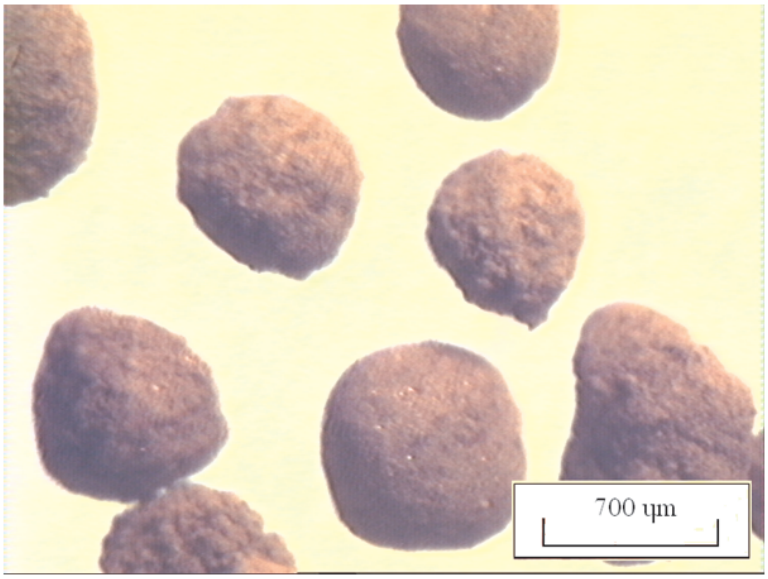

Figure 4.1. The image of the pellets produced from cement with the grain size distribution of the Standard sand 20 - 30 taken by microscope.

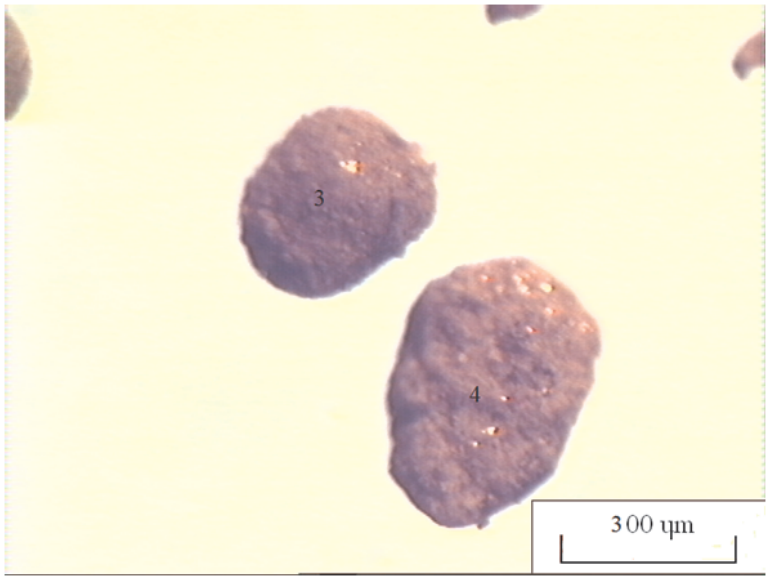

Figure 4.2. The image of the pellets produced from cement with the grain size distribution of the Standard sand well graded taken by microscope.

In Figure 4.1 and Figure 4.2, the images of pellets produced from cement in different grain size distributions are presented. It is clear that the pellets with uniformly graded size distribution are more spherical but they have more and bigger corners than the pellets well graded. The well graded pellets are more squeezed and, therefore, they have smaller roundness values than those of the uniformly graded pellets.

4.3. Constrained Modulus

In the following constrained modulus tests, it has been seen that pellets produced both from fly ash and cement are susceptible to crushing. If the pellets with grains size distribution of the Standard sand 20 - 30 are taken into the consideration, it is emerged that about 5% of the pellets, both produced from fly ash or cement, are under No. 30 sieve after the application of the stresses. If the crushabilty results of the natural and crushed sand are taken into the consideration, it is seen that 1% to 2% of the specimens are under No. 30 sieve. This concludes that, both pellets produced from fly ash and cement has a extra crushabilty degree of about 3% to 4% for the grain size distribution of the Standard sand 20 - 30.

Moreover, if the crushability degrees of the pellets with the grain size distribution of well graded are examined, it is occured that the percent passing from the No. 40 and No. 100 sieve are increasing about 5% of the material passed before in that sieves. That means crushing can be seen at all sizes. It is not particular to a single diameter size of pellets. It is also independent of the used material. For all samples produced from cement or fly ash, same observation is made.

If Figure 4.3 to Figure 4.6 are taken into the consideration, it can be seen that the graphs for pellets produced with cement in size distribution of well graded and 20 - 30 according to Standard sand are similar to each other. The void ratios are decreasing with decreasing D_{50}, because the intergranular voids are decreasing with decreasing D_{50}. Also, the changing grain size distribution from uniformly graded to well graded is a reason of decreasing void ratio, since the smaller grains are filling the voids between the larger grains.

At the recompression curves of Figure 4.3 and Figure 4.5, it is obvious that there is breaking point at 400 kPa. This behavior points out a decreasing decrease in the constrained modulus in comparison with natural and crushed sands. If the Figure 4.4 and Figure 4.6 are examined, it is easy to see that the strain recovery of the pellets in both grain size distributions are almost linear. In constrained modulus test with natural and crushed sand, it is expected that the void ratios have a increasing increase with decreasing pressure. This might be caused by the high flexibility and low strain recovery of the single grains. Differently from the natural or crushed sand, the single pellet grains can have large strain values as high as 10%.

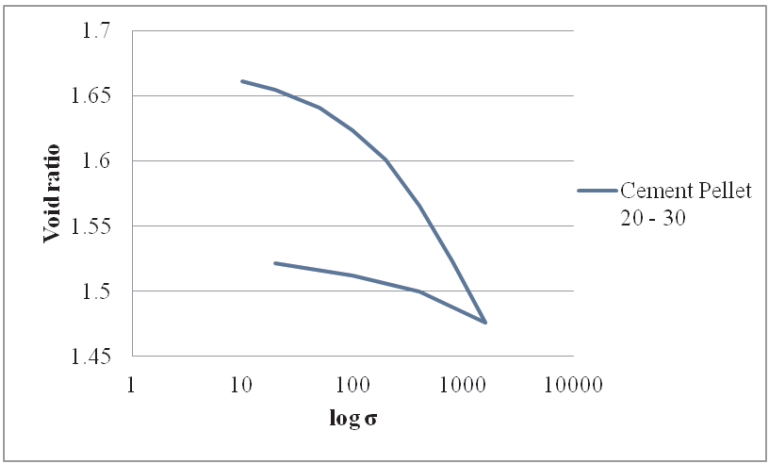

Figure 4.3. Void ratio vs. log σ for pellets produced by cement with grain size distribution of Standard sand 20 - 30.

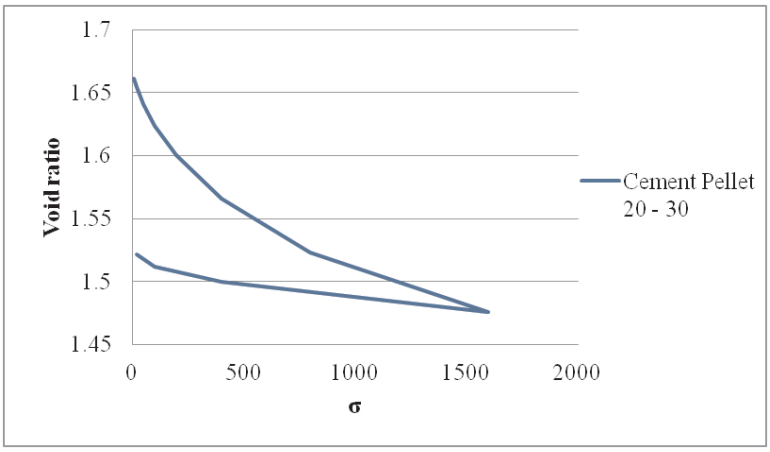

Figure 4.4. Void ratio vs. σ for pellets produced by cement with grain size distribution of Standard sand 20 - 30.

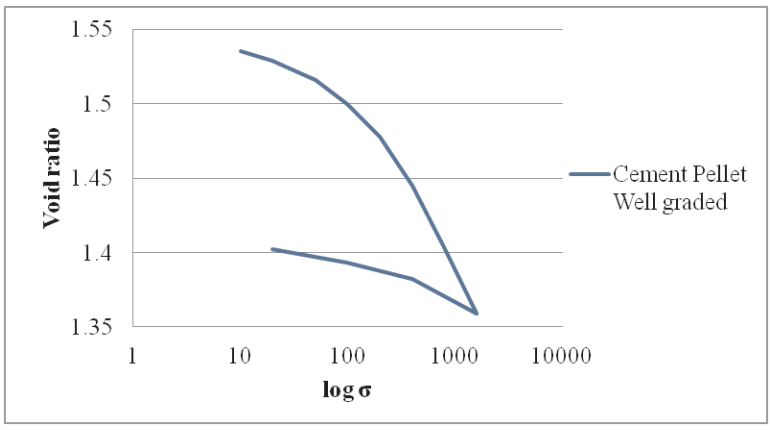

Figure 4.5. Void ratio vs. log σ for pellets produced by cement with grain size distribution of Standard sand well graded.

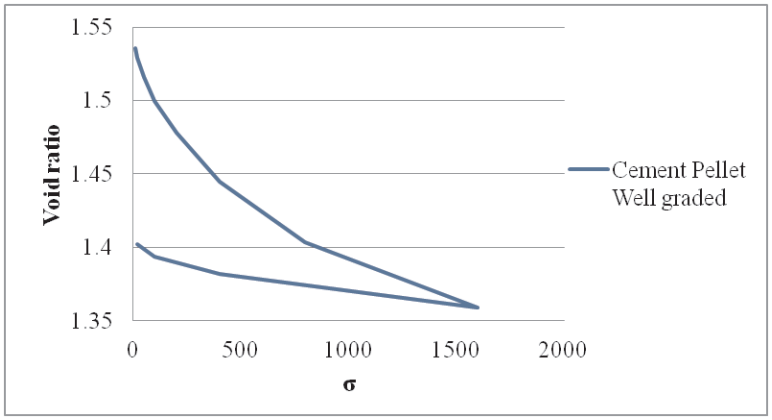

Figure 4.6. Void ratio vs. σ for pellets produced by cement with grain size distribution of Standard sand well graded.

In the following graphs (Figure 4.5, Figure 4.6, Figure 4.7 and Figure 4.8), the logaritmic vertical stress versus void ratio values and vertical stress versus void ratio values for crushed sand in grain size distribution of well graded and 20 - 30 according to Standard sand are presented. The first important fact about the crushed sand is the relatively smaller amount of void ratio in comparison with the pellets produced from cement. The reason is the intragranular voids of pellets. The intragranular voids are also calculated in void ratio calculations because it is not possible to understand whether the decrease in the voids ratios caused by the intergranular voids or intragranular voids.

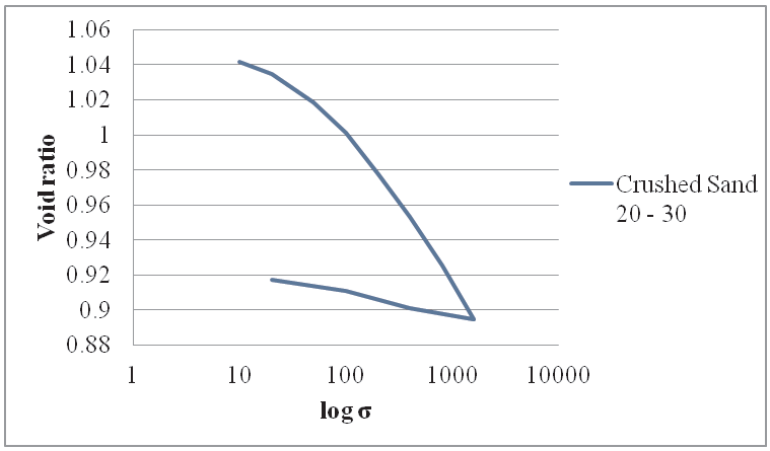

Figure 4.7. Void ratio vs. log σ for crushed sand with grain size distribution of Standard sand 20 - 30.

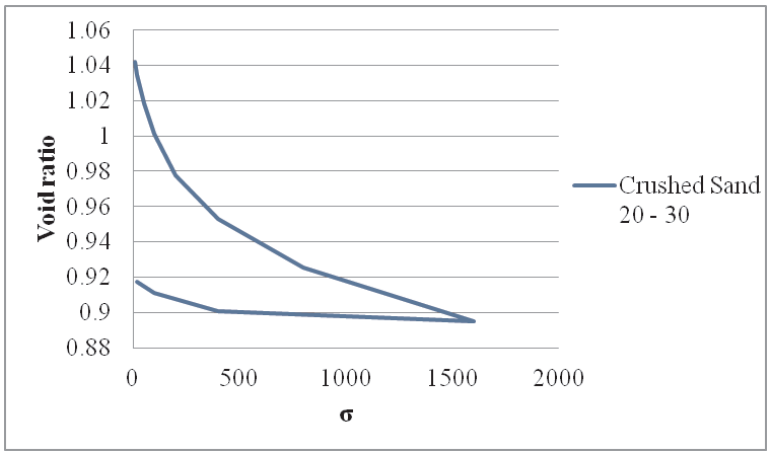

Figure 4.8. Void ratio vs. log σ for crushed sand with grain size distribution of Standard sand 20 - 30.

The recompression curves in Figure 4.7 and Figure 4.9 are almost linear, but the recompression curves in the Figure 4.3 and Figure 4.5 have a breaking point at 400 kPa stress and the curves are bilinear. In the linear representations in the graphs of Figure 4.8 and Figure 4.10, the recompresion curves have a different slope between 0 kPa to 400 kPa than the part between 400 kPa to 1600 kPa. This behavior shows that the crushed sand will gain more constrained modulus value than the pellets produced from cement and the strength of the soil increases. Furthermore, crushed sand shows less vertical displacement than the samples produced from cement at the same stress level under at rest condition.

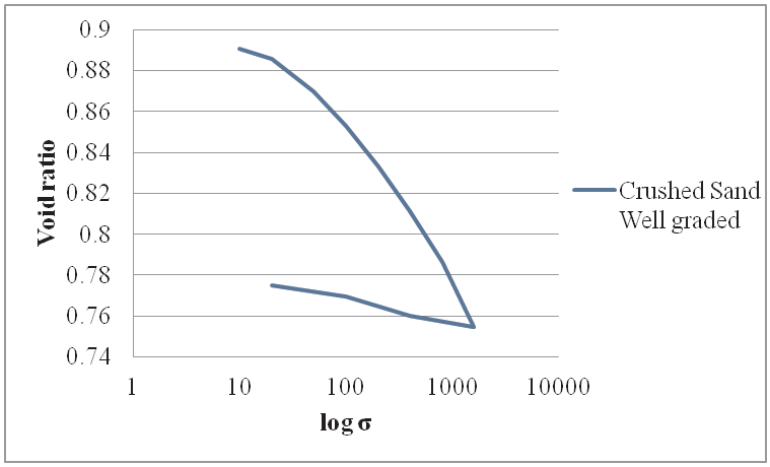

Figure 4.9. Void ratio vs. log σ for crushed sand with grain size distribution of Standard sand well graded.

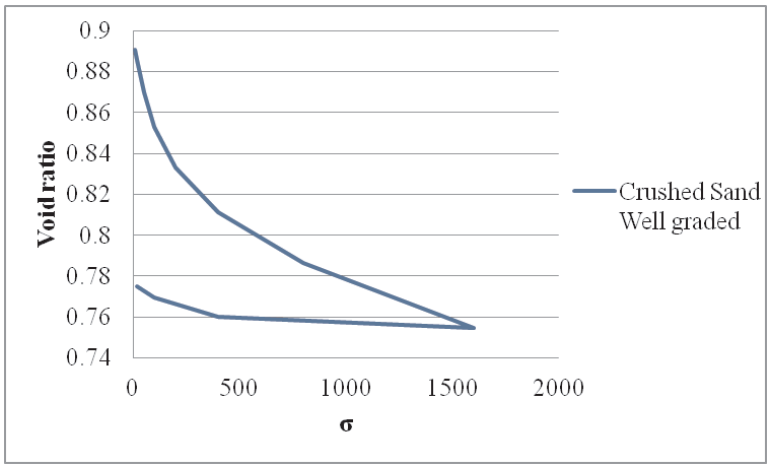

Figure 4.10. Void ratio vs. σ for crushed sand with grain size distribution of Standard sand well graded.

Figure 4.11 and Figure 4.13, the graphs of the logaritmic vertical stress versus void ratio values for pellets produced with fly ash in size distribution of well graded and 20 - 30 according to Standard sand, same behavior can be seen like in the Figure 4.3 and Figure 4.5 of the pellets produced by cement. The same behavior of decreasing decrease of the constrained modulus of the cement samples can be seen here, also. A strong decrease in the void ratio values in the virgin curve at the 100 kPa stress is occurred.

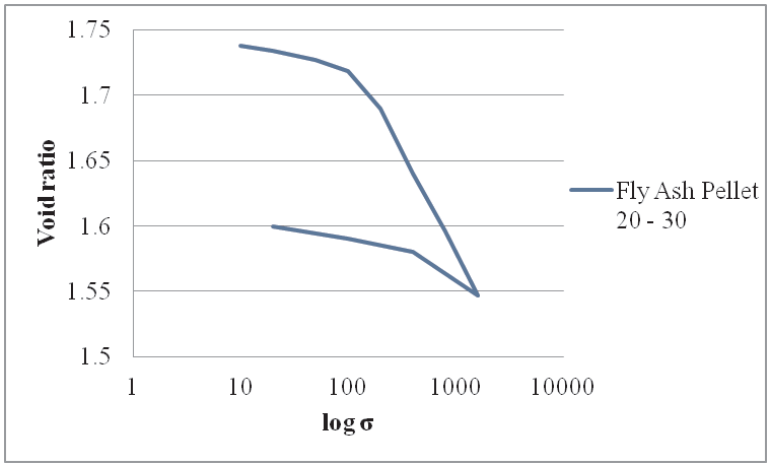

Figure 4.11. Void ratio vs. log σ for pellet produced with fly ash with grain size distribution of Standard sand 20 - 30.

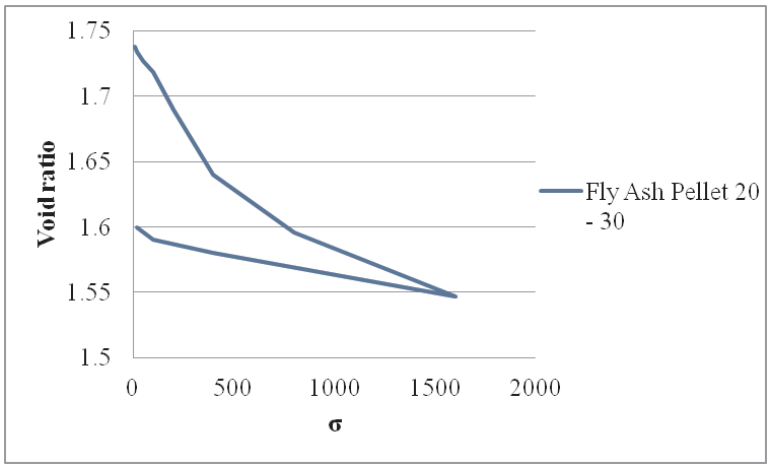

Figure 4.12. Void ratio vs. σ for pellet produced with fly ash with grain size distribution of Standard sand 20 - 30.

In comparison with the pellets produced from cement, this behavior can be a sign of sudden crushing of the grains produced from fly ash. The values of the void ratios of pellets produced by fly ash are much greater than the void ratio values of the pellets produced from cement because fly ash pellets have greater water absorption values than the pellets produced from cement.

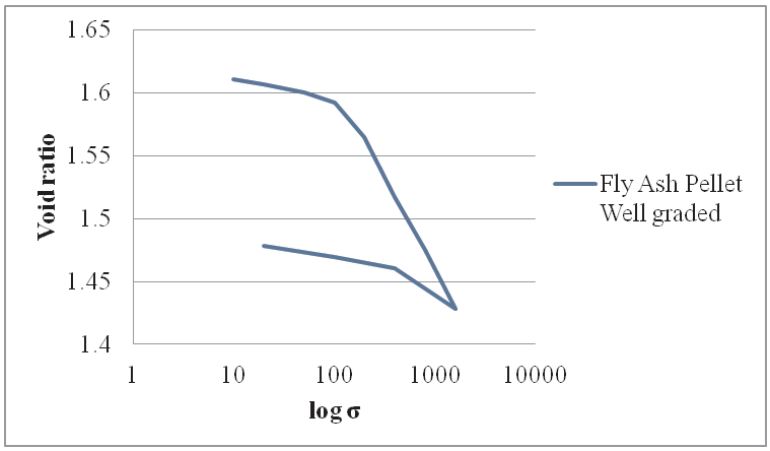

Figure 4.13. Void ratio vs. log σ for pellet produced with fly ash with grain size distribution of Standard sand well graded.

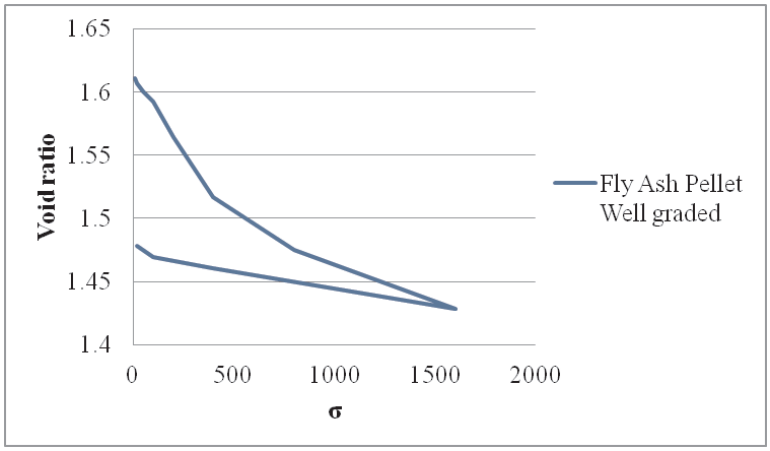

Figure 4.14. Void ratio vs. σ for pellet produced with fly ash with grain size distribution of Standard sand well graded.

In Figure 4.12 and Figure 4.14, the linear behavior of recompression curve is much clearer than the curves represented in Figure 4.4 and Figure 4.6. So, pellets produced from fly ash have almost no gain in the constrained modulus values in comparison of natural and crushed sand. Only after 10 kPa vertical stress in the recompression region, a small increase can be seen.

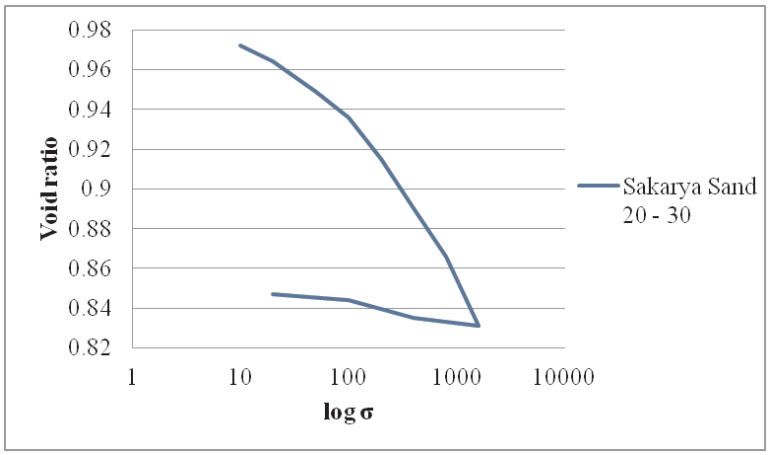

Figure 4.15. Void ratio vs. log σ for Sakarya sand with grain size distribution of Standard sand 20 - 30.

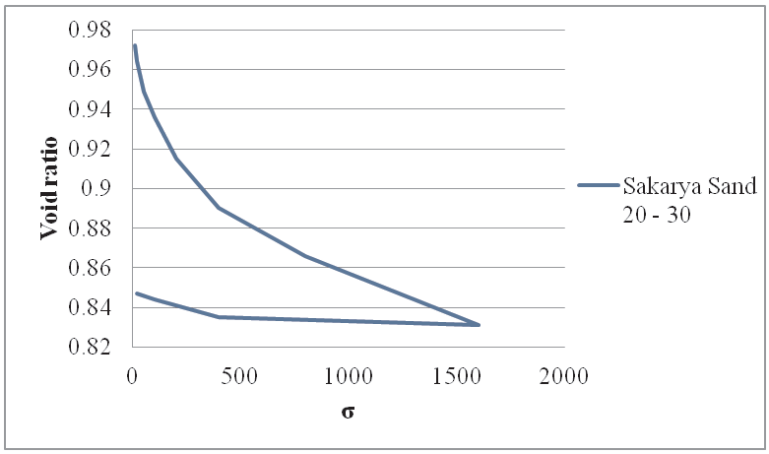

Figure 4.16. Void ratio vs. σ for Sakarya sand with grain size distribution of Standard sand 20 - 30.

In Figure 4.15 and Figure 4.17, the graphs of the logaritmic vertical stress versus void ratio values for Sakarya sand in size distribution of well graded and 20 - 30 according to Standard sand, the relatively small amount of void ratios can be seen. If it is taken into the consideration, that all samples are prepared in dense condition, the reason for this behavior can be explained with roundness and sphericity.

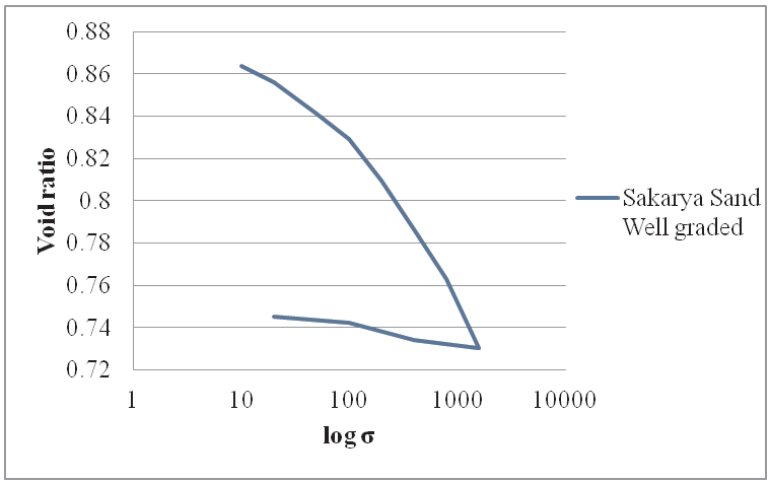

Figure 4.17. Void ratio vs. log σ for Sakarya sand with grain size distribution of Standard sand well graded.

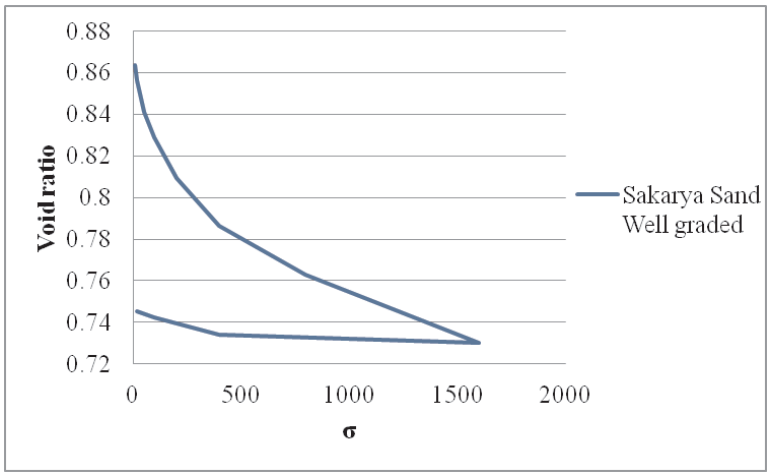

Figure 4.18. Void ratio vs. log σ for Sakarya sand with grain size distribution of Standard sand well graded.

The round samples of Sakarya sand can be more compacted than the relatively angular samples of crushed sand. The graphs Figure 4.15 and Figure 4.17 are more similar to the graphs log σ - e and σ - e of the pellets produced from cement. A breaking point, but with a smaller change in the slope of the line, at the stress level of 100 kPa in the virgin curve can be seen in the Figure 4.15 and Figure 4.17 and also in the Figure 4.3 and Figure 4.5.

In the Figure 4.16 and Figure 4.18, the recompression curves seem much more linear than the recompression curves of the σ - e graphs of the crushed sand. The gain of the constrained modulus value of natural sand is smaller than the gain of the constrained modulus value of the crushed sand. This behavior that is seen also in the pellets produced from fly ash and cement can be caused by the smaller roundness and sphericity values of the Sakarya sand. Differently from pellets, the constrained modulus value of the natural sand shows an increase after 100 kPa stress in the recompression zone like the crushed sand.

In the Table 4.5 and Table 4.6, the constrained modulus values of the samples are given. Although there is a difference between 20 - 30 and well graded specimens of both Sakarya sand and crushed sand, there is no significant change between 20 - 30 and well graded samples of pellets produced from fly ash and cement. Both natural

and crushed sand have smaller constrained modulus values than the pellets produced from fly ash and cement. The increase in the constrained moduli of the natural and crushed sand from first section (100 kPa - 400 kPa) to the second section (400 kPa - 1600 kPa) is greater than change of the constrained moduli values of the of pellets both produced from fly ash and cement between same sections. From second section to the third section (1600 kPa - 400 kPa), the increase in the constrained modulus value is very small for the pellets than the natural and crushed sand. The crushing behavior of the pellets and the strain gaining values of pellets can be the reason. Furthermore, the change between the third section to the second section (400 kPa - 100 kPa) in the recompression zones are greater for pellets produced from both, cement and fly ash. That means pellets are gaining smaller constrained modulus value in the recompression than the natural and crushed sands.

Table 4.5. Roundness, sphericity and regularity values of Sakarya sand, crushed sand, pellet produced with fly ash and cement with grain size distribution of Standard sand well graded.

Samples	Constrained modulus between 100 kPa - 200 kPa	Constrained modulus between 400 kPa - 1600 kPa
Fly Ash Pellet (20-30)	10985	35798
Fly Ash Pellet (Well Graded)	10683	35818
Sakarya Sand (20-30)	8695	40015
Sakarya Sand (Well Graded)	9052	38756
Cement Pellet (20-30)	11752	35821
Cement Pellet (Well Graded)	11765	35852
Crushed Sand (20-30)	9285	42105
Crushed Sand (Well Graded)	9523	40000

Table 4.6. Roundness, sphericity and regularity values of Sakarya sand, crushed sand, pellet produced with fly ash and cement with grain size distribution of Standard sand well graded.

Samples	Constrained modulus between 1600 kPa - 400 kPa	Constrained modulus between 400 kPa - 100 kPa
Fly Ash Pellet (20-30)	123568	59874
Fly Ash Pellet (Well Graded)	123245	58898
Sakarya Sand (20-30)	375627	230796
Sakarya Sand (Well Graded)	398129	232145
Cement Pellet (20-30)	133304	66632
Cement Pellet (Well Graded)	133333	66667
Crushed Sand (20-30)	400000	240000
Crushed Sand (Well Graded)	400052	240098

Table 4.7 to Table 4.14, the vertical and horizontal stress values are given. K_0 values are calculated. It can be seen that the K_0 values for all pellets and sands are changing with same manner. This is a surprising effect because an increase in the K_0 values is expected for pellets after the crushing of the grains.

Table 4.7. Vertical stresses, horizontal stresses and K_0 values for pellet produced from cement with grain size distribution of Standard sand 20 - 30.

Cement Pellet 20 - 30		
Vertical Stress (kPa)	Horizontal Stress (kPa)	K_0
10	4	0.40
20	6	0.30
50	19	0.38
100	41	0.41
200	79	0.40
400	154	0.39
800	311	0.39
1600	624	0.39
400	164	0.41
100	46	0.46
20	8	0.40

Table 4.8. Vertical stresses, horizontal stresses and K0 values for pellet produced from cement with grain size distribution of Standard sand well graded.

Cement Pellet Well Graded		
Vertical Stress (kPa)	Horizontal Stress (kPa)	K_0
10	4	0.40
20	6	0.30
50	21	0.42
100	39	0.39
200	82	0.41
400	155	0.39
800	317	0.40
1600	634	0.40
400	175	0.44
100	45	0.45
20	7	0.35

Table 4.9. Vertical stresses, horizontal stresses and K_0 values for crushed sand with grain size distribution of Standard sand 20 - 30.

Crushed Sand 20 - 30		
Vertical Stress (kPa)	Horizontal Stress (kPa)	K_0
10	5	0.50
20	7	0.35
50	21	0.42
100	42	0.42
200	81	0.41
400	163	0.41
800	319	0.40
1600	638	0.40
400	164	0.41
100	44	0.44
20	6	0.30

Table 4.10. Vertical stresses, horizontal stresses and K_0 values for crushed sand with grain size distribution of Standard sand well graded.

Crushed Sand Well Graded		
Vertical Stress (kPa)	Horizontal Stress (kPa)	K_0
10	5	0.50
20	7	0.35
50	21	0.42
100	42	0.43
200	81	0.41
400	163	0.41
800	319	0.40
1600	638	0.40
400	164	0.41
100	44	0.43
20	6	0.20

Table 4.11. Vertical stresses, horizontal stresses and K_0 values for pellet produced from fly ash with grain size distribution of Standard sand 20 - 30.

Fly Ash Pellet 20 - 30		
Vertical Stress (kPa)	Horizontal Stress (kPa)	K_0
10	3	0.30
20	6	0.30
50	19	0.38
100	39	0.39
200	74	0.37
400	145	0.36
800	301	0.38
1600	611	0.38
400	158	0.40
100	39	0.39
20	5	0.25

Table 4.12. Vertical stresses, horizontal stresses and K_0 values for pellet produced from fly ash with grain size distribution of Standard sand well graded.

Fly Ash Pellet Well Graded		
Vertical Stress (kPa)	Horizontal Stress (kPa)	K_0
10	3	0.38
20	6	0.38
50	19	0.38
100	39	0.39
200	74	0.37
400	145	0.36
800	301	0.37
1600	611	0.38
400	158	0.39
100	39	0.39
20	5	0.25

Table 4.13. Vertical stresses, horizontal stresses and K_0 values for Sakarya sand with grain size distribution of Standard sand 20 - 30.

Sakarya Sand 20 - 30		
Vertical Stress (kPa)	Horizontal Stress (kPa)	K_0
10	4	0.40
20	7	0.35
50	20	0.40
100	41	0.41
200	78	0.39
400	158	0.40
800	320	0.40
1600	642	0.40
400	161	0.40
100	41	0.41
20	7	0.35

Table 4.14. Vertical stresses, horizontal stresses and K_0 values for crushed sand with grain size distribution of Standard sand well graded.

Sakarya Sand Well Graded		
Vertical Stress (kPa)	Horizontal Stress (kPa)	K_0
10	4	0.40
20	8	0.40
50	22	0.44
100	43	0.43
200	77	0.39
400	160	0.40
800	319	0.40
1600	654	0.41
400	161	0.40
100	43	0.43
20	7	0.35

4.4. Direct Shear

The results of direct shear tests performed on uniformly graded (between 20 - 30 sieve sizes) fly ash pellets are presented in Figure 4.19. At low normal stresses of 50 and 100 kPa, fly ash pellets give lower peak shear stress values as compared to those of Sakarya sand and crushed sand. Dilation is observed under shear for the normal stress of 50 kPa in loose state and for all three normal stresses in dense state.

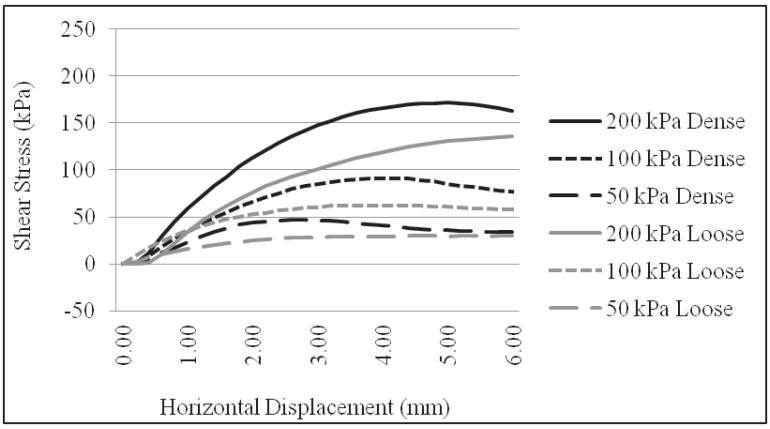

Figure 4.19. Shear stress vs. horizontal displacement curve for pellet produced with fly ash with grain size distribution of Standard sand 20 - 30.

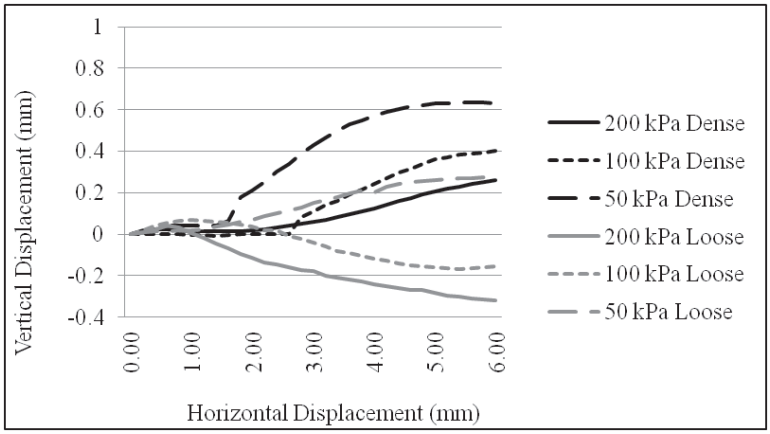

Figure 4.20. Vertical displacement vs. horizontal displacement curve for pellet produced with fly ash with grain size distribution of Standard sand 20 - 30.

It is surprising that all samples in dense state do not show any contraction behavior. The dilation values of fly ash pellets are comparatively higher than those of Sakarya Sand and crushed sand. Mobilization of peak shear strength occurs at higher horizontal displacement values for fly ash pellets in comparison with natural and crushed sand.

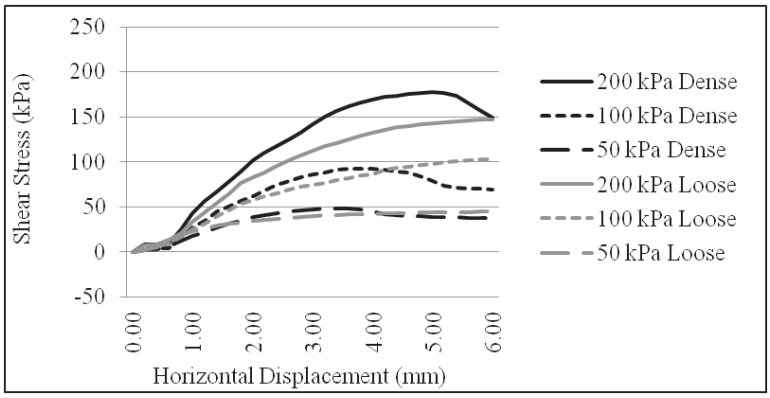

Figure 4.21. Shear stress vs. horizontal displacement curve for pellet produced with fly ash with grain size distribution of Standard sand well graded.

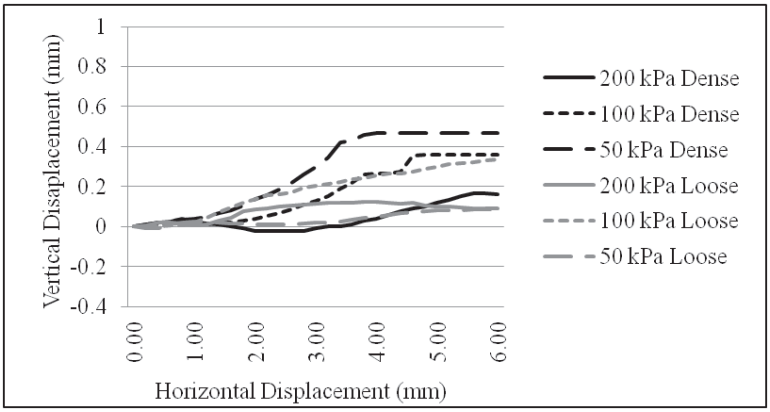

Figure 4.22. Vertical displacement vs. horizontal displacement curve for pellet produced with fly ash with grain size distribution of Standard sand well graded.

In Figure 4.21, the result of the direct shear tests of the pellets produced from fly ash with the grain size distribution of Standard sand well graded are presented. Although the peak shear strength values in dense state are almost same with the shear strength values of the uniformly graded samples produced from fly ash, the shear strength values of well graded samples produced from fly ash in the loose state are clearly higher than the uniformly graded samples in the same relative density and under same normal stresses.

In Figure 4.22, the vertical displacement versus horizontal displacement curves for pellets produced from fly ash with grain size distribution of Standard sand well graded is represented. Unlikely, all samples in loose state show a dilation behavior.

Except the sample under 200 kPa normal stress in dense condition, the other samples in dense state showing only a dilation behavior and all samples, also the sample under 200 kPa normal stress, in dense condition, reach critical state.

Dilation behavior of pellets produced from fly ash is similar to those samples of calcareous sands mentioned in the literature review section. At the large deformations and with smaller normal stresses, pellets in the loose condition are susceptible to dilation, differently from natural and crushed sand samples.

In comparison with samples produced from fly ash, Sakarya sand has higher peak shear strength values in all relative density values under all normal stresses. The horizontal displacement versus shear stress curves are similar to those of the curves that are represented in soil mechanics books. Differently from the graphs of the direct shear results of pellets produced from fly ash, the mobilization of the peak shear strength occurs at lower horizontal displacement values.

The horizontal displacement versus vertical displacement curves for Sakarya sand with uniformly graded grain size distribution are represented in Figure 4.19. Uniformly graded samples in dense condition are showing a contraction behavior at lower horizontal displacement values and higher dilation values than those of pellets at higher horizontal displacements. Like the uniformly graded Sakarya sand samples in dense condition, also the Sakarya sand samples with same gradation curves in loose condition show a contraction behavior at lower horizontal displacement values and dilation behavior at higher horizontal displacement values.

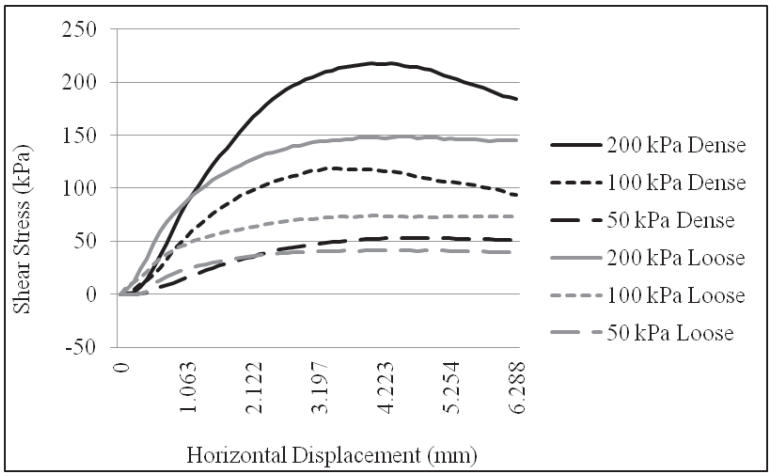

Figure 4.23. Shear stress vs. horizontal displacement curve for Sakarya sand with grain size distribution of Standard sand 20 - 30.

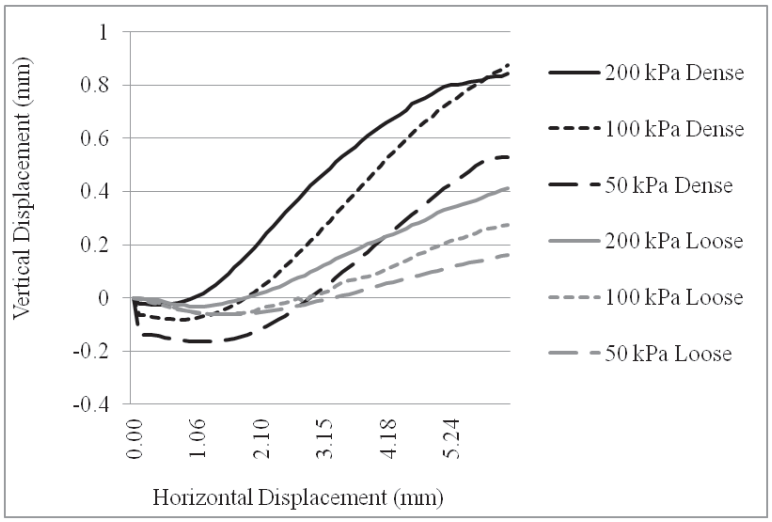

Figure 4.24. Vertical displacement vs. horizontal displacement curve for Sakarya sand with grain size distribution of Standard sand 20 - 30.

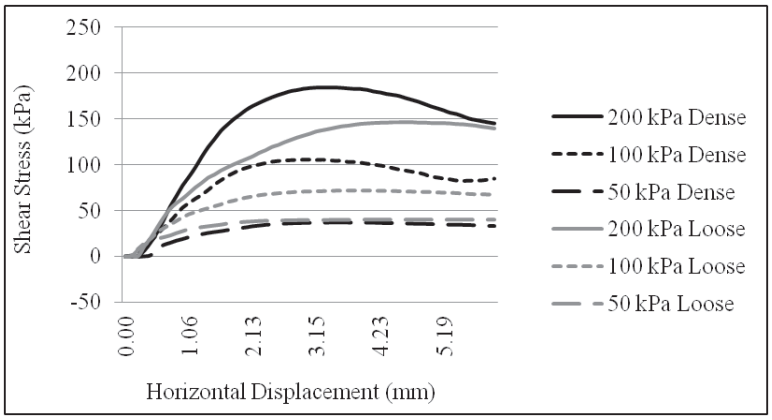

Figure 4.25. Shear stress vs. horizontal displacement curve for Sakarya sand with grain size distribution of Standard sand well graded.

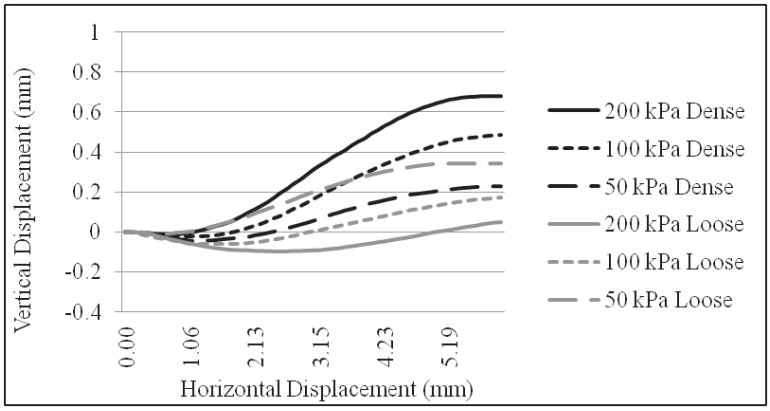

Figure 4.26. Vertical displacement vs. horizontal displacement curve for Sakarya sand with grain size distribution of Standard sand well graded.

The presentation of shear stress versus horizontal displacement curve for Sakarya sand with grain size distribution of Standard sand well graded is the Figure 4.25. Relatively smaller peak shear strength values are seen in comparison with those of Sakarya sand samples with uniformly graded grain size distribution. The mobilization of the peak shear strengths are seen at lower horizontal displacement values.

In Figure 4.26, vertical displacement versus horizontal displacement curves for well graded Sakarya sand is represented. For the samples prepared in dense state, the contraction behavior is smaller than those of the uniformly graded Sakarya samples at dense state. The dilation behavior after contraction behavior for the samples in

loose state is observed. The contraction behavior is more significant in this case in comparison with those of uniformly graded Sakarya sand samples at loose condition.

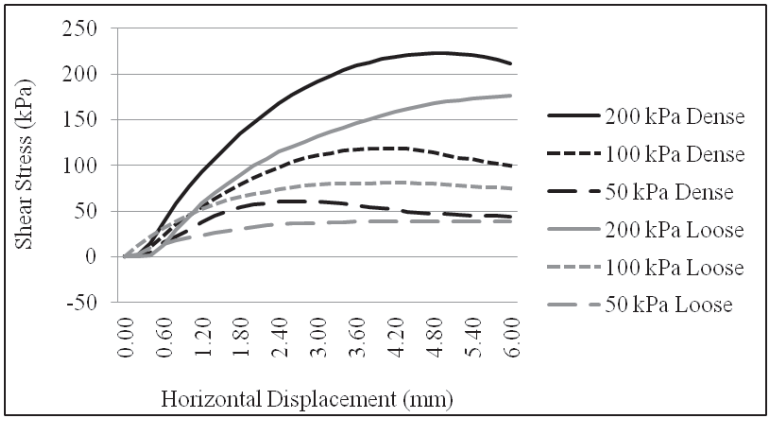

Figure 4.27. Shear stress vs. horizontal displacement curve for pellet produced with cement with grain size distribution of Standard sand 20 - 30.

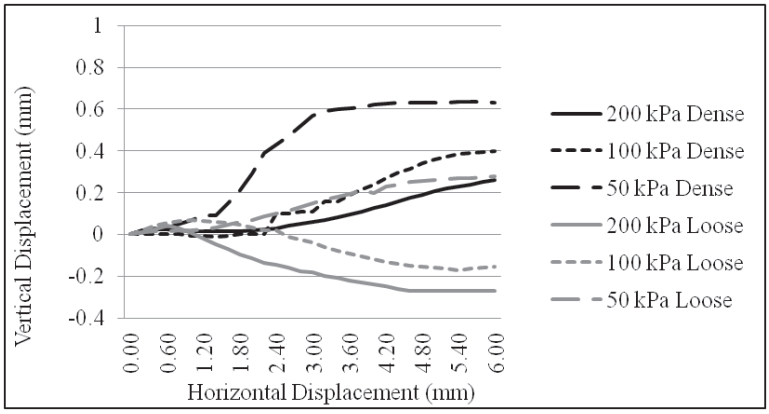

Figure 4.28. Vertical displacement vs. horizontal displacement curve for pellet produced with cement with grain size distribution of Standard sand 20 - 30.

The pellets produced with cement, presented in Figure 4.27, are showing a similar shear strength values like those of uniformly graded samples of Sakarya sand. However, the mobilization of peak shear strength values are seen at larger horizontal deformations.

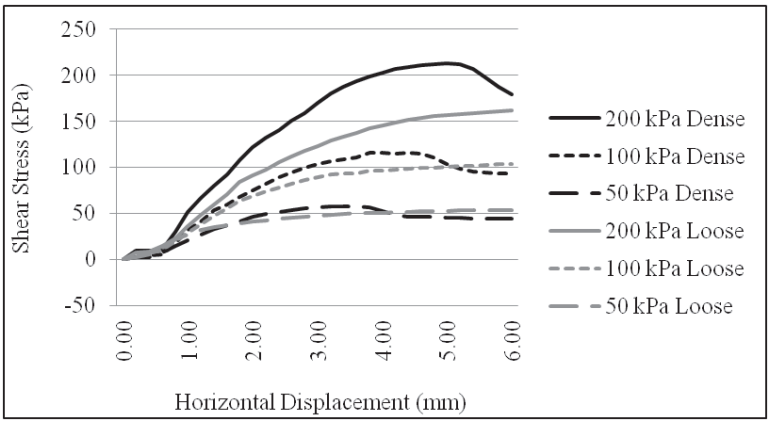

Figure 4.29. Shear stress vs. horizontal displacement curve for pellet produced with cement with grain size distribution of Standard sand well graded.

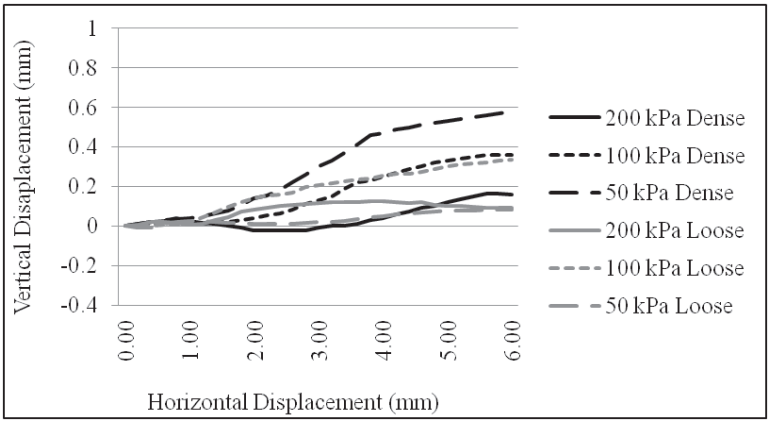

Figure 4.30. Vertical displacement vs. horizontal displacement curve for pellet produced with cement with grain size distribution of Standard sand well graded.

The vertical displacement versus horizontal displacement curves for uniformly graded pellet produced with cement is shown in Figure 4.28. Although the shear stress versus horizontal displacement curves are similar with those of uniformly graded Sakarya sand samples, the vertical displacement versus horizontal displacement curves are similar with those of uniformly graded fly ash pellets.

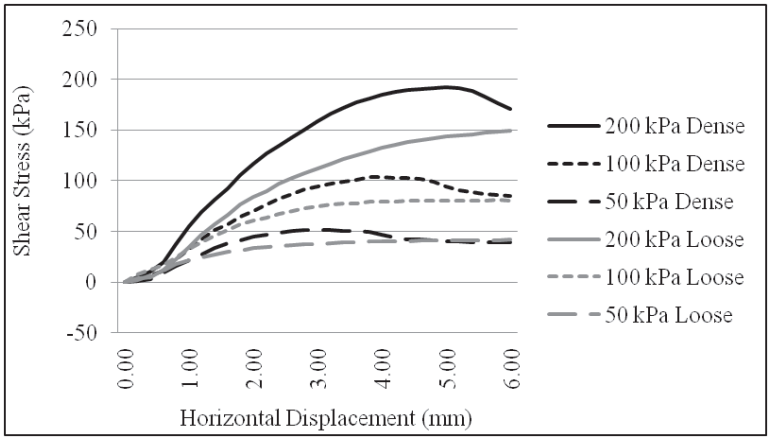

Figure 4.31. Shear stress vs. horizontal displacement curve for crushed sand with grain size distribution of Standard sand 20 - 30.

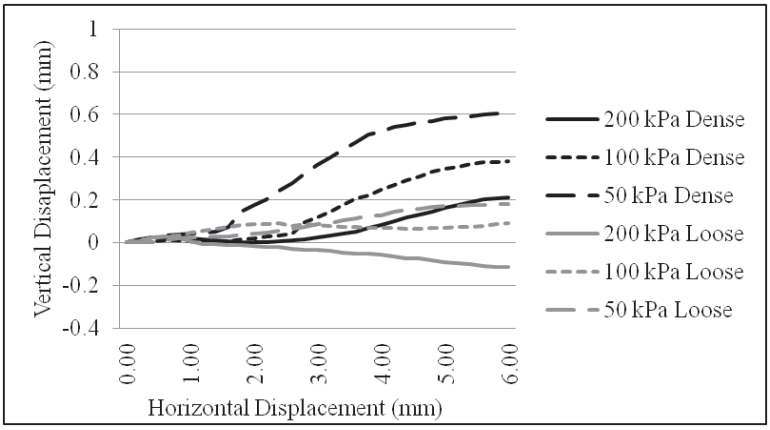

Figure 4.32. Vertical displacement vs. horizontal displacement curve for crushed sand with grain size distribution of Standard sand 20 - 30.

In Figure 4.29, shear stress versus horizontal displacement curves for well graded cement pellet are represented. The peak shear strength values are similar with those of uniformly graded pellet samples produced from cement. The mobilization of the peak shear strength is occurred similarly at higher horizontal deformation values but a larger and more sudden decrease of the shear strength can be observed for the residual stress plateau.

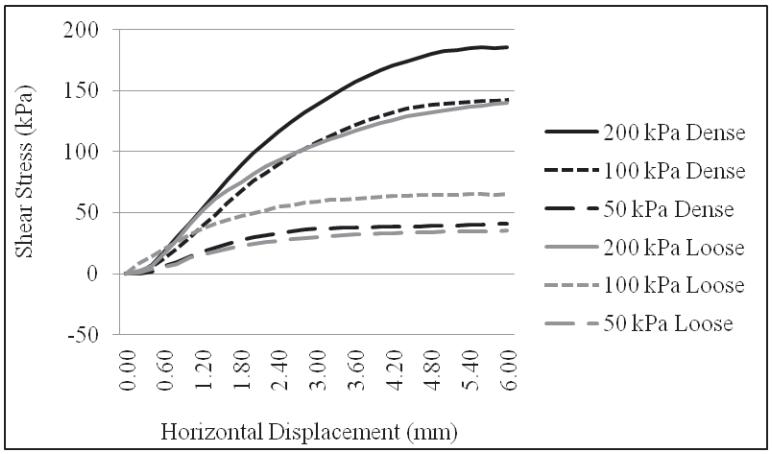

Figure 4.33. Shear stress vs. horizontal displacement curve for crushed sand with grain size distribution of Standard sand well graded..

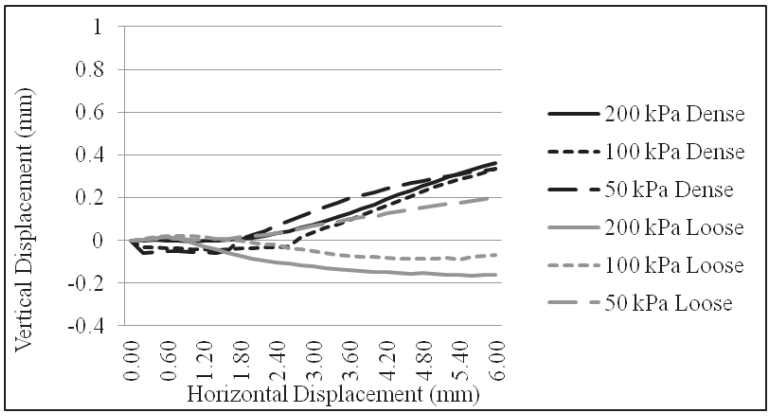

Figure 4.34. Vertical displacement vs. horizontal displacement curve for crushed sand with grain size distribution of Standard sand well graded.

In the Figure 4.30, a dilation behavior for all samples is at issue. For the samples in dense state a breaking point at approximately 3.50 mm can be observed. In Figure 4.31, uniformly graded crushed sand samples have relatively smaller peak shear strength values than those of uniformly graded Sakarya sand and cement pellet samples. Mobilization of peak shear strength is observed at higher horizontal displacement values like those of pellets produced from fly ash or cement. In comparison with uniformly graded Sakarya sand, uniformly graded crushed sand samples have lower vertical displacement values, shown in Figure 4.32. All samples, except the sample under 100 kPa normal stress in loose state, are showing dilation behavior.

In Figure 4.33 and Figure 4.34, the shear strength and vertical displacement values versus horizontal displacement values are represented for the well graded crushed sand. The peak shear strength values of the samples are relatively low. For the samples in dense state, a residual strength plateau does not appear. The crushed sand samples in dense state are showing a contraction and a following dilation behavior. Although the sample under 50 kPa in loose state is dilating, other samples in loose state are showing contraction behavior.

Table 4.15. Relative density and internal friction angle values of the various samples.

Samples Relative	Density State	Internal Friction Angle
Fly Ash Pellet (20-30)	Dense (97%)	39.60^O
Fly Ash Pellet (20-30)	Loose (9%)	36.23^O
Fly Ash Pellet (Well Graded)	Dense (97%)	40.71^O
Fly Ash Pellet (Well Graded)	Loose (8%)	32.83^O
Sakarya Sand (20-30)	Dense (96%)	37.50^O
Sakarya Sand (20-30)	Loose (9%)	33.60^O
Sakarya Sand (Well Graded)	Dense (97%)	39.83^O
Sakarya Sand (Well Graded)	Loose (7%)	36.37^O
CementPellet (20-30)	Dense (97%)	40.72^O
Cement Pellet (20-30)	Loose (9%)	37.43^O
Cement Pellet (Well Graded)	Dense (96%)	42.01^O
Cement Pellet (Well Graded)	Loose (9%)	33.96^O
Crushed Sand (20-30)	Dense (95%)	37.73^O
Crushed Sand (20-30)	Loose (10%)	35.04^O
Crushed Sand (Well Graded)	Dense (96%)	39.23^O
Crushed Sand (Well Graded)	Loose (9%)	37.87^O

In Table 4.15, the relative densities and internal friction angles for the samples are represented. The internal friction angles of the pellets produced from both fly ash and cement are showing similar or greater values in comparison with natural and crushed sand. Especially, the internal friction angle values for the pellets produced with cement

are occurred greater than all other samples. The difference in internal friction angle between the pellets produced with fly ash and cement can be caused by the greater crushability value of fly ash pellets.

4.5. Stress Path

In the following Figure 4.35 and Figure 4.36, the stress paths for the uniformly graded samples produced with fly ash in dense and loose condition are presented. To draw the graphs in Figure 4.35, the fly ash pellets are consolidated at rest condition. The angle between the K_0 line and s line is calculated as 27.24^o. For the first sample, a vertical stress of 50 kPa is applied. For the second one, 200 kPa of vertical stress is used. The angle between the K_f and s line comes out as 32.51^o.

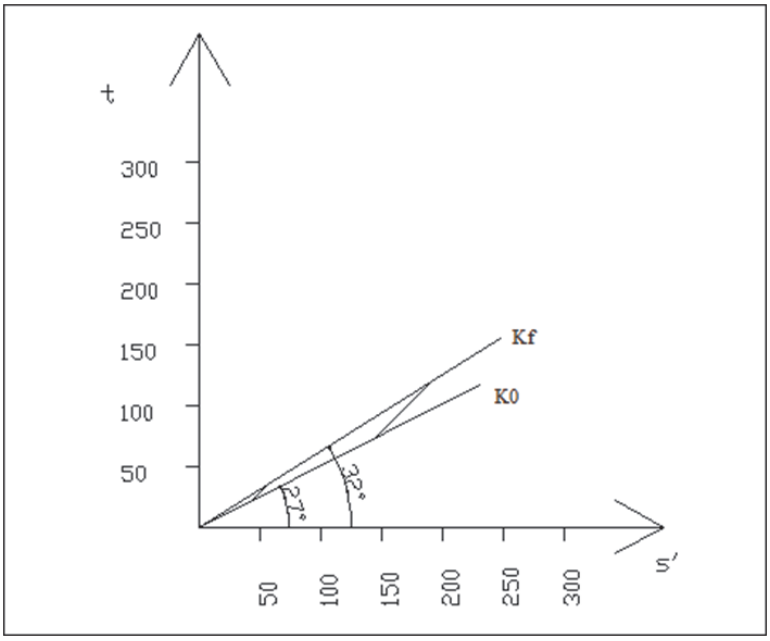

Figure 4.35. Stress path with K_f and K_0 lines for pellet produced with fly ash with grain size distribution of Standard sand 20 - 30 in dense state.

In Figure 4.36 the angle between the K_0 line and s line is 25.54^o. The decreased value of this angle in comparison of those in Figure 4.35 points out to an increasing value of K0. As mentioned before, a vertical stress of 50 kPa for the first sample and 200 kPa of vertical stress for the second one is applied. The angle between the K_f and

$\acute{s}$ line comes out as 30.58^o.

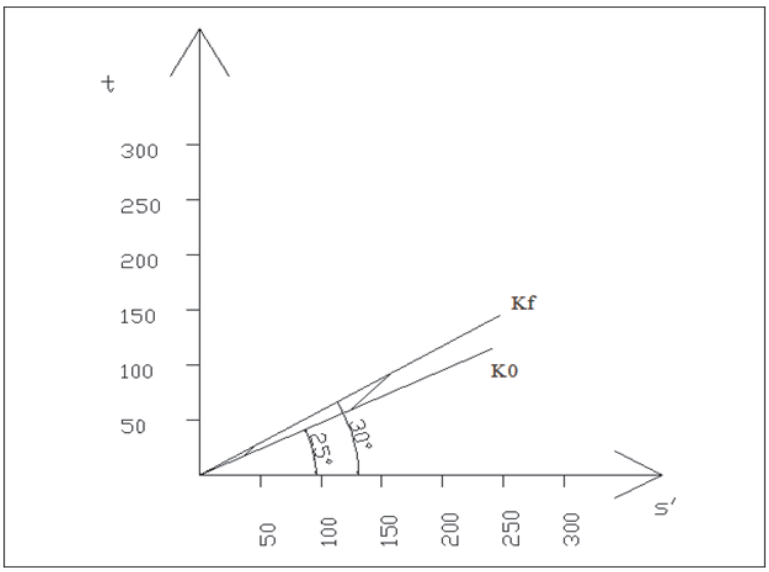

Figure 4.36. Stress path with Kf and K0 lines for pellet produced with fly ash with grain size distribution of Standard sand 20 - 30 in loose state.

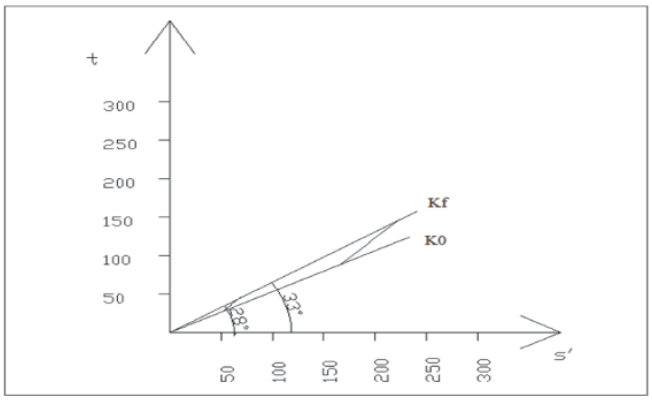

Figure 4.37. Stress path with Kf and K0 lines for pellet produced with fly ash with grain size distribution of Standard sand well graded in dense state.

In Figure 4.37, the angle θ is 33.11^o and α is 28.39^o. The well graded samples reaches higher σ_1 and σ_3 values at the point of failure. Because of the increase of α value, an increase in internal friction angle value and higher values of principle stresses at failure are expected.

In Figure 4.38, the angle between K_f line and $\acute{s}$ axis, θ, comes down till the value of 28.46^o and the angle between K_0 line and $\acute{s}$ axis, α, is occurred as 21.67^o for well

graded fly ash pellet. The decreased value of internal friction angle is a clear reason for these dropsin the values.

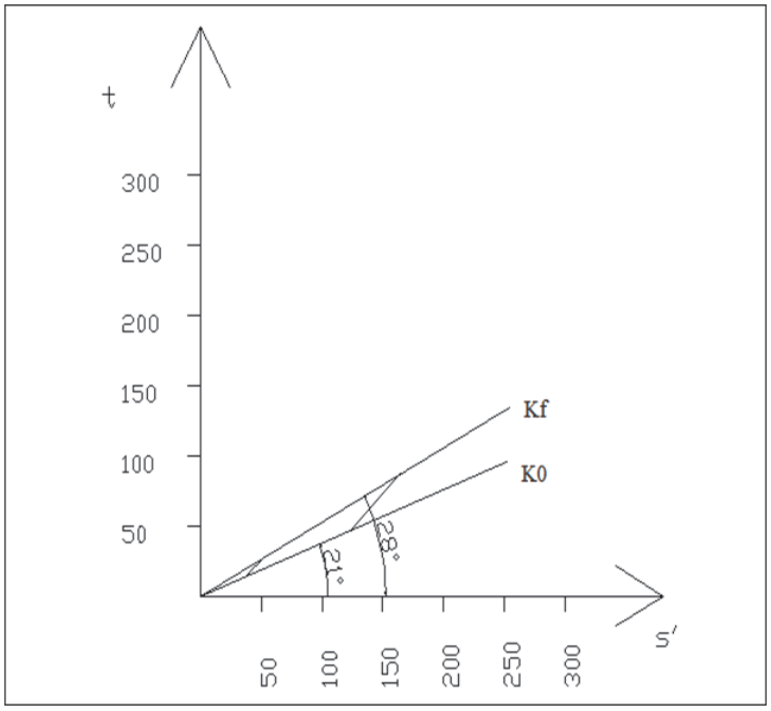

Figure 4.38. Stress path with K_f and K_0 lines for pellet produced with fly ash with grain size distribution of Standard sand well graded in loose state.

In Figure 4.39, the stress path of uniformly graded Sakarya sand at dense state is represented. The angle θ is 31.33^o and α is 25.87^o. In comparison with those of uniformly graded fly ash pellets, Sakarya sand samples have a smaller internal friction angle and, therefore, a decrease in θ and α angles.

As it is seen in all types sands used in this work, the change from the dense state to the loose state in relative density ends up with a decrease in internal friction angle and smaller θ and α angles, like represented in Figure 4.40. The angle θ is 28.96^o and α is 22.77^o for the uniformly graded Sakarya sand in dense state, presented in Figure 4.40.

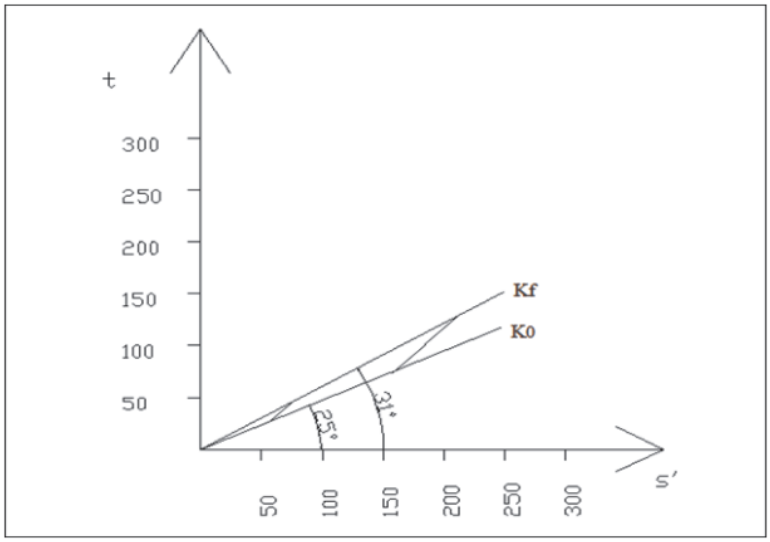

Figure 4.39. Stress path with K_f and K_0 lines Sakarya sand with grain size distribution of Standard sand 20 - 30 in dense state.

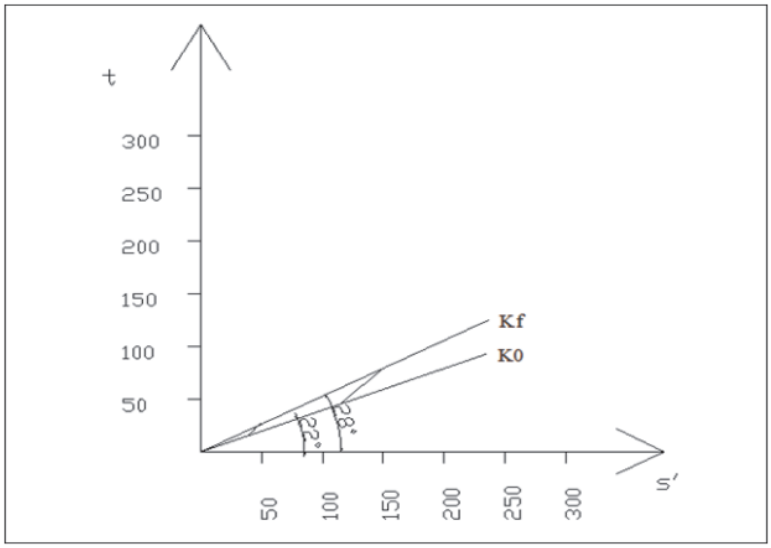

Figure 4.40. Stress path with K_f and K_0 lines Sakarya sand with grain size distribution of Standard sand 20 - 30 in loose state.

In Figure 4.41 and Figure 4.42, the stress paths of the well graded Sakarya sand samples are represented under dense and loose condition, respectively. The angle θ is 32.64^o and α is 26.43^o at dense condition. Under the loose condition, the angle θ is 30.67^o and α is 24.51^o.

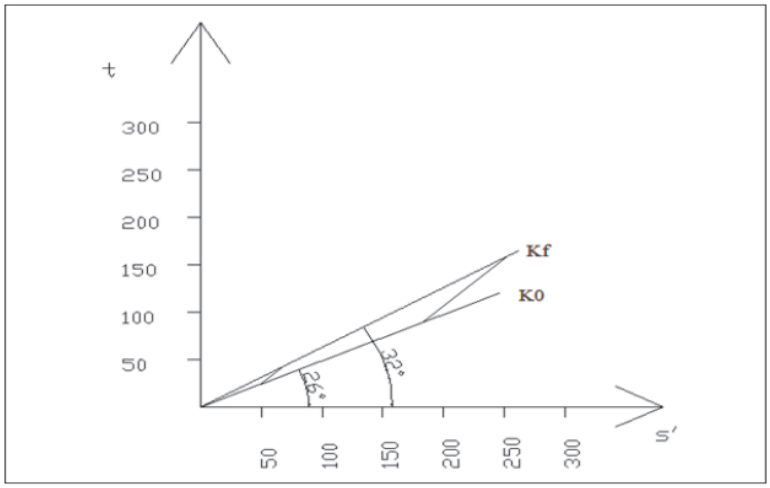

Figure 4.41. Stress path with K_f and K_0 lines Sakarya sand with grain size distribution of Standard sand well graded in dense state.

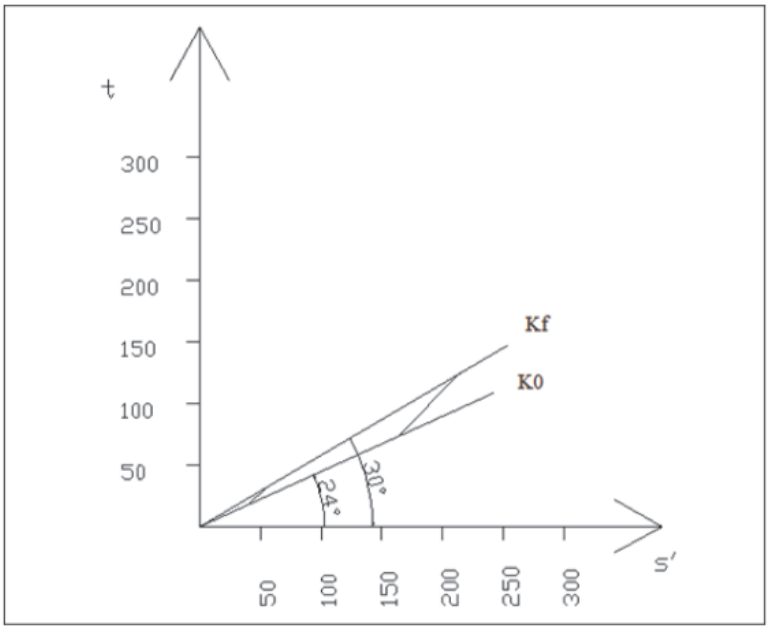

Figure 4.42. Stress path with K_f and K_0 lines Sakarya sand with grain size distribution of Standard sand well graded in loose state.

The decrese in the value of internal friction angle, the angle θ and α is again occurred as the relative density condition changes from dense to loose state. In comparison with those of uniformly graded Sakarya sand samples, well graded Sakarya sand samples have greater internal friction angle values and they reach to failure at greater maximum principal stress values.

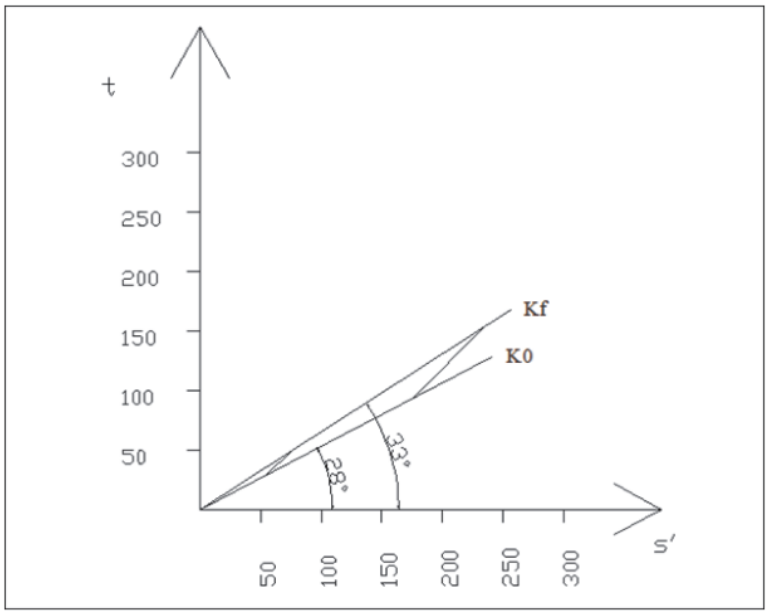

Figure 4.43. Stress path with K_f and K_0 lines for pellet produced with cement with grain size distribution of Standard sand 20 - 30 in dense state.

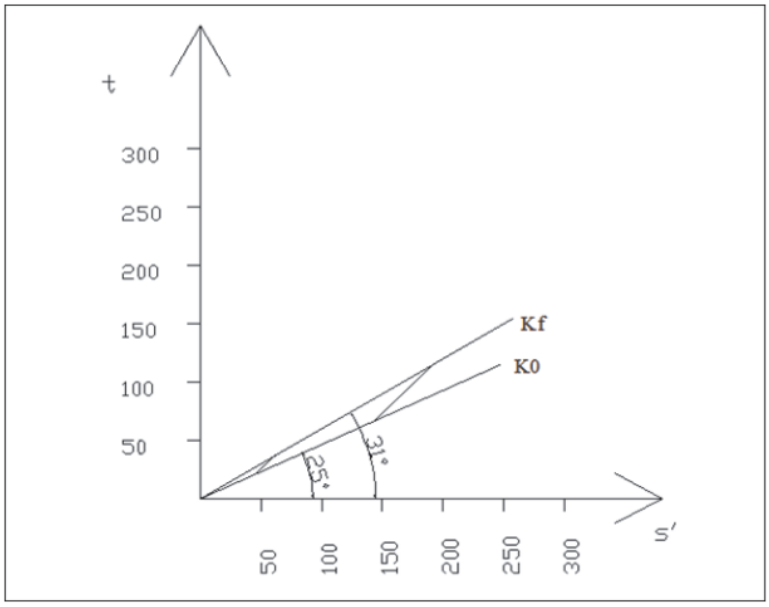

Figure 4.44. Stress path with K_f and K_0 lines for pellet produced with cement with grain size distribution of Standard sand 20 - 30 in loose state.

The stress paths for uniformly graded pellets produced with cement are represented in Figure 4.43 and Figure 4.44. The angles θ are 33.12^o and 31.29^o, the angles α are 28.16^o and 23.97^o at dense and loose relative density condition, respectively. The internal friction angles are showing the peak values under all other sand samples.

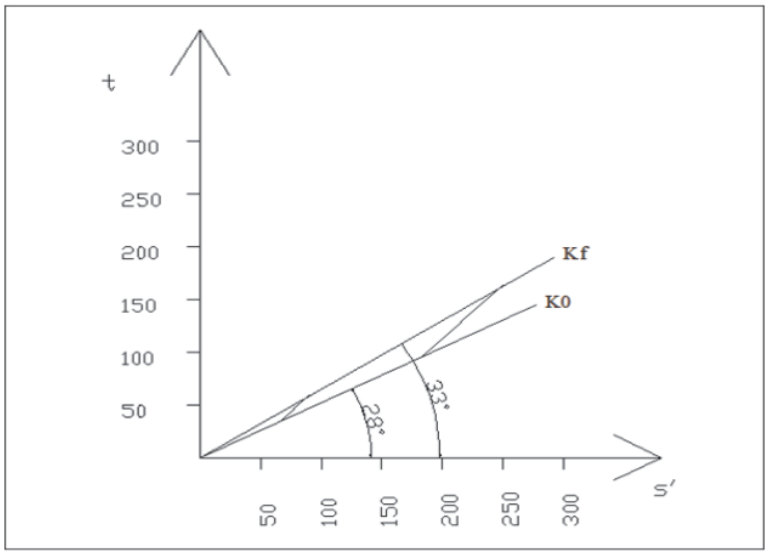

Figure 4.45. Stress path with K_f and K_0 lines for pellet produced with cement with grain size distribution of Standard sand well graded in dense state.

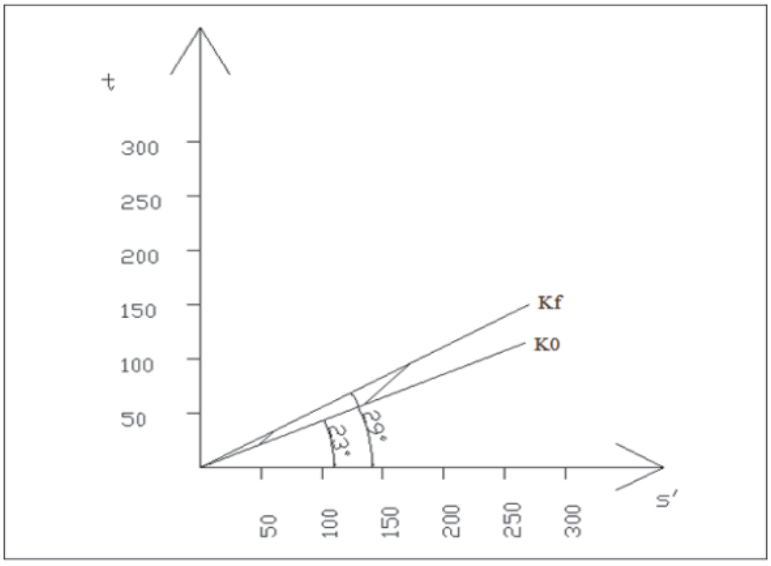

Figure 4.46. Stress path with K_f and K_0 lines for pellet produced with cement with grain size distribution of Standard sand well graded in loose state.

In Figure 4.45 and Figure 4.46, stress paths with well graded cement pellets in dense and loose state are represented. The angles θ and α are 33.79^o and $28,89^o$ for dense state, 29.19^o and 23.94^o for loose state, respectively. Like uniformly graded cement pellet samples, well graded cement samples reach high internal friction angle, K_f and K_0 values.

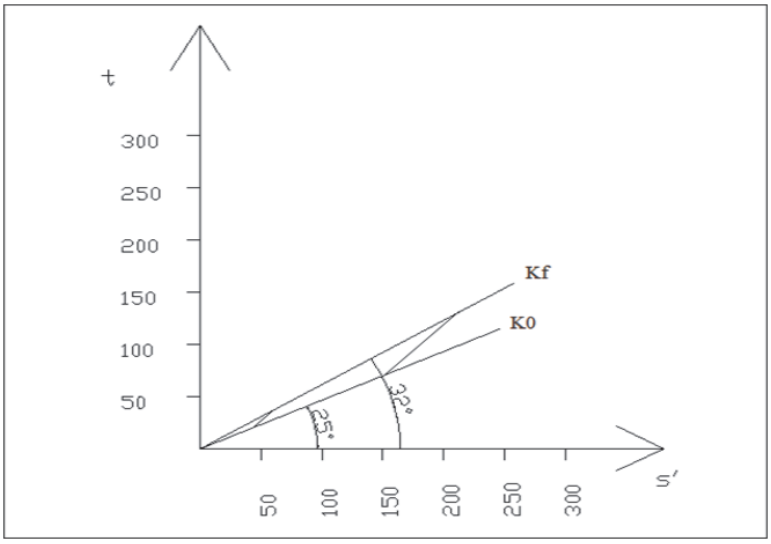

Figure 4.47. Stress path with K_f and K_0 lines for crushed sand with grain size distribution of Standard sand 20 - 30 in dense state.

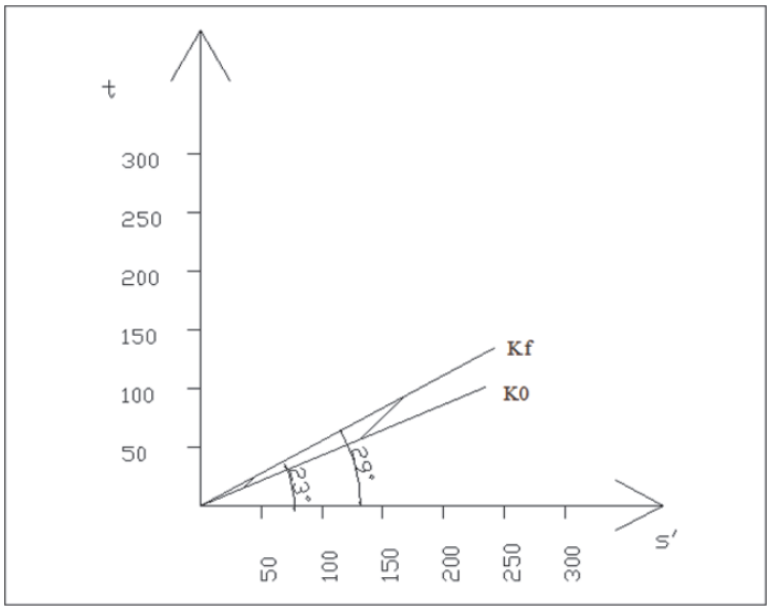

Figure 4.48. Stress path with K_f and K_0 lines for crushed sand with grain size distribution of Standard sand 20 - 30 in loose state.

Stress paths for uniformly graded crushed sand in dense and loose state are given in the Figure 4.47 and Figure 4.48. The angles θ are 32.03^o and 29.86^o for dense and loose relative density condition, respectively. The α angles are 27.41^o and 25.27^o for dense and loose condition, respectively. Even uniformly graded crushed sand cannot reach the internal friction values of the uniformly graded cement pellet.

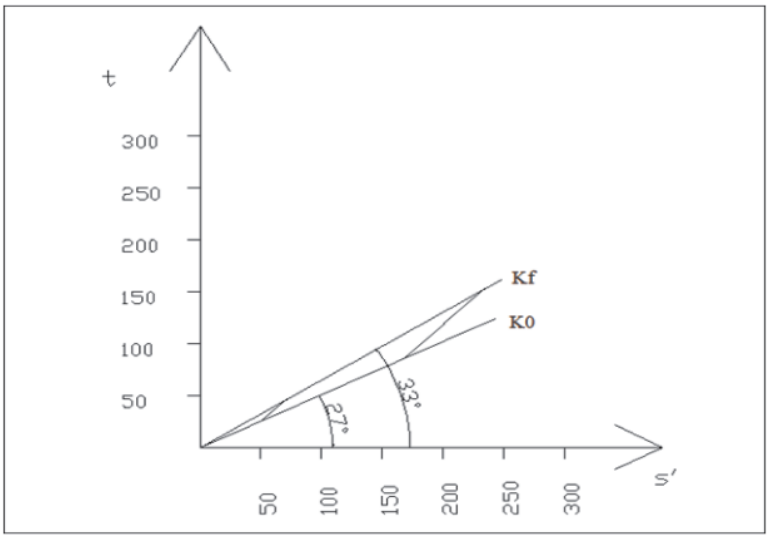

Figure 4.49. Stress path with K_f and K_0 lines for crushed sand with grain size distribution of Standard sand well graded in dense state.

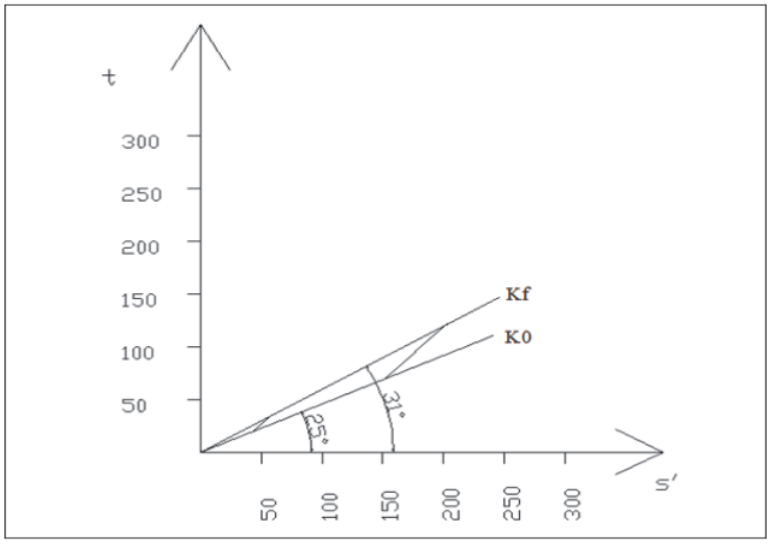

Figure 4.50. Stress path with K_f and K_0 lines for crushed sand with grain size distribution of Standard sand well graded in loose state.

In Figure 4.49 and Figure 4.50, stress paths for well graded crushed sand in dense and loose state are represented. The angle between the K_0 line and s'line, the angle θ is calculated as 27.75^o for Figure 4.49 and the angle between the K_f and s'line, the angle θ , comes out as 33.39^o. For graph 4.50, the angle between the K_0 line and s'line, the angle α is 25.64^o and the angle between the K_f and s'line, the angle θ, calculated as 31.54^o.

In Table 4.16, the relative density values and the angle θ values are given. The relative density values are similar to those of direct shear tests. The θ angles are in a correlation with those of internal friction angles in the direct shear tests.

Table 4.16. Relative density and the angle between K_f line and axis $\acute{s}(\theta)$ of the various samples.

Samples	Relative Density State	The angle between K_f line and axis $\acute{s}(\theta)$
Fly Ash Pellet (20-30)	Dense (92%)	32.51^o
Fly Ash Pellet (20-30)	Loose (13%)	30.58^o
Fly Ash Pellet (Well Graded)	Dense (94%)	33.11^o
Fly Ash Pellet (Well Graded)	Loose (11%)	28.46^o
Sakarya Sand (20-30)	Dense (91%)	31.33^o
Sakarya Sand (20-30)	Loose (10%)	28.96^o
Sakarya Sand (Well Graded)	Dense (89%)	32.64^o
Sakarya Sand (Well Graded)	Loose (14%)	30.67^o
Cement Pellet (20-30)	Dense (91%)	33.12^o
Cement Pellet (20-30)	Loose (10%)	31.29^o
Cement Pellet (Well Graded)	Dense (89%)	33.79^o
Cement Pellet (Well Graded)	Loose (11%)	29.19^o
Crushed Sand (20-30)	Dense (91%)	32.03^o
Crushed Sand (20-30)	Loose (11%)	29.86^o
Crushed Sand (Well Graded)	Dense (94%)	33.39^o
Crushed Sand (Well Graded)	Loose (12%)	31.54^o

4.6. Cyclic Triaxial

In this section, all cyclic triaxial tests are done with samples at loose condition. Similar relative densities in stress path tests are also reached in these experiments.

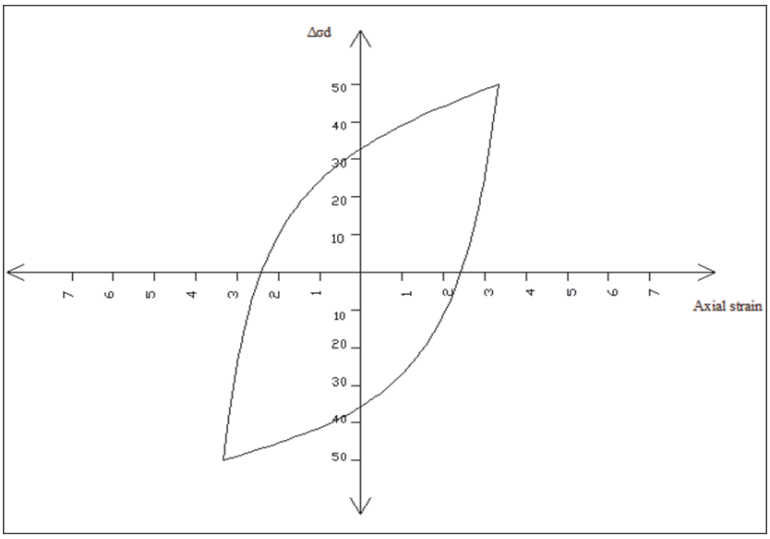

Figure 4.51. Axial strain vs $\triangle\sigma_d$ curve for pellet produced with cement with grain size distribution of Standard sand well graded in loose state.

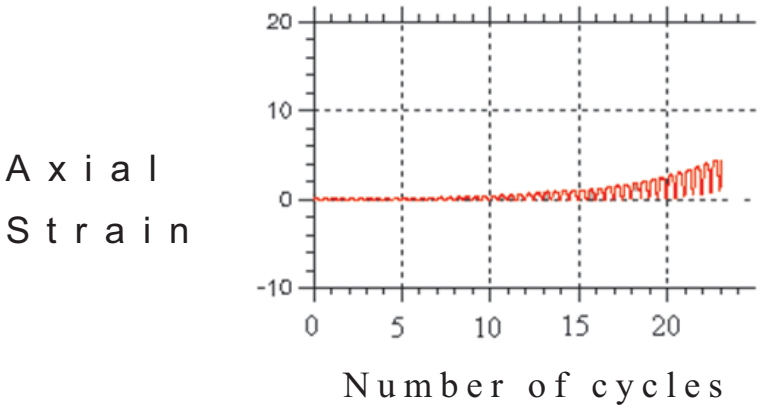

Figure 4.52. Number of cycles vs axial strain curve for pellet produced with cement with grain size distribution of Standard sand well graded in loose state.

Axial strain versus $\triangle\sigma_d$ curve for well graded cement pellet are represented in the Figure 4.51. The damping ratio is calculated as 1.906 for this test. The maximum strain before liquefaction is reached at 3.23% axial strain and after 23 cycles, as seen in the Figure 4.51 and Figure 4.52. Those results are similar with those result of the well graded fly ash pellets at loose state.

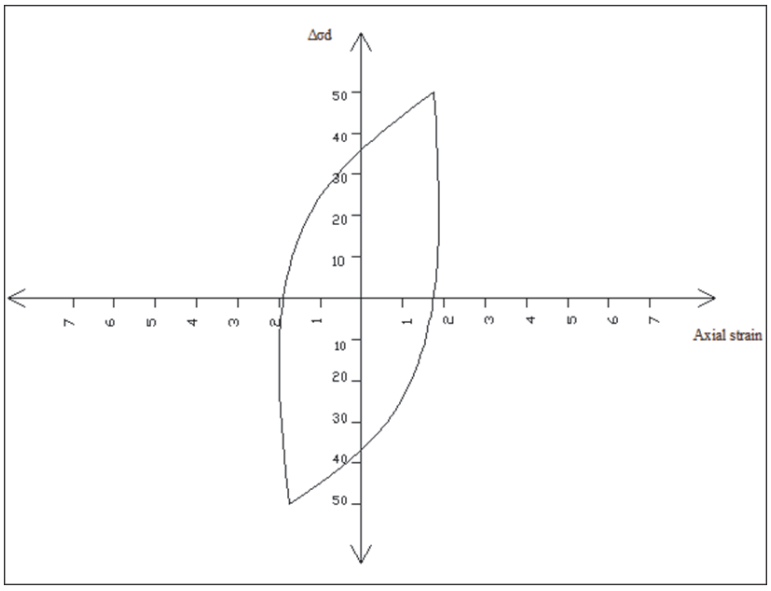

Figure 4.53. Axial strain vs $\triangle\sigma_d$ curve for crushed sand with grain size distribution of Standard sand well graded in loose state.

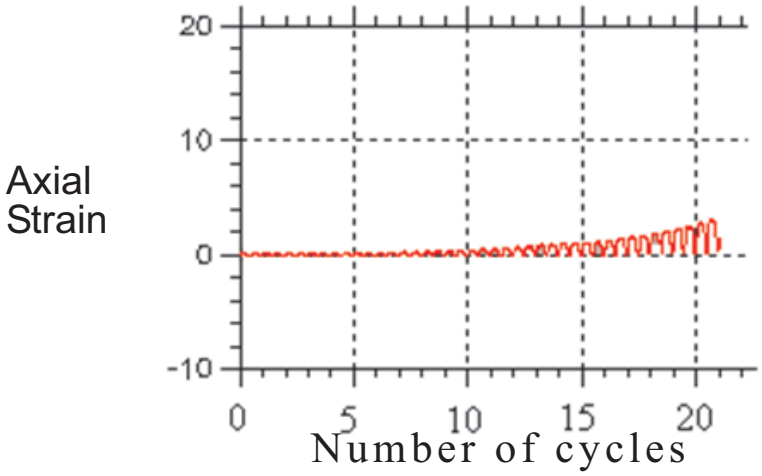

Figure 4.54. Number of cycles vs axial strain curve for crushed sand with grain size distribution of Standard sand well graded in loose state.

In Figure 4.53, the axial strain versus $\triangle\sigma_d$ curve for well graded crushed sand at loose state is represented. The damping ratio for this cyclic shear test is calculated as 2.525. As seen in Figure 4.53 and Figure 4.54, the maximum strain before liquefaction is reached at 1.73% axial strain and after 21 cycles.

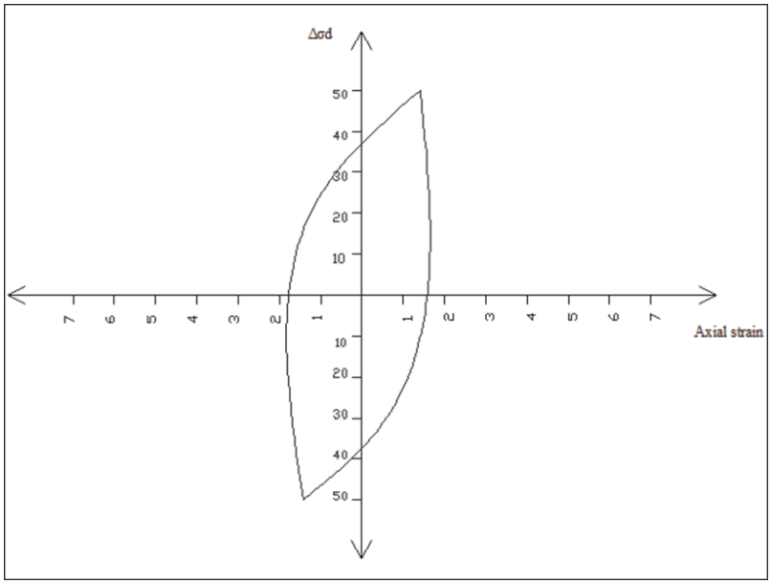

Figure 4.55. Axial strain vs. $\triangle\sigma_d$ curve for Sakarya sand with grain size distribution of Standard sand well graded in loose state.

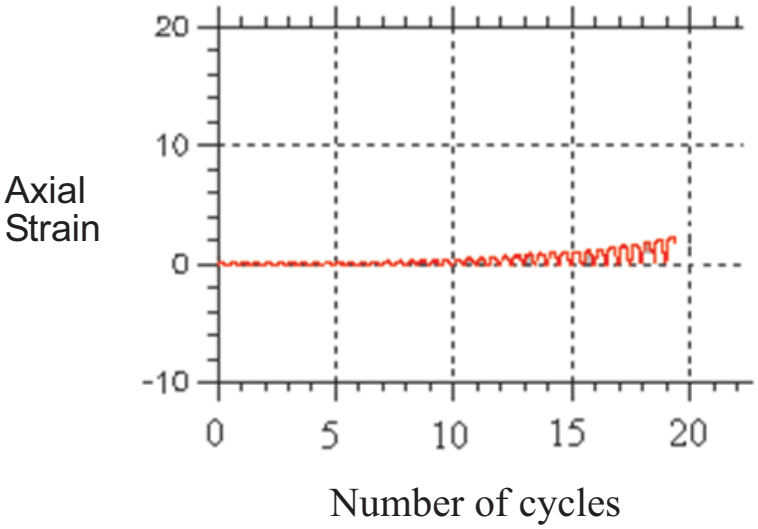

Figure 4.56. Number of cycles vs axial strain curve for Sakarya sand with grain size distribution of Standard sand well graded in loose state.

The axial strain versus $\triangle\sigma_d$ curve for well graded Sakarya sand at loose state is represented in Figure 4.55. The according damping ratio is found as 2.803. In Figure 4.55 and Figure 4.56, it can be seen that the liquefaction is reached at 1.59% strain

and after 19 cycles. From these results, it can be obtained that as the roundness and sphericity values increases among natural and crushed sand.

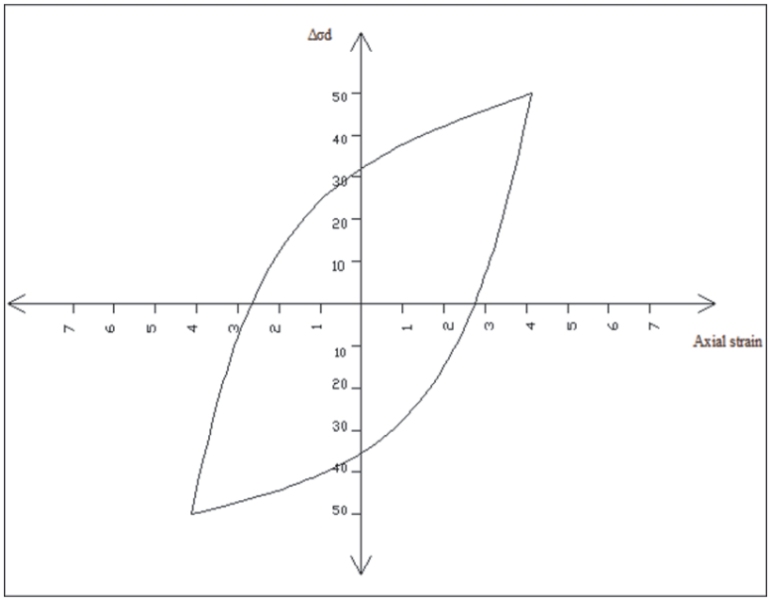

Figure 4.57. Axial strain vs $\triangle\sigma_d$ curve for pellet produced with fly ash with grain size distribution of Standard sand well graded in loose state.

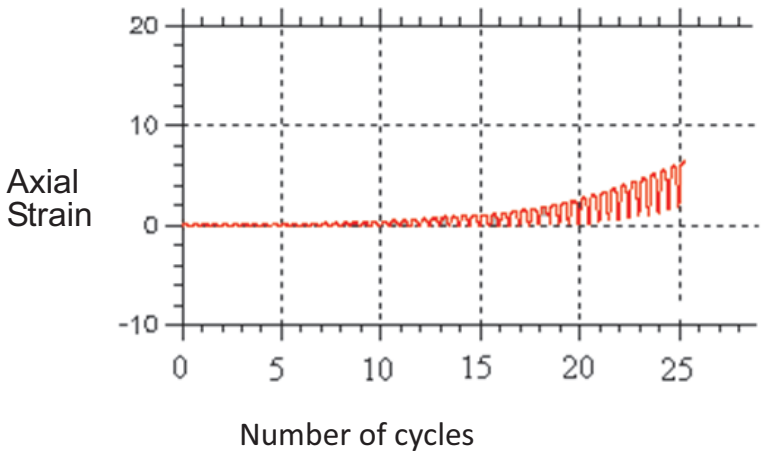

Figure 4.58. Number of cycles vs axial strain curve for pellet produced with fly ash with grain size distribution of Standard sand well graded in loose state.

Axial strain versus $\triangle\sigma_d$ curve and the number of cycles versus axial strain curve for well graded pellet produced with fly ash at loose state are represented in Figure 4.57 and Figure 4.58, respectively. It is calculated that the damping ratio of the fly

ash pellets are 1.772. According to Figure 4.57 and Figure 4.58, the liquefaction is occurring at the 3.81% axial strain and after 25 cyclic loading.

5. CONCLUSION

The pellets produced with fly ash or cement have desired strength values to use in geotechnical laboratory experiments, although they have less crushing strength. The reason for that are the assumptions that are made for shear strength experiments. For example, in the direct shear experiments, the area of shearing is the box area. This area is decreasing in one dimension with increasing horizontal displacement. It is assumed that this whole area carries the shear load on itself. But the voids in the shearing area are not considered. Because the every grain of pellets behaves in an elastic manner, the contact area between the particles is increasing. So, the shear load on the grains is similar to those of the natural sand grains.

The geotechnical properties of artificial sand are investigated without any prejudice like stated above. It is also known that natural sand samples are variable even in the same deposit and they are not suitable for parametric study concerning geotechnical laboratory experiments. The standards sands, also, can vary or become unavailable over the time. As the objective of this M.S. thesis, artificial sand is produced with fly ash and cement in order to use in geotechnical laboratory experiments and examining its geotechnical properties. As part of this study, the performance of artificial sand produced by pelletization is compared with natural sand samples (Sakarya sand) and crushed sand.

The properties, that can cause a difference in the results of experiments with changing sample of sand, are mineralogy, roundness, sphericity, specific gravity, water absorption, grain size distribution and internal friction angle. The usability of the pellets as artificial sand for laboratory uses can be decided by evaluating and comparing these parameters.

After the specific gravity and water absorption values of all samples are found, it is seen that the apparent specific gravity values are about 2.38 and 2.45 for the samples produced by fly ash and cement, respectively, where the apparent specific

gravity values are 2.68 and 2.84 for the natural sand samples and crushed sand samples, respectively. The intragranular voids and, as a result of this, the water absorption values are decreasing with the decreasing mean particle size D_{50}. The water absorption values for the samples produced by fly ash and cement are 27.82% and 24%. However, no significant water absorption values for Sakarya sand and crushed sand are seen. They are taken as zero. So, it is seen that the decrease in the specific gravity values of pellets are caused by the large intragranular voids. For an absolute explanation of the effect of the intragranular voids, different experiments and observations with different instruments like X - ray machine or scanning electron microscope should be used.

If the roundness, sphericity and regularity values of pellets produced with fly ash are compared with those values of the pellets produced from cement, there is no significant difference between those values. The roundness values for pellets are higher than the natural and crushed sand samples in both grain size distributions. These results have also another meaning: The pelletization process is a totally physical process. Furthermore, at the hands of an experienced operator and with a proper device; the mean diameter of the grains, the roundness, the sphericity and the regularity values will be the same independent of the material that is used for pelletization.

Constrained modulus tests are also conducted to specify the strain - stress behavior of the samples at rest, in K_0 condition. It is seen that, pellets cannot have the same strain gaining behavior like the natural and crushed sand samples in recovery region. However, the results are highly similar, even better in the virgin curve region. It is also seen that an excess of 3% to 4% crushability is occurred both in cement and fly ash pellets.

Direct shear tests are conducted to decide whether the artificial sand has the appropriate internal friction angle and crushability values. Same manner in the crushability has been observed. So, the crushability is affected by shearing very small. Internal friction angles of pellets, produced both from fly ash and cement, are close to the internal friction angle values of crushed sand and Sakarya sand.

In the stress path tests, it is seen that pellets have similar or better performance than the performance of natural and crushed sands under the condition of vertical loading after K_0 consolidation. In the cyclic triaxial tests, the samples produced from fly ash and cement reaches to the liquefaction failure after 25 and 23 cycles, whereas Sakarya sand and crushed sand reaches to the failure after 19 and 21 cycles. Pellets have also higher axial strain values at the time of failure. Therefore, they have better results for cyclic loading.

To sum up, it is seen that pellets can be used for geotechnical laboratory purposes. Especially by modeling of crushable sands, they have very similar behaviors. If the costs of taking samples from crushable sand deposits (calcareous sand deposits under the oceans) are taken into the consideration, modeling these sands with pellets is a promising solution in the future.

REFERENCES

Al-Douri, R. H., H. G., Poulos, 1991, "Static and cyclic direct shear tests on carbonate sands", *Geotechnical Testing Journal*, Vol. 15, No. 2, pp. 138-157.

ASTM C127, 2007, *Standard Test Method for Density, Relative Density (Specific Gravity), and Absorption of Coarse Aggregate*, American Society for Testing Materials, West Conshohocken.

ASTM C778, 2006, *Standard Specification for Standard Sand*, American Society for Testing Materials, West Conshohocken.

Arslan, H., 2003, *The Effect of Crushing on the Behavior of Granular Materials*, M.S. Thesis, Bogazici University.

Arslan, H. and G., Baykal, 2006, "Utilization of Fly-ash as Engineering Pellet Aggregates", *Environmental Geology Journal*, Vol. 50, No. 5, pp. 761 - 770.

Bardet, J. P., 1997, *Experimental Soil Mechanics*, Prentice Hall, New Jersey.

Baykal, G. and A. G., Döven, 2000, "Utilization of Fly Ash Pelletization Process; Theory, Application Areas and Research Results", *Resources Conservation and Recycling Journal*, Vol. 30, No. 7, pp. 59 - 77.

Bijen, J, 1986, "Fly Ash Aggregates", *ACI SP 79-26, American Concrete Institute.*

Bowles, J. E., 1998, *Engineering Properties of Soils and Their Measurements*, McGraw-Hill Science Engineering, New York.

Brandes, H. G., 2011, "Simple Shear Behavior of Calcareous and Quartz Sands", *Journal of Geotechnical and Geological Engineering*, Vol. 29, No. 8, pp. 113 - 126.

Brendan, C. O. and P. J., Naughton, 2009, "Study of the yielding of sand under

generalized stress conditions using a versatile hollow cylinder torsional apparatus", *Mechanics of Materials*, Vol. 41, pp. 187 - 198.

Celestino, T. B. and J. K., Mitchell, 1983, "Behavior of Carbonate Sands for Foundations of Offshore Structures", *Proceedings of Brazil Offshore, Rio de Janeiro*, pp. 85 - 102.

Chen, Y. P., 1985, *Liquefaction Potential of Coral Sand*, M.S. Thesis, Department of Civil Engineering, Colorado State University, Fort Collins, Colorado.

Coop, M. R., D. W., Airey, 2003, "Carbonate sands", *Characterization and engineering properties of natural soils*, Vol. 39, No. 2, pp. 1049-1086.

Çabalar, A.F., A., Çevik, and I. H., Güzelbey, 2010, "Constitutive modeling of Leighton Buzzard Sands using genetic programming", *Neural Computing and Applications*, Vol. 19, No. 1, pp. 657 - 665.

Danyıldız, E., 2007, *The Interface Behavior Between Granular Soils and Concrete*, Ph. D. Thesis, Boğaziçi University.

Das, B., 2007, *Principals of Geotechnical Engineering*, Thomson, New Jersey.

Das, B., 2011, *Principals of Soil Dynamics*, Cengage Learning, New Jersey.

Datta, M., S. K., Gulhati and G. V., Rao., 1979, "Crushing of calcareous sands during shear", *Proceedings of Offshore Technology Conference*, Houston, Vol 3., No.43, pp. 1459-1467.

Dehnavi, Y., 2011, "Numerical modeling of stress-strain behavior of sand under cyclic loading", *Engineering Geology*, Vol. 116, No. 4, pp. 53.

Döven, G., 1998, *Light Weight Aggregate Production Using Cold Bonding Agglomeration Process*, Ph.D. Thesis, Boğaziçi University.

Eşidir, Y., 2010, *Evaluation of the Intergranular Coefficient of Friction Using Distinct Element Modelling*, M.S. Thesis, Boğaziçi University.

Head, K. H., 1981, *Manual of Soil Laboratory Testing*, Vol. 2, No. 8, Halstead.

Head, K. H., 1998, *Manual of Soil Laboratory Testing*, Vol. 3, No. 19, Halstead.

Holmes, A., 1978, *Principles of Physical Geology*, Cengage Learning, Australia.

Ishihara, K., H. Tsuchiya, Y. Huang and K., Kamada, 2001, "Recent studies on liquefaction resistance of sand effect of saturation", *Proceeding* 4^{th} *International Conference Recent Advances in Geotechnical Earthquake Engineering and Soil Dynamics*, Keynote Lecture, San Diego, p.1-7.

Jewell, R. J., 1993, *An Introduction to Calcareous Sediments*, Research Report No. G1075, Department of Civil Engineering, The University of Western Australia, pp. 45.

Jia, Y., S., Chi and G., Lin, 2009,*Rock and Soil Mechanics*, State Key Laboratory of Coastal and Offshore Engineering, Dalian University of Technology.

Kong, D., B., Zhang and X., Sun, 2010, "Triaxial Tests on Artificial Rockfill Materials of Steel Balls", *Journal of Hydroelectric Engineering*, Vol. 37, pp. 106 - 111.

Kuwano, R. and J. R., Jardine, 2002, "On Measuring Creep Behaviour in Granular Materials through Triaxial Testing", *Canadian Geotechnical Journal*, Vol. 39, pp. 1061 - 1074.

Kwag, J. M., H., Ochiai and N., Yasufuku, 1999, "Yielding stress characteristics of carbonate sand in relation to individual particle fragmentation strength", Proceedings of the 2^{nd} International Conference on Engineering for Calcareous Sediments, Bahrain, Vol. 1, pp. 79-86.

Lee, J. Y., J. C., Santamarina and C., Ruppel, 2011, "Volume change associated

with formation and dissociation of hydrate in sediment", *Geochemical Geophysical Geosystems*, Vol. 8, No. 49, pp. 219-223.

Lo Presti, D. C. F., O., Pallara, R., Lancellota, M., Armandi and R., Maniscalco, 1993, "Monotonic and Cyclic Loading Behavior of Two Sands at Small Strains", *Geotechnical Testing Journal*, Vol. 16, No. 4, pp. 409-424.

Mayne, D. Q., 2001, "Control of constrained dynamic systems", *European Journal of Control*, Vol. 7, pp. 87-99.

Mao, X., M., Fahey, 2003, "Behaviour of Calcareous Soils in Undrained Cyclic Simple Shear", *Geotechnique*, Vol. 53, No. 8, pp. 715-727.

Marchetti, S., 1999, *On the calibration of the DMT membrane*, L'Aquila University, Unpublished report.

McClelland, B., 1988, "Calcareous sediments: an Engineering Enigma", *Proceeding of the International Conference on Calcerous Sediments, Perth*, Vol. 2, pp. 777 - 784.

Meigh, A. C., 1987, *Cone Penetration Testing-Methods and Interpretation*, CIRIA, Butterworths.

Mejia, L. H. and M. R., Yeung, 1995, "Liquefaction of Coralline Soils during the 1993 Guam Earthquake", *Earthquake-induced Movements and Seismic Remediation of Existing Foundations and Abutments, Geotechnical special publication* No. 55, ASCE, pp 33-48.

Mitchell, J. K. and K., Soga, 2005, *Fundamentals of Soil Behavior*, John Wiley and Sons.

Moore, D. and G., McCabe, 2003, *Introduction to the Practice of Statistics*, W.H. Freeman, New York.

Morioka, B. T. and P. G., Nicholson, 2000, "Evaluation of the Liquefaction Potential of Calcareous Sand", *Proceedings of the* 10^{th} *International Offshore and Polar Engineering Conference, Brest, France*, Vol. 2, pp. 494 - 500.

Nicholson, P. G., 2006, "Liquefaction Evaluation Discrepancies in Tropical Lagoonal Soils", *Journal of Geotechnical and Geological Engineering*, Vol. 24, No. 5, pp.1259 - 1269.

Ong, S. E., H. A., Joer and M. F., Randolph, 1999, "Frictional behavior in calcareous soils", *Proceedings of the* 2^{nd} *International Conference on Engineering for Calcareous Sediments, Bahrain*, Vol. 1, pp. 219-228.

Patel, A., P. P., Bartake and D. N., Singh, 2009, "An Empirical Relationship for Determining Shear Wave Velocity in Granular Materials Accounting for Grain Morphology", *Geotechnical Testing Journal*, Vol. 32, pp. 1 - 10.

Porcino, D., G., Caridi and V. N., Ghionna, 2008, "Undrained Monotonic and Cyclic Simple Shear Behaviour of Carbonate Sand", *Geotechnique*, Vol. 58, No. 8, pp. 635 - 644.

Richard, J., 2002, "On Measuring Creep Behaviour in Granular Materials Through Triaxial Testing". *Canadian Geotechnical Journal*, Vol. 39, no. 5, pp. 1061-1074.

Reinson, J. R., D. G., Fredlund and G. W., Wilson, 2005, "Unsaturated Flow in Coarse Porous Media", *Canadian Geotechnical Journal*, Vol. 42, pp. 252 - 262.

Rollins, K. M., P., Nicholson, J. D., Lane and R. E., Rollins, 2004, "Liquefaction Hazard Assessment Using Controlled-blasting Techniques", *Proceedings of* 11^{th} *International Conference on Soil Dynamics and Earthquake Engineering and* 3^{rd} *International Conference on Earthquake Geotechnical Engineering*, Vol. 2, pp. 630 - 637.

Rouse, P., R. J., Fannin, and D. A., Shuttle, 2008, "Influence of roundness on the void

ratio and strength of uniform sand", *Geotechnique*, Vol. 58, pp. 227-231.

Sangrelat, G., 1970, *The Penetrometer and Soil Exploration*, Elsevier, Amsterdam, pp. 464.

Sastry, K. V., 1995, "Pelletization of Fine Coals", *Final Report U.S. Department of Energy Technology Center*, E and FN Spon, Los Angeles.

Seidman, J., 2007, *Static and Dynamic Properties of Various Sands Using a Direct Simple Shear Apparatus*, M.S. Thesis, University of Hawaii.

Semple, R. M., 1988, "The mechanical properties of carbonate soils", *Proceedings of the International Conference on Calcareous Sediments, Perth*, Vol. 2, pp. 807-836.

Shahnazari, H., Y., Dehnavi and A. H., Alavi, 2010, "Numerical Modeling of Stress-strain Behavior of Sand under Cyclic Loading", *Engineering Geology*, Vol.116, pp. 53-72.

Sharma, S. S., M., Fahey, 2003a, "Evaluation of Cyclic Shear Strength of Two Cemeneted Calcareous Soils", *Journal of Geotechnical and Geoenvironmental Engineering*, Vol. 129, No. 7, pp. 608 - 618.

Sharma, S. S., M., Fahey, 2003b, "Degradation of Stiffness of Cemented Calcareous Soil in Cyclic Triaxial Tests", *Journal of Geotechnical and Geoenvironmental Engineering*, Vol. 129, No. 7, pp. 619 - 629.

Takahashi, A. and R. J., Jardine, 2007, "Assessment of Standard Research Sand for Laboratory Testing", *Quarterly Journal of Engineering Geology and Hydrogeology*, Vol. 40, pp. 93-103.

Unklesbay, A. G. and J. D., Vineyard, 1992, *Missouri Geology - Three Billion Years of Volcanoes, Seas, Sediments, and Erosion*, University of Missouri Press.

Use of Fly Ash in Concrete, ACI Committee 232, 2003.

Vallejo, L.E., 2001, "Interpretation of the Limits in Shear Strength in Binary Granular Mixtures", *Canadian Geotechnical Journal*, Vol. 38, No. 5, pp. 1097-1104.

Vuppala, M. K., D. M., Parikh and H. R., Bhagat, 1997, "Application of Powder-layering Technology and Film Coating for Manufacture of Sustained-release Pellets Using a Rotary Fluid Bed Processor", *Drug Development Indian Pharmacy*, Vol. 23, No. 7, pp. 687 - 694.

Walker, G. R., 1991, *The Behaviour of a new Ham River Sand with Special Reference to the Triaxial Test*, Thesis M.S., Imperial College, University of London.

Xia, H. and T., Hu, 1991, "Effects of Saturation and Back Pressure on Sand Liquefaction", *Journal of Geotechnical Engineering*, Vol. 117, No. 9, pp. 1347 - 1362.

Yoshimi, Y., K., Tanaka and K., Tokimatsu, 1989, "Liquefaction resistance of partially saturated sand", *Soils and foundations*, Vol. 29, pp. 157 - 162.

Yukio, N., K., Yoshinori and M., Hidekazu, 1999, "Properties of Compression and Single Particle Crushing for Crushable Soil", *PrIJC. of Sym. on Engineering problem on Crushable Ground*, Kagoshima, pp.15-20.

Yun, T. S. and J. C., Santamarina, 2008, "Fundamental study of thermal conduction in dry soils", *Granular Matter*, Vol. 10, pp. 197 - 207.